

Rapid post-merger signal of circularly polarized gravitational wave from magnetic black hole superradiance: novel approach to detect magnetic monopole

Zhong-Hao Luo,^{1,*} Fa Peng Huang,^{1,†} Pengming Zhang,^{2,‡} and Chen Zhang³

¹ MOE Key Laboratory of TianQin Mission, TianQin Research Center for Gravitational Physics & School of Physics and Astronomy,

Frontiers Science Center for TianQin, Gravitational Wave Research Center of CNSA, Sun Yat-sen University (Zhuhai Campus), Zhuhai 519082, China

² School of Physics and Astronomy, Sun Yat-sen University, Zhuhai 519082, China

³ Liaoning Key Laboratory of Cosmology and Astrophysics, College of Sciences, Northeastern University, Shenyang 110819, China

We present an analytic framework demonstrating that a spinning black hole endowed with a net magnetic charge exhibits a dramatically amplified superradiant instability against charged scalar fields—enhanced by several orders of magnitude compared with the neutral Kerr case. The amplification arises from a monopole-induced reduction of the centrifugal barrier, $\ell(\ell+1) \rightarrow \ell(\ell+1) - q^2$, encoded by an effective quantum number ℓ_q , with $q = eP = N/2$ fixed by Dirac quantization. This shift deepens the gravitational bound-state potential well and produces a parametrically larger instability growth rate. This resulting rapid growth yields a macroscopic boson cloud that acts as a coherent source of near-monochromatic continuous gravitational waves (GWs). We find an enhanced GW power, $P_{\text{GW}}^{\pm} \propto (E_c/M)^2 \alpha^{4\ell_q+8}$ (instead of $\alpha^{4\ell+10}$). Monopole-harmonic selection rules restrict the emission from the north/south clouds to $(\tilde{\ell}, \tilde{m}) = (2q, \pm 2q)$, corresponding to opposite helicities. Their superposition generates an (approximately) circularly polarized continuous GWs at a fixed sky location within parity-even general relativity, distinct from the generic elliptical polarization of the Kerr case. In light of these new findings, we propose a potential smoking-gun search strategy for magnetic monopole and ultralight boson: the rapid post-merger follow-up GW signals from binary-black-hole merger remnants through ground-based and space-based GW experiments. In contrast to the Kerr case, where the signal turn-on can be delayed to decades–centuries, a magnetic remnant can form a cloud and emit a stronger, circularly polarized continuous GWs within weeks to months. Taking the magnetic supermassive remnants ($M \sim 10^6 M_\odot$) as an example, we demonstrate that the rapid follow-up GW signal appears just in few weeks after binary black hole mergers and the GW strain scales as $h \sim 10^{-19}$ in the mHz band. Moreover, future polarization (ellipticity) measurements can distinguish the magnetic scenario from Kerr while providing a parity-even mechanism for circularly polarized GWs in general relativity.

Introduction—Black-hole superradiance extracts rotational energy from spinning black holes (BHs) and, in the presence of light bosonic fields, can trigger superradiant instabilities that build macroscopic bosonic condensates around the BH [1–15]. These clouds generically emit long-lived, nearly monochromatic gravitational waves (GWs), making them well-motivated targets for ground- and space-based interferometers [16–21]. Recent developments have sharpened waveform modeling, including cloud depletion, frequency evolution, and level-transition features [22–26].

Most studies focus on neutral Kerr BHs, but superradiant instabilities can be qualitatively modified if the BH carries magnetic charge sourced by magnetic monopoles. Magnetic monopoles are a classic prediction of grand unified theories [27–30]. Establishing their existence would probe high-scale gauge unification, and would provide a direct test of Dirac charge quantization. Their classical description is captured by the Wu–Yang construction [31, 32]. In the absence of definitive laboratory evidence so far [33–35], it is timely to pursue new observational avenues, with astrophysical environments providing a complementary discovery space. Motivated by this, Pérez-Gómez *et al.* [36] recently performed a numeri-

cal study of charged-scalar superradiance around rotating magnetic BHs and found dramatically shorter instability timescales, even for an order-one monopole number. They also uncovered “north” and “south” monopole-harmonic modes: rather than forming an equatorial torus as in Kerr, the most unstable clouds align with the rotation axis and localize into opposite hemispheres.

Despite this progress, several key issues remain open. First, the *physical origin* and analytic structure of the instability enhancement in rotating magnetic black holes remain unclear. Here we present an analytic derivation for an electrically charged massive scalar on a magnetically charged background and treat the Dirac-quantized parameter $q \equiv eP = N/2$ as a free parameter [31]. We show that the magnetic charge effectively reduces the centrifugal barrier via $\ell(\ell+1)/r^2 \rightarrow [\ell(\ell+1) - q^2]/r^2 \equiv \ell_q(\ell_q+1)/r^2$, which implies the scaling $\omega_I \propto \alpha^{4\ell_q+5}$ with $\alpha \equiv \mu M$ and explains the large growth-rate enhancement relative to Kerr.

Second, GW emission from hemispherically localized monopole-harmonic clouds has not been computed systematically. We identify the dominant bound states as the north/south monopole-harmonic modes $Y_{qq\pm q}^{\pm}$ [36] and compute the GW power from scalar self-annihilation

in a flat-spacetime approximation. For $\ell = q$ and $m = \pm q$ we find $P_{\text{GW}}^\pm \propto (E_c/M)^2 \alpha^{4\ell_q+8}$, together with a helicity selection rule in which the north (south) cloud radiates dominantly into $(\tilde{\ell}, \tilde{m}) = (2q, +2q)$ [$(2q, -2q)$].

Third, the enhanced growth motivates a self-consistent treatment of backreaction and GW depletion [37–40]. We therefore integrate the coupled BH–cloud evolution and translate the modified growth history and helicity-selective emission into observable continuous-wave waveforms and polarization signatures.

Finally, these effects translate into observables: a rapidly spinning *post-merger* remnant from a binary-BH merger provides the high spin needed for superradiance, and the monopole-induced enhancement can reduce the cloud build-up time from the neutral Kerr scale (years-to-centuries, depending on α) to days-to-weeks (or \sim year) in the magnetic case, bringing the onset of monochromatic GWs into the same observing window. Moreover, the coherent superposition of the $\tilde{m} = \pm 2q$ sectors yields near-circular polarization; future measurements of the GW ellipticity [41–44] can distinguish the magnetic case from Kerr and provide a source-based route to circular polarization within parity-even general relativity.

This work provides an analytic explanation for the magnetic-BH enhancement of superradiance and identifies distinctive GW power and polarization signatures that can serve as smoking-gun targets in future searches.

Setup and monopole-harmonic clouds— We consider a rotating black hole of mass M and spin $a = J/M$ that carries a magnetic charge P after capturing magnetic monopoles [45–47]. An electrically charged massive scalar Ψ with mass μ and charge e obeys the covariant Klein–Gordon equation

$$(\nabla^\rho - ieA^\rho)(\nabla_\rho - ieA_\rho)\Psi = \mu^2\Psi, \quad (1)$$

with a Dirac-type potential $A_\phi = -P \cos \theta$ and Dirac quantization [48]

$$q \equiv eP = \frac{N}{2}, \quad N \in \mathbb{Z}_{\geq 0}. \quad (2)$$

Separability with $\psi = e^{-i\omega t + im\phi} S(\theta)R(r)$ yields monopole harmonics $Y_{q\ell m}(\theta, \phi)$ in the ultralight limit [31, 36]. Moreover, the north-south monopole modes $Y_{qq\pm q}^\pm$ are the most superradiant unstable modes, which take the form

$$Y_{qq\pm q}^\pm = A_{\pm q} (1 \pm \cos \theta)^q e^{\pm iq\phi}, \quad (3)$$

with $A_{\pm q} = \sqrt{(2q+1)/(4\pi)}$. Here $Y_{qq\pm q}^\pm$ denote the monopole harmonics on the north/south patches. The apparent phase singularity $e^{\pm iq\phi}$ at the poles is a gauge artifact and can be removed by an intermediate gauge choice [36], so the harmonics are regular on the z axis ($\cos \theta = \pm 1$) and behave as

$$Y_{qq\pm q}^\pm \sim (1 \pm \cos \theta)^q. \quad (4)$$

As a result, the maximally superradiant modes are localized toward the rotation axis and suppressed near the equator, yielding a characteristic north–south two-lobe cloud profile that is symmetric under $z \rightarrow -z$. (see Fig. S1 in Supplemental Material (SM), Sec. II.c for further details)

Result I: Analytic origin of the superradiance rate enhancement in the presence of a magnetic monopole— In the far region ($r \gg M$) the radial equation reduces to

$$\frac{d^2(rR)}{dr^2} + \left[\omega^2 - \mu^2 \left(1 - \frac{2M}{r} \right) - \frac{\ell(\ell+1) - q^2}{r^2} \right] (rR) = 0. \quad (5)$$

Thus the centrifugal barrier is weakened by the monopole charge. We define the reduced orbital index ℓ_q via

$$\ell(\ell+1) - q^2 \equiv \ell_q(\ell_q+1), \quad \ell_q = \sqrt{\left(\ell + \frac{1}{2} \right)^2 - q^2} - \frac{1}{2}, \quad (6)$$

which is precisely the Wu–Yang structure for charged motion around a monopole [31]. A smaller ℓ_q deepens the effective potential well and increases the number of superradiant amplification cycles (Fig. S2).

Matched asymptotics in the overlap region (derivation in SM, Sec. III.b) give the imaginary part of the bound-state frequency,

$$\omega_I = \frac{\delta\nu_I}{M} \left(\frac{\alpha}{n_r + \ell_q + 1} \right)^3 \left[1 - \left(\frac{\alpha}{n_r + \ell_q + 1} \right)^2 \right]^{-1/2}, \quad (7)$$

with $\alpha \equiv \mu M$ and $\delta\nu$ determined by Gamma-function matching (see Eq. (S39) in SM, Sec. III.a). In the small-coupling limit, the scaling is

$$\omega_I \propto \alpha^{4\ell_q+5}, \quad (8)$$

to be contrasted with the Kerr scaling $\omega_I^{(\text{Kerr})} \propto \alpha^{4\ell+5}$. Since $\ell_q < \ell$ for $q \neq 0$, the exponent is reduced and the growth can be enhanced by orders of magnitude. For the dominant magnetic mode $(\ell, m) = (q, q)$ with $N = 3$ ($q = 3/2$), $\ell_q \simeq 0.82$, implying $\omega_I/\omega_{I(\text{Kerr})} \sim \mathcal{O}(10^2)$ near the peak (for the BH spin $a/M = 0.9$, see Fig. S3 in SM, Sec. II); this agrees at the order-of-magnitude level with the numerical results of [36] and with our analytic curves in Fig. S3.

Result II: Power enhancement and opposite-helicity emission from north/south clouds— The cloud emits nearly monochromatic GWs through scalar self-annihilation at $\tilde{\omega} \simeq 2\omega \simeq 2\mu$. Working in the flat-spacetime approximation for the sourced wave equation [49] (see SM, Sec. III), we find that monopole-harmonic selection rules fix the dominant radiative modes as

$$(\tilde{\ell}, \tilde{m}) = (2q, \pm 2q) \quad \text{for} \quad (\ell, m) = (q, \pm q), \quad (9)$$

corresponding to opposite-helicity GW emission from the north/south clouds (Fig. 1). Having fixed the dominant radiative channel, we obtain the GW power from the north/south clouds as

$$P_{\text{GW}}^{\pm} = C_{n\ell\ell_q}^{\pm} \left(\frac{E_c}{M} \right)^2 \alpha^{4\ell_q+8}. \quad (10)$$

Here E_c is the cloud energy and $C_{n\ell\ell_q}^{\pm}$ is a dimensionless coefficient determined by angular integrals and radial normalization (see SM, Sec. III III.c). This approximation captures the parametric α -scaling and the monopole-harmonic selection rules; curvature corrections only enter as order-unity factors. Eq. (10) should be contrasted with the Kerr result $P_{\text{GW}} \propto \alpha^{4\ell+10}$ [17]. The comparison between the neutral and charged cases is illustrated in Fig. 2. Physically, the enhancement arises from two effects: (i) the reduced ℓ_q weakens the small- r suppression of the bound-state wavefunction, increasing the coherent overlap with outgoing GW modes, and (ii) for monopole harmonics the Kerr angular identities that enforce leading-order cancellations no longer apply, removing an extra α^2 suppression.

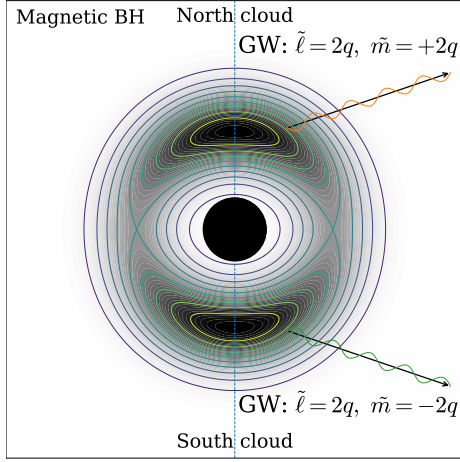


FIG. 1. Schematic illustration of helicity-polarized GW emission from hemispherically localized charged scalar clouds around a magnetically charged black hole. Angular-momentum selection rules imply that the north cloud in the $m = +q$ mode radiates GWs dominantly in $(\tilde{\ell}, \tilde{m}) = (2q, +2q)$, while the south cloud in the $m = -q$ mode radiates in $(\tilde{\ell}, \tilde{m}) = (2q, -2q)$, producing opposite GW helicities in the two hemispheres.

Result III: Novel GW signatures—rapid post-merger GW signal and (approximately) circular polarization—A rapid post-merger onset follows from the enhanced growth found in Result I: in the linear regime $M_c(t) \simeq M_{c,0} e^{2\omega_I t}$, so a useful idealized scale is the e-folding time $\tau_e \equiv (2\omega_I)^{-1}$, which using $\omega_I \sim \mu \alpha^{4\ell_q+5}$ implies

$$\frac{\tau_e}{M} \sim \alpha^{-(4\ell_q+6)}, \quad (11)$$

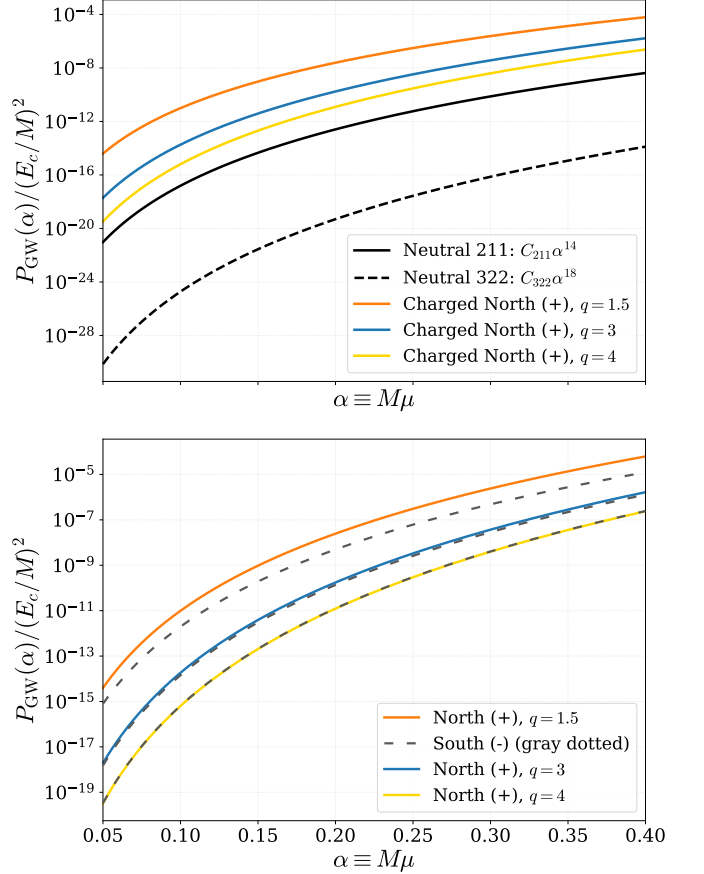


FIG. 2. Normalized GW power $P_{\text{GW}}(\alpha)/(E_c/M)^2$ for the dominant annihilation channel. Top: neutral Kerr (211, 322) versus charged clouds with $\ell = q$ for representative q . Bottom: north (+) versus south (-) branches; the convergence at larger q reflects the emergent north–south symmetry.

BH mass M	Magnetic $N = 3$		Neutral 211
	$M\omega_I \sim 10^{-6}$	$M\omega_{I(\text{Kerr})} \sim 2 \times 10^{-8}$	$M\omega_{I(\text{Kerr})} \sim 2 \times 10^{-8}$
$10 M_\odot$	2.47×10^1 s (0.41 min)	1.23×10^3 s (20.5 min)	
$10^4 M_\odot$	2.47×10^4 s (6.86 hr)	1.23×10^6 s (14.3 d)	
$10^6 M_\odot$	2.47×10^6 s (28.6 d)	1.23×10^8 s (3.9 yr)	

TABLE I. Using representative peak growth rates for a BH spin $a/M = 0.9$, we estimate the e-folding time $\tau_e = (2\omega_I)^{-1}$.

and a rough build-up time $t_{\text{grow}} \sim \tau_e \ln(M_c/M_{c,0})$; adopting peak growth rates $M\omega_I \sim 10^{-6}$ for the magnetic $N = 3$ mode and $M\omega_I \sim 2 \times 10^{-8}$ for the neutral 211 mode gives the illustrative estimates in Table I. However, τ_e is a naive estimate: it neglects GW back-reaction, which in Kerr typically satisfies $\tau_{\text{SR}} \ll \tau_{\text{GW}}$ during growth so the cloud approaches $m\Omega_H \simeq \omega_R$ before GW losses matter, whereas for magnetically charged BHs the power enhancement in Eq. (10) can make P_{GW} competitive already during growth and quench the instability, shifting the effective turn-on time; a self-consistent

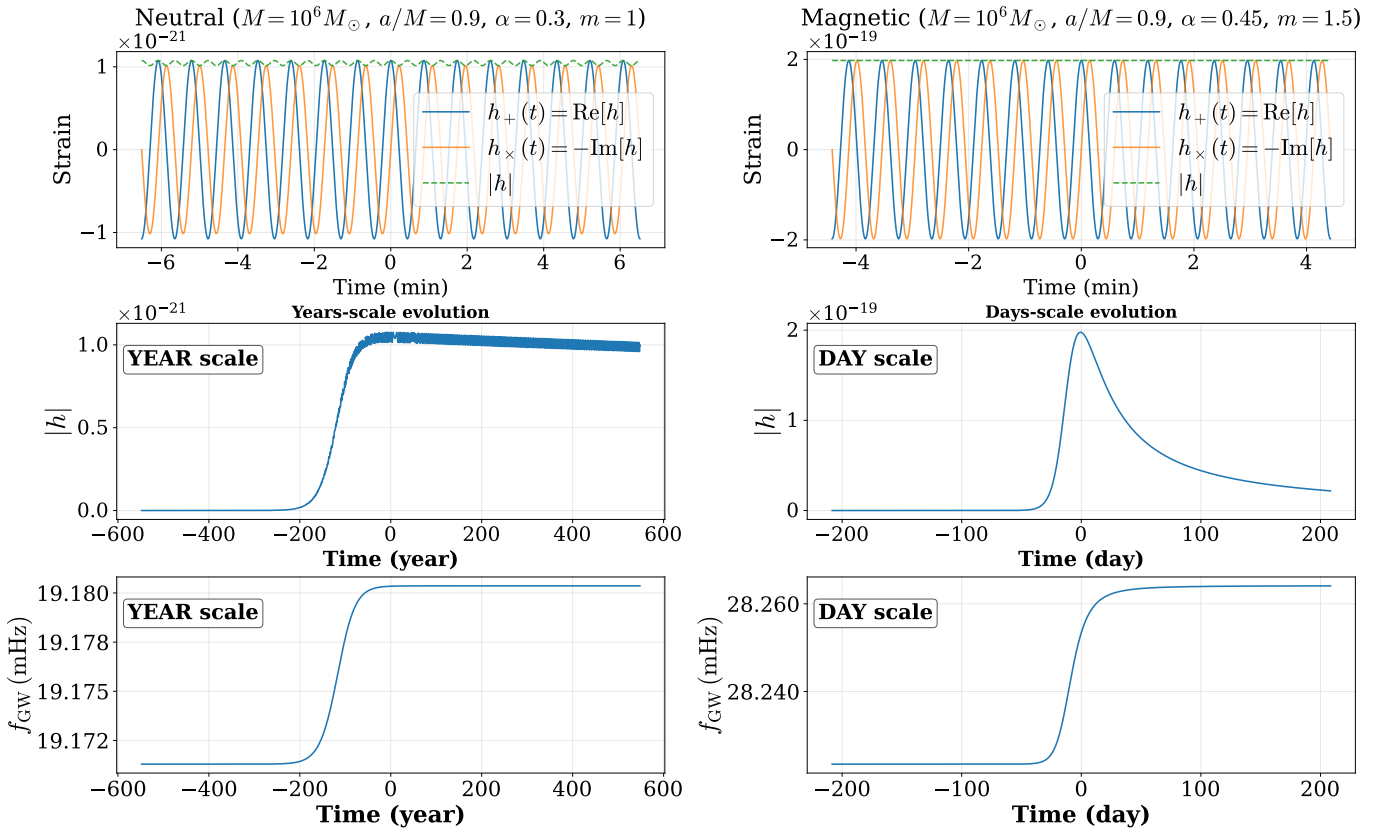


FIG. 3. GW strain from boson clouds around a rotating black hole with $M = 10^6 M_\odot$. Left: neutral case ($\alpha = 0.3$, $\mu \simeq 4.0 \times 10^{-17}$ eV), dominated by a single mode, yielding elliptical polarization and a beat in $|h|$. Right: magnetic case ($\alpha = 0.45$, $\mu \simeq 6.0 \times 10^{-17}$ eV), where north/south monopole-harmonic clouds populate opposite-helicity modes $(\tilde{\ell}, \tilde{m}) = (2q, \pm 2q)$; their superposition gives near-circular polarization with an almost constant envelope. Top: short-window waveforms $h_+ = \text{Re}[h]$, $h_x = -\text{Im}[h]$, and $|h|$. Middle/bottom: strain envelope and instantaneous frequency $f_{\text{GW}}(t)$ during cloud growth and depletion.

evolution therefore requires integrating [3, 37]

$$\frac{dM}{dt} = -2\omega_I M_c, \quad (12)$$

$$\frac{dJ}{dt} = -\frac{2m\omega_I}{\omega_R} M_c, \quad (13)$$

$$\frac{dM_c}{dt} = 2\omega_I M_c - P_{\text{GW}}, \quad (14)$$

with $P_{\text{GW}} = P_{\text{GW}}^+ + P_{\text{GW}}^-$. In the Kerr case, one typically has $\tau_{\text{SR}} \ll \tau_{\text{GW}}$ during the growth stage, so the cloud approaches the superradiant threshold $m\Omega_H \simeq \omega_R$ before GW losses become important. For magnetically charged BHs, the enhancement in Eq. (10) can make GW losses relevant already during the growth stage, so a self-consistent evolution requires integrating Eqs. (12)–(14) with $P_{\text{GW}} = P_{\text{GW}}^+ + P_{\text{GW}}^-$ (see Fig. S4) [3, 37]. The same integration fixes the spin evolution: $a(t)/M(t) = J(t)/M(t)^2$ decreases while the cloud extracts angular momentum, but GW quenching turns on earlier in the magnetic case, leaving only a modest $\Delta(a/M)$ in our fiducial examples (bottom panels of Fig. S4).

The resulting $M_c(t)$ sets the GW luminosity and strain envelope through $P_{\text{GW}}[M_c(t)]$, while the evolving BH pa-

rameters shift $\omega_R(t)$ and hence the instantaneous GW frequency $f_{\text{GW}}(t)$, as shown in Fig. 3. In the nonrelativistic regime the frequency is set primarily by the boson mass, $f_{\text{GW}} \simeq \tilde{\omega}/(2\pi) \simeq \mu/\pi$; Equivalently, at fixed coupling $\alpha = \mu M$ the frequency scales as $f_{\text{GW}} \propto 1/M$, so supermassive, intermediate-mass, and stellar-mass remnants populate the space-based [50–55], decihertz [56–58], and ground-based bands [59–63], respectively. For the examples in Fig. 3, one finds $f_{\text{GW}} \simeq 19.18$ mHz (neutral, $\mu \simeq 4.0 \times 10^{-17}$ eV) and $f_{\text{GW}} \simeq 28.26$ mHz (charged, $\mu \simeq 6.0 \times 10^{-17}$ eV), squarely in the LISA/TianQin/Taiji band [50, 51, 53, 54]. For a quasi-monochromatic signal, a coherent integration over duration T gives an order-of-magnitude matched-filter signal-to-noise ratio $\rho \sim h_0 \sqrt{T/S_n(f_{\text{GW}})}$ [50, 51]. In our fiducial examples the characteristic strain level is $h_0 \sim 10^{-21}$ (neutral) and can reach $h_0 \sim 10^{-19}$ (Magnetic), and Fig. 3 shows that the charged signal turns on and reaches this level within $\mathcal{O}(10)$ days. This motivates prompt post-merger follow-ups: a tens-of-days coherent baseline can already accumulate substantial signal-to-noise ratio, with longer baselines further improving sensitivity.

A second, independent observable is the polarization.

Writing the complex strain $h \equiv h_+ - ih_\times$ as

$$h(t, \theta, \phi) = \frac{1}{r} \sum_{\ell, m} h_{\ell m}(t) {}_{-2}Y_{\ell m}(\theta, \phi), \quad (15)$$

we emphasize a key reconstruction difference between Kerr and magnetic cases. For a neutral Kerr BH with a single superradiant cloud, the GW is dominated by one positive-frequency mode, typically $(\tilde{\ell}, \tilde{m}) = (2\ell, 2\ell)$; the accompanying $-\tilde{m}$ contribution in the *real* waveform is not an independent opposite-helicity sector but is fixed by the conjugation condition relating (m, ω) to $(-m, -\omega)$, i.e. $h_{\tilde{\ell}, -\tilde{m}}$ is determined by $h_{\tilde{\ell}, \tilde{m}}^*$ [37, 64]. As a result, at a fixed sky location the two linear polarizations are generically not in the special circular limit, yielding an elliptically polarized signal and a residual $2\tilde{\omega}$ modulation (“breathing”) in the instantaneous magnitude $|h(t)| \equiv \sqrt{h_+^2(t) + h_\times^2(t)}$ (as shown in Fig. 3).

By contrast, for magnetically charged BHs monopole-harmonic selection rules populate two *independent* positive-frequency components emitted by the north/south clouds (as illustrated in Fig. 1), $(\tilde{\ell}, \tilde{m}) = (2q, \pm 2q)$. Keeping only these dominant modes,

$$h(t, \theta, \phi) \simeq \frac{e^{-i\tilde{\omega}t}}{r} \left[h_{2q, 2q} {}_{-2}Y_{2q, 2q} + h_{2q, -2q} {}_{-2}Y_{2q, -2q} \right], \quad (16)$$

with independent $h_{2q, \pm 2q} = |h_{2q, \pm 2q}| e^{i\delta_{\pm}}$. The instantaneous envelope then satisfies (see SM, Sec. IV IV.b)

$$\begin{aligned} |h(\theta, \phi)|^2 &= \frac{1}{r^2} \left[|h_{2q, 2q}|^2 {}_{-2}S_{2q, 2q}^2(\theta) \right. \\ &+ |h_{2q, -2q}|^2 {}_{-2}S_{2q, -2q}^2(\theta) \\ &+ 2|h_{2q, 2q}| |h_{2q, -2q}| {}_{-2}S_{2q, 2q}(\theta) {}_{-2}S_{2q, -2q}(\theta) \\ &\left. \cos(\delta_- - \delta_+ - 4q\phi) \right]. \end{aligned} \quad (17)$$

which is independent of the fast phase $\tilde{\omega}t$. Thus, in this dominant-mode approximation the polarization ellipse at fixed (θ, ϕ) has essentially time-independent semi-axes and undergoes an (approximately) rigid rotation rather than a $2\tilde{\omega}$ breathing (Fig. S5). Importantly, Fig. 2 shows $P_{\text{GW}}^+ \simeq P_{\text{GW}}^-$ over a broad range of q , indicating that both azimuthal sectors typically contribute appreciably to the reconstruction (and making the near-circular signature robust once subdominant modes are included).

To quantify polarization in a way directly tied to the presence/absence of breathing, we use the normalized Stokes parameter

$$\Pi_{\text{circ}} \equiv \frac{V}{I}, \quad I \equiv |h_+|^2 + |h_\times|^2, \quad V \equiv 2 \text{Im}(h_+ h_\times^*), \quad (18)$$

where $h_{+, \times}$ denote the complex amplitudes of the positive-frequency component at a fixed sky location

$(h_{+, \times}(t) = h_{+, \times} e^{-i\tilde{\omega}t})$. A short calculation (SM, App. IV IV.c) gives

$$|h(t)|^2 = \frac{I}{2} \left[1 + \sqrt{1 - \Pi_{\text{circ}}^2} \cos(2\tilde{\omega}t - \varphi) \right], \quad (19)$$

so the $2\tilde{\omega}$ breathing amplitude is controlled by $\sqrt{1 - \Pi_{\text{circ}}^2}$. Therefore $|\Pi_{\text{circ}}| = 1$ corresponds to (approximately) circular polarization (no breathing), whereas $0 \leq |\Pi_{\text{circ}}| < 1$ corresponds to elliptical polarization, with the linear limit at $|\Pi_{\text{circ}}| = 0$ (up to a convention-dependent sign of V) [41, 42].

Conclusion and discussion—We have shown that magnetic charge sourced by monopoles can qualitatively reshape charged-boson superradiance. Through the replacement $\ell(\ell + 1) \rightarrow \ell(\ell + 1) - q^2$ (encoded in ℓ_q), the centrifugal barrier is reduced and the bound states deepen, yielding a parametrically faster instability than in the neutral Kerr case and enabling cloud growth and a near-monochromatic continuous-wave signal on observationally relevant timescales (days–years). Monopole-harmonic selection rules further imply a distinctive polarization pattern: north/south clouds radiate dominantly into $(\tilde{\ell}, \tilde{m}) = (2q, \pm 2q)$ with opposite helicities, so their superposition can produce an approximately circularly polarized signal within parity-even general relativity. Together with the enhanced GW power relative to Kerr at comparable parameters, these features motivate targeted continuous-wave searches and prompt post-merger follow-up of rapidly spinning remnants. A practical caveat is the fate of the cloud’s gauge charge if the boson is electromagnetically charged, since ambient plasma could neutralize or screen the cloud and weaken charged-cloud imprints; nevertheless, in the supermassive-BH regime the cloud can form within $\mathcal{O}(10)$ days, plausibly faster than environmental neutralization, with dark $U(1)$ (or sufficiently feebly coupled) charges providing an additional long-lived possibility. In this window, the prompt emergence of a helicity-polarized, nearly circularly polarized continuous signal would offer a robust discriminator of magnetically charged remnants and provide a novel probe of magnetic monopoles by GW observation.

Acknowledgments—This work is supported by the National Natural Science Foundation of China (NNSFC) under Grant No.12475111, No.12205387, No. 12375084 and the Fundamental Research Funds for the Central Universities, Sun Yat-sen University.

* luozhh58@mail2.sysu.edu.cn

† Corresponding author. huangfp8@sysu.edu.cn

‡ zhangpm5@mail.sysu.edu.cn

[1] A. A. Starobinskii, Amplification of waves during reflection from a rotating “black hole”, Sov. Phys. JETP **37**, 28 (1973).

[2] T. J. M. Zouros and D. M. Eardley, INSTABILITIES OF MASSIVE SCALAR PERTURBATIONS OF A ROTATING BLACK HOLE, *Annals Phys.* **118**, 139 (1979).

[3] R. Brito, V. Cardoso, and P. Pani, Superradiance: New Frontiers in Black Hole Physics, *Lect. Notes Phys.* **906**, pp.1 (2015), arXiv:1501.06570 [gr-qc].

[4] V. Cardoso, O. J. C. Dias, J. P. S. Lemos, and S. Yoshida, The Black hole bomb and superradiant instabilities, *Phys. Rev. D* **70**, 044039 (2004), [Erratum: Phys. Rev. D 70, 049903 (2004)], arXiv:hep-th/0404096.

[5] S. Detweiler, Klein-gordon equation and rotating black holes, *Phys. Rev. D* **22**, 2323 (1980).

[6] S. R. Dolan, Instability of the massive Klein-Gordon field on the Kerr spacetime, *Phys. Rev. D* **76**, 084001 (2007), arXiv:0705.2880 [gr-qc].

[7] S. R. Dolan, Instability of the Proca field on Kerr spacetime, *Phys. Rev. D* **98**, 104006 (2018), arXiv:1806.01604 [gr-qc].

[8] W. E. East, Superradiant instability of massive vector fields around spinning black holes in the relativistic regime, *Phys. Rev. D* **96**, 024004 (2017), arXiv:1705.01544 [gr-qc].

[9] N. Xie and F. P. Huang, Imprints of ultralight axions on the gravitational wave and pulsar timing measurement, *Sci. China Phys. Mech. Astron.* **67**, 210411 (2024), arXiv:2207.11145 [hep-ph].

[10] S. Alexander and N. Yunes, Chern-Simons Modified General Relativity, *Phys. Rept.* **480**, 1 (2009), arXiv:0907.2562 [hep-th].

[11] J. M. Cornwall, Speculations on primordial magnetic helicity, *Phys. Rev. D* **56**, 6146 (1997), arXiv:hep-th/9704022.

[12] T. Kahnashvili, G. Gogoberidze, and B. Ratra, Polarized cosmological gravitational waves from primordial helical turbulence, *Phys. Rev. Lett.* **95**, 151301 (2005).

[13] A. Roper Pol, S. Mandal, A. Brandenburg, T. Kahnashvili, and A. Kosowsky, Numerical simulations of gravitational waves from early-universe turbulence, *Phys. Rev. D* **102**, 083512 (2020), arXiv:1903.08585 [astro-ph.CO].

[14] N. Seto and A. Taruya, Measuring a Parity Violation Signature in the Early Universe via Ground-based Laser Interferometers, *Phys. Rev. Lett.* **99**, 121101 (2007), arXiv:0707.0535 [astro-ph].

[15] T. Vachaspati, Estimate of the primordial magnetic field helicity, *Phys. Rev. Lett.* **87**, 251302 (2001), arXiv:astro-ph/0101261.

[16] A. Arvanitaki, M. Baryakhtar, and X. Huang, Discovering the QCD Axion with Black Holes and Gravitational Waves, *Phys. Rev. D* **91**, 084011 (2015), arXiv:1411.2263 [hep-ph].

[17] H. Yoshino and H. Kodama, Gravitational radiation from an axion cloud around a black hole: Superradiant phase, *PTEP* **2014**, 043E02 (2014), arXiv:1312.2326 [gr-qc].

[18] R. Brito, S. Ghosh, E. Barausse, E. Berti, V. Cardoso, I. Dvorkin, A. Klein, and P. Pani, Gravitational wave searches for ultralight bosons with LIGO and LISA, *Phys. Rev. D* **96**, 064050 (2017), arXiv:1706.06311 [gr-qc].

[19] M. Isi, L. Sun, R. Brito, and A. Melatos, Directed searches for gravitational waves from ultralight bosons, *Phys. Rev. D* **99**, 084042 (2019), [Erratum: Phys. Rev. D 102, 049901 (2020)], arXiv:1810.03812 [gr-qc].

[20] J. Yang and F. P. Huang, Gravitational waves from axions annihilation through quantum field theory, *Phys. Rev. D* **108**, 103002 (2023), arXiv:2306.12375 [hep-ph].

[21] R. Abbott, others (LIGO Scientific Collaboration, V. Collaboration, and K. Collaboration), All-sky search for gravitational wave emission from scalar boson clouds around spinning black holes in ligo o3 data, *Phys. Rev. D* **105**, 102001 (2022), arXiv:2111.15507 [gr-qc].

[22] N. Siemonsen, T. May, and W. E. East, Modeling the black hole superradiance gravitational waveform, *Phys. Rev. D* **107**, 104003 (2023).

[23] D. Baumann, H. S. Chia, J. Stout, and L. ter Haar, The Spectra of Gravitational Atoms, *JCAP* **12**, 006, arXiv:1908.10370 [gr-qc].

[24] D. Baumann, H. S. Chia, R. A. Porto, and J. Stout, Gravitational Collider Physics, *Phys. Rev. D* **101**, 083019 (2020), arXiv:1912.04932 [gr-qc].

[25] N. Xie and F. P. Huang, Self-interaction effects on the Kerr black hole superradiance and their observational implications, *Phys. Rev. D* **112**, 055028 (2025), arXiv:2503.10347 [hep-ph].

[26] J. Yang, N. Xie, and F. P. Huang, Implication of nano-Hertz stochastic gravitational wave background on ultra-light axion particles, *JCAP* **11**, 045, arXiv:2306.17113 [hep-ph].

[27] P. Langacker and S.-Y. Pi, Magnetic monopoles in grand unified theories, *Phys. Rev. Lett.* **45**, 1 (1980).

[28] G. 't Hooft, Magnetic Monopoles in Unified Gauge Theories, *Nucl. Phys. B* **79**, 276 (1974).

[29] A. M. Polyakov, Particle Spectrum in Quantum Field Theory, *JETP Lett.* **20**, 194 (1974).

[30] P. Langacker and S.-Y. Pi, Magnetic Monopoles in Grand Unified Theories, *Phys. Rev. Lett.* **45**, 1 (1980).

[31] T. T. Wu and C. N. Yang, Dirac Monopole Without Strings: Monopole Harmonics, *Nucl. Phys. B* **107**, 365 (1976).

[32] T. T. Wu and C. N. Yang, Concept of nonintegrable phase factors and global formulation of gauge fields, *Phys. Rev. D* **12**, 3845 (1975).

[33] G. Giacomelli and L. Patrizii, Magnetic monopole searches, *ICTP Lect. Notes Ser.* **14**, 121 (2003), arXiv:hep-ex/0302011.

[34] G. Aad *et al.* (ATLAS), Search for magnetic monopoles and stable particles with high electric charges in $\sqrt{s} = 13$ TeV pp collisions with the ATLAS detector, *JHEP* **11**, 112, arXiv:2308.04835 [hep-ex].

[35] K. Nakamura *et al.* (Particle Data Group), Review of particle physics, *J. Phys. G* **37**, 075021 (2010).

[36] D. Perniguel, M. de Amicis, R. Brito, and R. Panosso Macedo, Superradiant Instability of Magnetic Black Holes, *Phys. Rev. D* **110**, 104001 (2024), arXiv:2402.05178 [gr-qc].

[37] N. Siemonsen, T. May, and W. E. East, Modeling the black hole superradiance gravitational waveform, *Phys. Rev. D* **107**, 104003 (2023), arXiv:2211.03845 [gr-qc].

[38] Y.-d. Guo, S.-s. Bao, and H. Zhang, Subdominant modes of the scalar superradiant instability and gravitational wave beats, *Phys. Rev. D* **107**, 075009 (2023), arXiv:2212.07186 [gr-qc].

[39] R. Brito, V. Cardoso, and P. Pani, Black holes as particle detectors: evolution of superradiant instabilities, *Class. Quant. Grav.* **32**, 134001 (2015), arXiv:1411.0686 [gr-qc].

[40] W. E. East, Massive Boson Superradiant Instability of Black Holes: Nonlinear Growth, Saturation, and Gravitational Radiation, *Phys. Rev. Lett.* **121**, 131104 (2018), arXiv:1807.00043 [gr-qc].

[41] N. Seto and A. Taruya, Polarization analysis of gravitational-wave backgrounds from the correlation signals of ground-based interferometers: Measuring a circular-polarization mode, *Phys. Rev. D* **77**, 103001 (2008), [arXiv:0801.4185 \[astro-ph\]](#).

[42] N. Seto, Prospects for direct detection of circular polarization of gravitational-wave background, *Phys. Rev. Lett.* **97**, 151101 (2006), [arXiv:astro-ph/0609504](#).

[43] J. Chen, C. Liu, and Y.-L. Zhang, Circularly polarized gravitational wave background search with a network of space-borne triangular detectors, *JCAP* **05**, 050, [arXiv:2410.18916 \[gr-qc\]](#).

[44] H. Su, B. Xu, J. Chen, C. Liu, and Y.-L. Zhang, Detectability of the chiral gravitational wave background from audible axions with the LISA-Taiji network, *Commun. Theor. Phys.* **77**, 115403 (2025), [arXiv:2503.20778 \[astro-ph.CO\]](#).

[45] R. Moulard and D. Tong, On the Hilbert Space of Dyons, *Phys. Rev. D* **110**, 085014 (2024), [arXiv:2401.01924 \[hep-th\]](#).

[46] Y. S. Myung, Superradiant instability of dyonic Reissner–Nordström black holes, *Eur. Phys. J. C* **82**, 933 (2022), [arXiv:2206.01390 \[gr-qc\]](#).

[47] Y.-F. Zou, J.-H. Xu, Z.-F. Mai, and J.-H. Huang, Dyonic Reissner–Nordstrom black holes and superradiant stability, *Eur. Phys. J. C* **81**, 855 (2021), [arXiv:2105.14702 \[gr-qc\]](#).

[48] P. A. M. Dirac, Quantised singularities in the electromagnetic field, *Proc. Roy. Soc. Lond. A* **133**, 60 (1931).

[49] A. Arvanitaki and S. Dubovsky, Exploring the string axisiverse with precision black hole physics, *Phys. Rev. D* **83**, 044026 (2011).

[50] P. Amaro-Seoane *et al.* (LISA), Laser interferometer space antenna (2017), [arXiv:1702.00786 \[astro-ph.IM\]](#).

[51] T. Robson, N. J. Cornish, and C. Liu, The construction and use of LISA sensitivity curves, *Classical and Quantum Gravity* **36**, 105011 (2019), [arXiv:1803.01944 \[astro-ph.HE\]](#).

[52] C. Cutler, Angular resolution of the LISA gravitational wave detector, *Physical Review D* **57**, 7089 (1998).

[53] J. Luo *et al.*, Tianqin: a space-borne gravitational wave detector, *Classical and Quantum Gravity* **33**, 035010 (2016), [arXiv:1512.02076 \[astro-ph.IM\]](#).

[54] W.-R. Hu and Y.-L. Wu, The Taiji program in space for gravitational wave physics and the nature of gravity, *National Science Review* **4**, 685 (2017).

[55] W.-H. Ruan, Z.-K. Guo, R.-G. Cai, and Y.-Z. Zhang, Taiji program: Gravitational-wave sources (2020), [arXiv:1807.09495 \[gr-qc\]](#).

[56] N. Seto, S. Kawamura, and T. Nakamura, Possibility of direct measurement of the acceleration of the universe using 0.1-Hz band laser interferometer gravitational wave antenna in space, *Phys. Rev. Lett.* **87**, 221103 (2001), [arXiv:astro-ph/0108011](#).

[57] K. Yagi and N. Seto, Detector configuration of DECIGO/BBO and identification of cosmological neutron-star binaries, *Phys. Rev. D* **83**, 044011 (2011), [Erratum: *Phys. Rev. D* 95, 109901 (2017)], [arXiv:1101.3940 \[astro-ph.CO\]](#).

[58] J. Crowder and N. J. Cornish, Beyond LISA: Exploring future gravitational wave missions, *Phys. Rev. D* **72**, 083005 (2005), [arXiv:gr-qc/0506015](#).

[59] B. P. Abbott *et al.*, Sensitivity of the Advanced LIGO detectors at the beginning of gravitational wave astronomy, *Phys. Rev. D* **93**, 112004 (2016), [Addendum: *Phys. Rev. D* 97, 059901 (2018)], [arXiv:1604.00439 \[astro-ph.IM\]](#).

[60] F. Acernese *et al.* (VIRGO), Advanced Virgo: a second-generation interferometric gravitational wave detector, *Class. Quant. Grav.* **32**, 024001 (2015), [arXiv:1408.3978 \[gr-qc\]](#).

[61] T. Akutsu *et al.* (KAGRA), Overview of KAGRA: Detector design and construction history, *PTEP* **2021**, 05A101 (2021), [arXiv:2005.05574 \[physics.ins-det\]](#).

[62] D. Reitze *et al.*, Cosmic Explorer: The U.S. Contribution to Gravitational-Wave Astronomy beyond LIGO, *Bull. Am. Astron. Soc.* **51**, 035 (2019), [arXiv:1907.04833 \[astro-ph.IM\]](#).

[63] A. Abac *et al.* (ET), The science of the einstein telescope (2025), [arXiv:2503.12263 \[gr-qc\]](#).

[64] S. Ghosh, E. Berti, R. Brito, and M. Richartz, Follow-up signals from superradiant instabilities of black hole merger remnants, *Phys. Rev. D* **99**, 104030 (2019), [arXiv:1812.01620 \[gr-qc\]](#).

[65] T. M. MacRobert, Higher transcendental functions, *Nature* **175**, 317 (1955).

[66] E. W. Leaver, An Analytic representation for the quasi normal modes of Kerr black holes, *Proc. Roy. Soc. Lond. A* **402**, 285 (1985).

[67] D. J. Griffiths and D. F. Schroeter, *Introduction to Quantum Mechanics*, 3rd ed. (Cambridge University Press, 2018).

[68] E. T. Whittaker and G. N. Watson, *A Course of Modern Analysis*, 4th ed., Cambridge Mathematical Library (Cambridge University Press, 1996).

[69] G. Ficarra, P. Pani, and H. Witek, Impact of multiple modes on the black-hole superradiant instability, *Phys. Rev. D* **99**, 104019 (2019).

[70] Y.-d. Guo, S.-s. Bao, and H. Zhang, Subdominant modes of the scalar superradiant instability and gravitational wave beats, *Phys. Rev. D* **107**, 075009 (2023).

[71] M. Baryakhtar, M. Galanis, R. Lasenby, and O. Simon, Black hole superradiance of self-interacting scalar fields, *Phys. Rev. D* **103**, 095019 (2021).

[72] C. W. Misner, K. S. Thorne, and J. A. Wheeler, *Gravitation* (W. H. Freeman, 1973).

[73] E. Newman and R. Penrose, An Approach to gravitational radiation by a method of spin coefficients, *J. Math. Phys.* **3**, 566 (1962).

[74] S. A. Teukolsky, Perturbations of a rotating black hole. 1. Fundamental equations for gravitational electromagnetic and neutrino field perturbations, *Astrophys. J.* **185**, 635 (1973).

[75] P. L. Chrzanowski, Vector potential and metric perturbations of a rotating black hole, *Phys. Rev. D* **11**, 2042 (1975).

[76] T. Regge and J. A. Wheeler, Stability of a schwarzschild singularity, *Phys. Rev.* **108**, 1063 (1957).

[77] F. J. Zerilli, Gravitational field of a particle falling in a schwarzschild geometry analyzed in tensor harmonics, *Phys. Rev. D* **2**, 2141 (1970).

[78] E. Wigner, über nicht kombinierende terme in der neueren quantentheorie. ii. teil, *Zeitschrift für Physik* **40**, 883 (1927).

[79] M. Zaldarriaga and U. c. v. Seljak, All-sky analysis of polarization in the microwave background, *Phys. Rev. D* **55**, 1830 (1997).

Supplemental Material

Zhong-Hao Luo, Fa Peng Huang, Pengming Zhang, and Chen Zhang

CONTENTS

I. Magnetic Kerr background and monopole-harmonic clouds	1
I.a. Metric, horizons, and electromagnetic potential	1
I.b. Angular separation equation of the charged Klein–Gordon equation	2
I.c. Monopole harmonics and the north/south cloud morphology	2
I.d. Why the centrifugal barrier is reduced: an intuitive angular-momentum picture	3
II. Superradiant growth rate: scaling estimate and matched-asymptotic derivation	4
II.a. Scaling estimate from the reduced angular barrier $\ell \rightarrow \ell_q$	4
II.b. Matched-asymptotic derivation of the growth rate	7
Far region: hydrogenic solution and the reduced orbital index ℓ_q	7
Near region: hypergeometric solution and horizon boundary condition	8
Overlap matching and analytic expression for $\delta\nu$	10
III. gravitational-wave power from electrically charged scalar clouds	11
III.a. General setup: GW equation and homogeneous-mode expansion	12
III.b. Outgoing modes in the Newman-Penrose formalism	12
III.c. GW emission in the flat-spacetime approximation	14
North/south selection rules and helicity-polarized emission	15
Enhancement scaling with the reduced orbital index ℓ_q of the GW power	17
III.d. Technical ingredients	20
Local inner product $u_{\mu\nu}^* T^{\mu\nu}$ in the Chrzanowski formalism	20
Angular source integrals I_1, I_2, I_3 and the $(\tilde{\ell}, \tilde{m}) = (2q, \pm 2q)$ selection rule	21
Radial source integral of the function $\mathcal{F}_{\tilde{\ell}\tilde{m}}(\tilde{r})$	24
IV. Mass evolution and gravitational-wave waveform of electrically charged scalar clouds	25
IV.a. Coupled BH-cloud mass and spin evolution for charged scalar clouds	25
IV.b. Waveform construction: circularly polarized instantaneous strain	27
IV.c. Breathing amplitude and the Stokes parameter	30

I. MAGNETIC KERR BACKGROUND AND MONOPOLE-HARMONIC CLOUDS

This Supplemental Material collects technical steps that underlie the results quoted in the main text. We work in units $G = c = \hbar = 1$ and follow the sign conventions of the main paper.

I.a. Metric, horizons, and electromagnetic potential

A rotating *magnetically* charged black hole is described by the Kerr–Newman family with vanishing electric charge and magnetic charge P . In Boyer–Lindquist coordinates (t, r, θ, ϕ) the metric is

$$ds^2 = - \left(1 - \frac{2Mr - P^2}{\Sigma} \right) dt^2 + \frac{\Sigma}{\Delta} dr^2 + \Sigma d\theta^2 + \left[(r^2 + a^2) + \frac{(2Mr - P^2)a^2 \sin^2 \theta}{\Sigma} \right] \sin^2 \theta d\phi^2 - \frac{2a(2Mr - P^2) \sin^2 \theta}{\Sigma} dt d\phi, \quad (\text{S1})$$

where

$$\Sigma \equiv r^2 + a^2 \cos^2 \theta, \quad \Delta \equiv r^2 - 2Mr + a^2 + P^2 = (r - r_+)(r - r_-). \quad (\text{S2})$$

The outer/inner horizons are

$$r_{\pm} = M \pm \sqrt{M^2 - a^2 - P^2}, \quad (\text{S3})$$

so regular horizons require $a^2 + P^2 \leq M^2$. The horizon angular velocity and surface gravity are

$$\Omega_H = \frac{a}{r_+^2 + a^2}, \quad \kappa = \frac{r_+ - r_-}{2(r_+^2 + a^2)}. \quad (\text{S4})$$

A magnetic monopole cannot be described globally by a single smooth vector potential; one uses Wu–Yang north/south patches [31]. A convenient choice is the Dirac form of the gauge potential of magnetic charges $A_\rho = (0, 0, 0, -P \cos \theta)$ [36, 45, 48]. While the Dirac gauge potential needs to introduce the Dirac quantization

$$q \equiv eP = \frac{N}{2} \geq 0, \quad N \in \mathbb{Z}. \quad (\text{S5})$$

with $N = 0, 1, 2, \dots$, this condition eliminates the global singularity. Notably, we define the magnetic parameter $q \geq 0$ to be non-negative, which differs by a sign from the convention used in [36].

I.b. Angular separation equation of the charged Klein–Gordon equation

The electrically charged massive scalar perturbation Ψ in the magnetic BH background can be described by the covariant Klein–Gordon equation [36, 46, 47]

$$[(\nabla_\mu - ieA_\mu)(\nabla^\mu - ieA^\mu) - \mu^2] \Psi = 0. \quad (\text{S6})$$

Because the background is stationary and axisymmetric, we take the ansatz

$$\Psi(t, r, \theta, \phi) = e^{-i\omega t} R(r) S(\theta) e^{im\phi}, \quad (\text{S7})$$

with (ω, m) conserved quantum numbers. Separation leads to an angular equation of the angular function $S(\theta)$

$$\frac{1}{\sin \theta} \frac{d}{d\theta} \left(\sin \theta \frac{dS}{d\theta} \right) + \left[a^2(\omega^2 - \mu^2) \cos^2 \theta - \frac{(m + q \cos \theta)^2}{\sin^2 \theta} - 2a\omega q \cos \theta - q^2 + \Lambda_{q\ell m} \right] S(\theta) = 0. \quad (\text{S8})$$

Here, $\Lambda_{q\ell m}$ represents the separation constant. For bound states of scalar fields around magnetic BHs, the frequency–mass relationship implies $\omega \approx \mu$. In the ultralight limit $\mu M \ll 1$ (and hence $\omega M \ll 1$), the above angular equation Eq. (S8) reduces to

$$-\frac{1}{\sin \theta} \frac{d}{d\theta} \left(\sin \theta \frac{dS(\theta)}{d\theta} \right) + \frac{(m + q \cos \theta)^2}{\sin^2 \theta} S(\theta) = (\Lambda_{q\ell m} - q^2) S(\theta), \quad (\text{S9})$$

which is identical to Eq. (22) in [31], except for the form of separation constant $\Lambda_{q\ell m} \approx \ell(\ell + 1) + O(a\omega)$. The approximate expansion of $\Lambda_{q\ell m}$ stems from neglecting the terms $a^2(\omega^2 - \mu^2) \cos^2 \theta$ and $2a\omega q \cos \theta$ in Eq. (S8). Hence, the separation constant $\Lambda_{q\ell m}$ is approximated as $\Lambda_{q\ell m} \simeq \ell(\ell + 1)$. More importantly, the spheroidal harmonics $S(\theta) e^{im\phi}$ reduce to the monopole harmonics $Y_{q\ell m}(\theta, \phi)$ [31, 36, 47], rather than the usual spherical harmonics $Y_{\ell m}(\theta, \phi)$.

I.c. Monopole harmonics and the north/south cloud morphology

A standard explicit representation of monopole harmonics is [31]

$$Y_{q\ell m} = S(\theta) e^{im\phi} = N_{q\ell m} (1 - \cos \theta)^{\alpha_J/2} (1 + \cos \theta)^{\beta_J/2} P_{\zeta}^{\alpha_J, \beta_J}(\cos \theta) e^{im\phi}, \quad (\text{S10})$$

$$\ell = |q|, |q| + 1, \dots, \quad m = -\ell, -\ell + 1, \dots, \ell,$$

where $\alpha_J = -q - m$, $\beta_J = q - m$, and $\zeta = \ell + m$. The quantity $N_{q\ell m}$ is normalization constant, and $P_{\zeta}^{\alpha_J, \beta_J}(\cos \theta)$ represents the Jacobi polynomial [65]. The mode that maximizes the superradiant growth rate is the *lowest* allowed ℓ

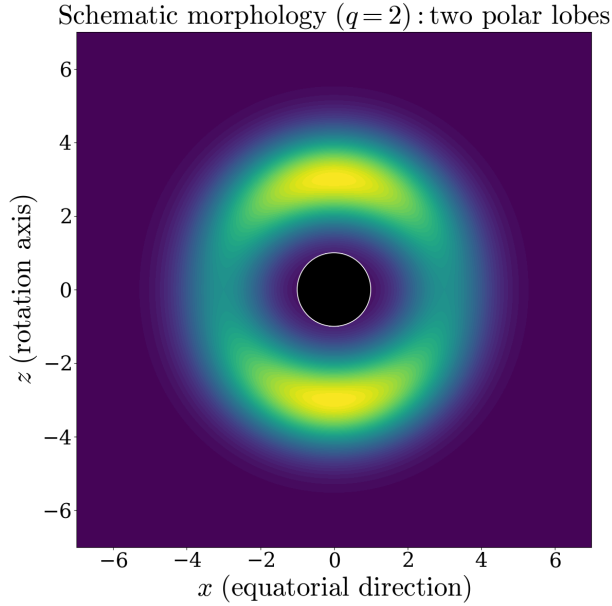


FIG. S1. Schematic meridional (x - z) slice of the cloud profile built from the maximally unstable monopole-harmonic modes Y_{qqq}^+ (north) and $Y_{qq,-q}^-$ (south).

for a given q , namely $\ell = q$, with $|m| = q$. Moreover, the north-south monopole modes $Y_{qq\pm q}^\pm$ are the most superradiant unstable modes, which take the form

$$Y_{qqq}^+ = A_q e^{iq\phi} \left(\cos \frac{\theta}{2} \right)^{2q}, \quad Y_{qq,-q}^- = A_q e^{-iq\phi} \left(\sin \frac{\theta}{2} \right)^{2q}, \quad (\text{S11})$$

with $N_{qqq} \equiv A_q = N_{qq,-q} \equiv A_{-q} = \sqrt{(2q+1)/(4\pi)}$. Here $Y_{qq\pm q}^\pm$ represent the monopole harmonics in the north and south hemispheres respectively. It is noteworthy that the phase singularity $e^{\pm iq\phi}$ at the north and south poles can be removed by the intermediate gauge [36]. Consequently, the monopole harmonics are regular at both poles of the z -axis $\cos \theta = \pm 1$

$$Y_{qqq}^+ \propto (1 + \cos \theta)^q \quad (\theta \simeq 0), \quad Y_{qq,-q}^- \propto (1 - \cos \theta)^q \quad (\theta \simeq \pi), \quad (\text{S12})$$

so the scalar density is enhanced around the rotation axis and suppressed near the equator, yielding the characteristic north-south two-lobe morphology (Fig. S1).

I.d. Why the centrifugal barrier is reduced: an intuitive angular-momentum picture

The key analytic effect of the monopole is the weakening of the centrifugal barrier in the far region, which can be understood directly from gauge-covariant angular momentum. For a charged particle in a monopole background, the canonical momentum is $\boldsymbol{\pi} = \mathbf{p} - e\mathbf{A}$ and the gauge-invariant total angular momentum is [31]

$$\mathbf{J} = \mathbf{r} \times \boldsymbol{\pi} - q \hat{\mathbf{r}}, \quad (\text{S13})$$

where $\hat{\mathbf{r}}$ is the radial unit vector. Squaring gives

$$J^2 = (\mathbf{r} \times \boldsymbol{\pi})^2 + q^2, \quad \Rightarrow \quad (\mathbf{r} \times \boldsymbol{\pi})^2 = J^2 - q^2. \quad (\text{S14})$$

Upon separation one has $J^2 \rightarrow \ell(\ell+1)$, so the centrifugal term becomes

$$\frac{\ell(\ell+1)}{r^2} \rightarrow \frac{\ell(\ell+1) - q^2}{r^2} = \frac{\ell_q(\ell_q+1)}{r^2}, \quad (\text{S15})$$

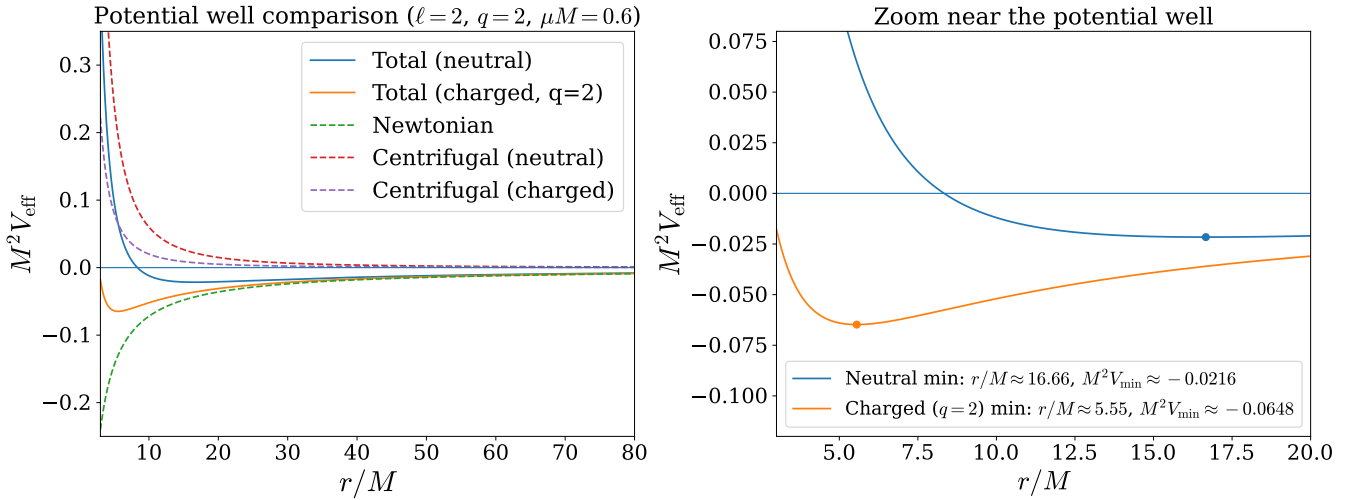


FIG. S2. Comparison of the far-region effective potential for Kerr ($q = 0$) and magnetic Kerr ($q \neq 0$). The reduced barrier for $q \neq 0$ deepens the potential well and increases the number of superradiant ‘‘bounces’’.

which defines the reduced effective index ℓ_q . Equivalently,

$$\ell_q = \sqrt{\left(\ell + \frac{1}{2}\right)^2 - q^2} - \frac{1}{2}, \quad (\text{S16})$$

as quoted in Eq. (6) of the main text. Since $\ell_q < \ell$ for $q \neq 0$, the effective potential barrier is reduced, leading to a deeper bound-state well and (as quantified in see SM, Sec. II) a much larger superradiant growth rate.

II. SUPERRADIANT GROWTH RATE: SCALING ESTIMATE AND MATCHED-ASYMPTOTIC DERIVATION

II.a. Scaling estimate from the reduced angular barrier $\ell \rightarrow \ell_q$

The radial separation equation of Eq. (S6) determines the growth rate of charged scalar clouds

$$\frac{d}{dr} \left(\Delta(r) \frac{d}{dr} R(r) \right) + \left[\frac{\left((r^2 + a^2) \omega - ma \right)^2}{\Delta(r)} - \mu^2 r^2 - \Lambda_{q\ell m} + q^2 + 2am\omega - a^2\omega^2 \right] R(r) = 0. \quad (\text{S17})$$

In [36], the numerical results of the growth rate have been computed via the Leaver method [6, 66], revealing that the superradiant instability of magnetic BHs can be up to two orders of magnitude faster than that of neutral Kerr BHs. Although this dramatic enhancement is robustly supported by numerical computations, the underlying physical mechanism remains unclear. We therefore aim to elucidate the physical mechanism by solving the radial equation analytically [1, 23], through matching the far-region and near-region solutions of Eq. (S17) in the overlap region.

In the far region ($r \gg M$ and $r \sim \ell/\omega$), we find that the radial equation reduces to

$$\frac{d^2(rR)}{dr^2} + \left[\omega^2 - \mu^2 \left(1 - \frac{2M}{r} \right) - \frac{\ell(\ell+1) - q^2}{r^2} \right] (rR) = 0, \quad (\text{S18})$$

where the centrifugal potential term $\frac{\ell(\ell+1) - q^2}{r^2}$ is weakened compared to the neutral case. This potential structure also appears in the case of a charged scalar field around a magnetic monopole given by Wu-Yang in Eq. (53) of [31]. Apart from the gravitational binding from the Newtonian potential $-\frac{2M\mu^2}{r}$, the charged scalar field is additionally bound by the magnetic charges of the BH. Qualitatively, this extra binding creates a deeper effective potential well around the magnetic BH as shown in Fig. S2. As a result, the bound state consequently undergoes more cycles of superradiant amplification, ultimately leading to an enhanced instability. Quantitatively, however, the precise growth rate requires matching the radial solutions across the overlap region.

After the calculation in Sec. III**b**, we find that, significantly, although the $\ell(\ell+1)$ term in the centrifugal potential is modified to $\ell(\ell+1) - q^2 \equiv \ell_q(\ell_q + 1)$ in Eq. (S18), the far-region radial solution can still be expressed in terms of confluent hypergeometric functions, simply by replacing the usual orbital quantum number ℓ with ℓ_q relative to the neutral scalar cloud case

$$R(r) = (2kr)^{\ell_q} e^{-kr} U(\ell_q + 1 - \nu, 2\ell_q + 2; 2kr), \quad (\text{S19})$$

where

$$\begin{aligned} \ell_q &\equiv \sqrt{(\ell + 1/2)^2 - q^2} - 1/2, \\ \ell(\ell + 1) &\rightarrow \ell(\ell + 1) - q^2 \equiv \ell_q(\ell_q + 1). \end{aligned} \quad (\text{S20})$$

Here $\nu \equiv M\mu^2/k$ with $k^2 \equiv \mu^2 - \omega^2$, and $U(\ell_q + 1 - \nu, 2\ell_q + 2; 2kr)$ is the confluent hypergeometric function. Analogous to the hydrogen atom [67], we define $\nu_0 \equiv n_r + \ell_q + 1 = n_r + \sqrt{(\ell + 1/2)^2 - q^2} + 1/2$. However, the presence of the horizon introduces a small complex correction $\nu = \nu_0 + \delta\nu$. Consequently, the solution in Eq. (S19) can be rewritten as

$$R(r) = (2kr)^{\ell_q} e^{-kr} U(-n_r - \delta\nu, 2\ell_q + 2; 2kr). \quad (\text{S21})$$

Using the asymptotic properties of confluent hypergeometric functions and Gamma functions in Eq. (S62) and Eq. (S63), the far-region solution can be expanded in the overlap region ($2kr \rightarrow 0$) as the centrifugal potential series

$$\begin{aligned} R(r) &= (2kr)^{\ell_q} e^{-kr} U(-n_r - \delta\nu, 2\ell_q + 2; 2kr) \\ &\simeq (-1)^{n_r} \frac{\Gamma(2\ell_q + n_r + 2)}{\Gamma(2\ell_q + 2)} (2kr)^{\ell_q} + (-1)^{n_r + 1} \Gamma(n_r + 1) \Gamma(2\ell_q + 1) \delta\nu (2kr)^{-\ell_q - 1}. \end{aligned} \quad (\text{S22})$$

Notably, the non-integer nature of ℓ_q precludes the use of the factorials as in [1] and necessitates the generalized Gamma function formalism.

In the near region, under the coordinate transformation $z \equiv \frac{r - r_+}{r_+ - r_-}$, the radial equation in Eq. (S23) can be approximated as

$$z(z+1) \frac{d}{dz} \left[z(z+1) \frac{dR}{dz} \right] + [p^2 - (\ell(\ell+1) - q^2)z(z+1)] R = 0, \quad (\text{S23})$$

where the sign of p determines whether superradiance is active. This parameter is expressed in terms of the BH's angular velocity $\Omega_H = \frac{a}{r_+^2 + a^2}$ and surface gravity $\kappa = \frac{r_+ - r_-}{2(r_+^2 + a^2)}$ as

$$p \equiv -\frac{\omega_*}{2\kappa} = -\frac{\omega - m\Omega_H}{2\kappa}. \quad (\text{S24})$$

The near-region radial equation (S23) possesses three regular singularities at $\{0, -1, \infty\}$. Its fundamental solutions $R(z)$ can be expressed as a linear combination of two linearly independent hypergeometric functions [65], characterized by six indices $(x_0^\pm, x_{-1}^\pm, x_\infty^\pm)$ corresponding to these singularities. Solving the indicial equation (S52) of Eq. (S23), we find that the indices at infinity x_∞^\pm precisely coincide with the ℓ_q factor

$$x_\infty^+ = 1/2 + \sqrt{(\ell + 1/2)^2 - q^2} = \ell_q + 1, \quad (\text{S25})$$

$$x_\infty^- = 1/2 - \sqrt{(\ell + 1/2)^2 - q^2} = -\ell_q. \quad (\text{S26})$$

Physically, these indices x_∞^\pm correspond to the power-law behavior of the centrifugal potential series in the overlap region. Considering the asymptotic form ($r \gg M$) of the hypergeometric functions w_3, w_4 in Eq. (S56), the solution behaves as

$$\begin{aligned} R(r) &\simeq A \left(\frac{-r}{r_+ - r_-} \right)^{-x_\infty^-} + B \left(\frac{-r}{r_+ - r_-} \right)^{-x_\infty^+} \\ &= A \left(\frac{-r}{r_+ - r_-} \right)^{\ell_q} + B \left(\frac{-r}{r_+ - r_-} \right)^{-\ell_q - 1}. \end{aligned} \quad (\text{S27})$$

where A, B are the linear coefficients.

Consequently, matching becomes possible in the overlap region between the far-region solution Eq. (S22) and near-region solution Eq. (S27), as both exhibit the same power-law dependence on ℓ_q in their centrifugal potential forms. The linear coefficients A and B are thereby determined by

$$A = (-1)^{n_r + \ell_q} [2k(r_+ - r_-)]^{\ell_q} \frac{\Gamma(2\ell_q + n_r + 2)}{\Gamma(2\ell_q + 2)}, \quad (\text{S28})$$

$$B = (-1)^{n_r + \ell_q} [2k(r_+ - r_-)]^{-\ell_q - 1} \Gamma(n_r + 1) \Gamma(2\ell_q + 1) \delta\nu. \quad (\text{S29})$$

Meanwhile, the near-region solution $R(z)$ can be expressed as the combination of the ingoing (z^{-ip}) and outgoing (z^{ip}) modes, which are associated with the hypergeometric function basis (w_1, w_2) near the horizon. This basis can be transformed from the basis (w_3, w_4) in Eq. (S58), which corresponds to the centrifugal potential in the overlap region,

$$\begin{aligned} R(z) &= (Af_{13} + Bf_{14})R_1 + (Af_{23} + Bf_{24})R_2 \\ &\simeq (Af_{13} + Bf_{14})z^{ip} + (Af_{23} + Bf_{24})z^{-ip}, \end{aligned} \quad (\text{S30})$$

where $f_{13}, f_{23}, f_{14}, f_{24}$ are the connection coefficients between different hypergeometric function bases, as given by Eq. (S59). Imposing the boundary condition at the event horizon (purely ingoing waves), the BH's reflectivity must vanish $\mathcal{R} \equiv \frac{Af_{13} + Bf_{14}}{Af_{23} + Bf_{24}} = 0$. This immediately implies the relation between the coefficients A and B

$$f_{13}A + f_{14}B = 0. \quad (\text{S31})$$

Substituting the expressions for A and B in Eqs. (S28)–(S29) into the relation in Eq. (S31) yields the horizon-corrected frequency parameter $\nu = \nu_0 + \delta\nu$, connected to the angular frequency via $\omega = \sqrt{\mu^2 - \frac{M\mu^2}{\nu}}$

$$\begin{aligned} \delta\nu &= 2ip [2k(r_+ - r_-)]^{2\ell_q + 1} \times \left| \frac{\Gamma(1 + \ell_q + 2ip)}{\Gamma(1 + 2ip)} \right|^2 \\ &\times \frac{\Gamma(2\ell_q + n_r + 2)}{\Gamma(n_r + 1)} \left[\frac{\Gamma(\ell_q + 1)}{\Gamma(2\ell_q + 1)\Gamma(2\ell_q + 2)} \right]^2. \end{aligned} \quad (\text{S32})$$

This result generalizes Detweiler's finding in [5] by replacing factorials with Gamma functions and introducing ℓ_q . Otherwise, if ℓ_q is a half-integer, continuing to use the factorial form would lead to an underestimation of the result. The superradiant factor $2p \propto (m\Omega_H - \omega)$ governs the superradiance condition. The radial transmission factor $[2k(r_+ - r_-)]^{2\ell_q + 1}$ determines the amplitude scale, while the phase coupling factor $\left| \frac{\Gamma(1 + \ell_q + 2ip)}{\Gamma(1 + 2ip)} \right|^2$ captures wave-horizon interaction phases. The remaining term $\frac{\Gamma(2\ell_q + n_r + 2)}{\Gamma(n_r + 1)} \left[\frac{\Gamma(\ell_q + 1)}{\Gamma(2\ell_q + 1)\Gamma(2\ell_q + 2)} \right]^2$ is the normalization coefficient.

Given the definitions $k = \frac{M\mu^2}{\nu}$ and $k^2 = \mu^2 - \omega^2$, the parameter $\nu = \nu_0 + \delta\nu$ induces expansions for both wavevector k and angular frequency ω . First, the wavevector expands as $k \simeq k_0 + \delta k$,

$$\begin{aligned} k &= \frac{\alpha^2}{M(\nu_0 + \delta\nu)} \simeq \frac{\alpha^2}{M\nu_0} - \frac{\alpha^2}{M\nu_0^2} \delta\nu = k_0 + \delta k, \\ k_0 &= \frac{\alpha^2}{M\nu_0}, \quad \delta k = -\frac{\alpha^2}{M\nu_0^2} \delta\nu \end{aligned} \quad (\text{S33})$$

with $\nu_0 \equiv \ell_q + n_r + 1$ and $\alpha \equiv M\mu$. The corresponding angular frequency expansion $\omega \simeq \omega_0 + \delta\omega$ yields

$$\omega = \sqrt{\mu^2 - (k_0 + \delta k)^2} \simeq \omega_0 - \frac{k_0}{\omega_0} \delta k = \omega_0 + \delta\omega. \quad (\text{S34})$$

$$\omega_0 = \mu \left[1 - \left(\frac{\alpha}{\nu_0} \right)^2 \right]^{1/2}, \quad \delta\omega = \frac{\delta\nu}{M} \left(\frac{\alpha}{\nu_0} \right)^3 \left[1 - \left(\frac{\alpha}{\nu_0} \right)^2 \right]^{1/2}. \quad (\text{S35})$$

Finally, the growth rate of this scalar cloud, determined by the imaginary part of the frequency shift $\delta\omega$, takes the form

$$\omega_I = \text{Im}[\delta\omega] = \frac{\delta\nu_I}{M} \left(\frac{\alpha}{\nu_0} \right)^3 \left[1 - \left(\frac{\alpha}{\nu_0} \right)^2 \right]^{-1/2}, \quad (\text{S36})$$

where we define $\delta\nu_I \equiv \text{Im}[\delta\nu]$.

The growth rate enhancement factor $\omega_I/\omega_{I(\text{Kerr})}$ is estimated to be several orders of magnitude by comparing the α -scaling in both Kerr and magnetic cases. The radial transmission factor

$$[2k(r_+ - r_-)]^{2\ell_q+1} \propto k^{2\ell_q+1} \sim \alpha^{4\ell_q+2}, \quad (\text{S37})$$

with $k \sim \alpha^2/M$ in $\delta\nu_I$ (Eq. (S32)) and the additional factor α^3 in Eq. (S36) set the α -dependence of the growth rate. For the neutral Kerr case [1, 3, 23], $\omega_{I(\text{Kerr})}$ scales as

$$\omega_{I(\text{Kerr})} = \frac{\delta\nu_I}{M} \left(\frac{\alpha_{(\text{Kerr})}}{\ell + n_r + 1} \right)^3 \propto \alpha_{(\text{Kerr})}^{4\ell+5}. \quad (\text{S38})$$

However, for the magnetic case,

$$\omega_I = \frac{\delta\nu_I}{M} \left(\frac{\alpha}{\ell_q + n_r + 1} \right)^3 \propto \alpha^{4\ell_q+5}. \quad (\text{S39})$$

Here $\ell_q < \ell$. This reduction in the exponent, combined with the small-coupling limit $\alpha, \alpha_{(\text{Kerr})} \ll 1$, leads to an enhancement of up to several orders of magnitude. As a concrete example, the peak growth rate for neutral scalar cloud ($\ell = m = 1$) around a Kerr BH at $\alpha_{(\text{Kerr})} \approx 0.3$ scales as

$$\omega_{I(\text{Kerr})} \propto \alpha_{(\text{Kerr})}^{4\ell+5} = \alpha_{(\text{Kerr})}^9 \approx 0.3^9 \approx 2.0 \times 10^{-5}. \quad (\text{S40})$$

For a charged scalar cloud ($\ell = m = q = N/2 = 3/2$) around a magnetic BH with $N = 3$ magnetic charges at $\alpha \approx 0.45$, with $\ell_q \approx 0.82$, the scaling is

$$\omega_I \propto \alpha^{4\ell_q+5} = \alpha^{8.3} \approx 0.45^{8.3} \approx 1.3 \times 10^{-3}, \quad (\text{S41})$$

yielding a growth rate enhancement

$$\omega_I/\omega_{I(\text{Kerr})} \approx 10^2. \quad (\text{S42})$$

Therefore, the growth rate of the charged scalar cloud around the magnetic BH with $N = 3$ magnetic charges can be about two orders of magnitude larger than that of the neutral scalar cloud around the Kerr BH. The above enhancement is illustrated in Fig. S3. Furthermore, the numerical results in Fig. 3 of [36] are consistent at the order-of-magnitude level with this estimate and our analytical results presented in Fig. S3.

II.b. Matched-asymptotic derivation of the growth rate

The analytical calculation of the growth rate for charged scalar clouds around magnetic BHs is performed using a matched-asymptotic expansion. This involves solving the radial equation (S17) separately in the far region and near region, with the growth rate ultimately extracted via matching of these solutions in the overlap region.

Far region: hydrogenic solution and the reduced orbital index ℓ_q

In the far region limit ($r \gg M$ and $r \sim \ell/\omega$), the radial equation (S17) can be approximated to a hydrogen-atom-like equation

$$\frac{d^2(rR)}{d\tilde{r}^2} + \left[\omega^2 - \mu^2 \left(1 - \frac{2M}{r} \right) - \frac{\ell(\ell+1) - q^2}{r^2} \right] (rR) = 0. \quad (\text{S43})$$

Introducing $\rho = 2kr$ transforms the equation into the Whittaker form [68]

$$\frac{d^2(\rho R)}{d\rho^2} + \left[-\frac{1}{4} + \frac{\nu}{\rho} - \frac{\ell(\ell+1) - q^2}{\rho^2} \right] (\rho R) = 0, \quad (\text{S44})$$

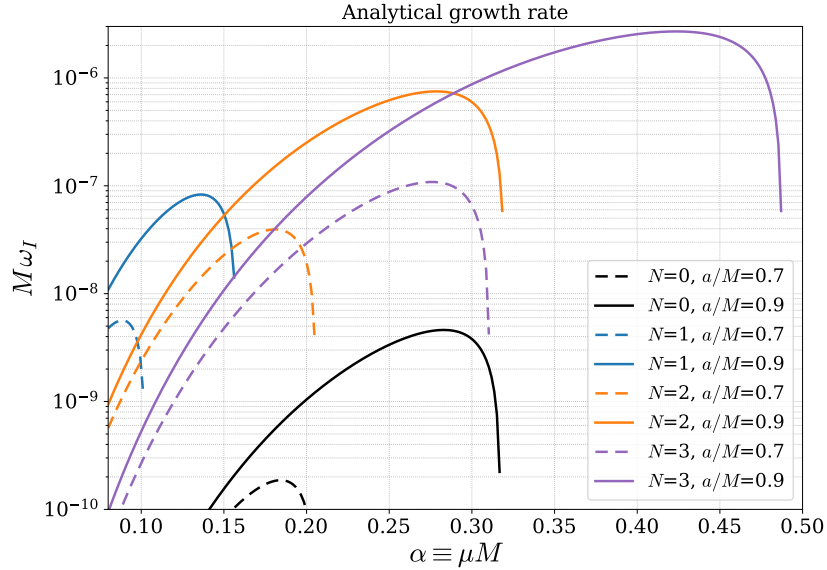


FIG. S3. Analytical growth rate $M\omega_I$ of charged scalar clouds around a magnetic BH as a function of $\alpha \equiv \mu M$. Solid (dashed) curves correspond to $a/M = 0.9$ ($a/M = 0.7$). We take the fundamental radial mode $n_r = 0$ and set $P/M \sim 10^{-19}$. Colors label the monopole number: black/blue/orange/purple denote $N = 0, 1, 2, 3$, respectively. For $N = 0$, we take $\ell = m = 1$. For $N \geq 1$, we take $\ell = m = q = N/2$ with $\ell_q = \sqrt{(\ell + 1/2)^2 - q^2} - 1/2$. The analytical results agree with the numerical values of Ref. [36] to within an order of magnitude.

where $k \equiv \sqrt{\mu^2 - \omega^2}$ and $\nu \equiv M\mu^2/k$. Its solution is given by the Whittaker function, expressed in terms of the confluent hypergeometric function

$$\rho R(\rho) = e^{-\rho/2} \rho^{\frac{1}{2} + \sqrt{(\ell + \frac{1}{2})^2 - q^2}} U\left(\frac{1}{2} + \sqrt{(\ell + \frac{1}{2})^2 - q^2} - \nu, 2\sqrt{(\ell + \frac{1}{2})^2 - q^2} + 1; \rho\right), \quad (\text{S45})$$

Defining $\ell_q + 1 \equiv \sqrt{(\ell + \frac{1}{2})^2 - q^2} + \frac{1}{2}$, the far-region radial solution can be rewritten as

$$R(r) = (2kr)^{\ell_q} e^{-kr} U(\ell_q + 1 - \nu, 2\ell_q + 2; 2kr), \quad (\text{S46})$$

where $U(\ell + 1 - \nu, 2\ell + 2; 2kr)$ is the confluent hypergeometric function [65]. Remarkably, although the centrifugal term $\ell(\ell+1)$ is modified to $\ell(\ell+1) - q^2$ in Eq. (S43), the solution retains the same confluent hypergeometric functional form as in the neutral case, simply by replacing ℓ with ℓ_q . In addition, the event horizon of the BH induces a complex shift $\nu = \nu_0 + \delta\nu$, with the correction

$$\nu_0 \equiv n_r + \ell_q + 1 = n_r + \sqrt{(\ell + \frac{1}{2})^2 - q^2} + \frac{1}{2}, \quad (\text{S47})$$

leading to the alternative representation

$$R(r) = (2kr)^{\ell_q} e^{-kr} U(-n_r - \delta\nu, 2\ell_q + 2; 2kr). \quad (\text{S48})$$

Near region: hypergeometric solution and horizon boundary condition

In the near region, we introduce the rescaled radial coordinate

$$z \equiv \frac{r - r_+}{r_+ - r_-}, \quad \Delta = z(z+1)(r_+ - r_-)^2. \quad (\text{S49})$$

In the limit $r \ll \ell/\omega$ and $r \ll \ell/\mu$, the radial equation in Eq. (S17) reduces to

$$z(z+1) \frac{d}{dz} \left[z(z+1) \frac{dR}{dz} \right] + [p^2 - (\ell(\ell+1) - q^2)z(z+1)] R = 0, \quad (\text{S50})$$

with the superradiant parameter

$$p \equiv -\frac{\omega_*}{2\kappa} = -\frac{\omega - m\Omega_H}{2\kappa}, \quad (\text{S51})$$

where $\Omega_H = \frac{a}{r_+^2 + a^2}$ and $\kappa = \frac{r_+ - r_-}{2(r_+^2 + a^2)}$ are the angular velocity and surface gravity of the BH respectively. The differential equation (S50) possesses three regular singularities at $\{0, -1, \infty\}$. Its solutions $R(z)$ take the standard form in terms of hypergeometric functions [65], characterized by six indices $(x_0^\pm, x_{-1}^\pm, x_\infty^\pm)$ corresponding to these singularities. The indices are determined by the indicial equations

$$x_n(x_n - 1) + A_n + B_n = 0, \quad (\text{S52})$$

where A_n is the first-order characteristic coefficient and B_n is the second-order characteristic coefficient for n -th singularity. Substituting the specific coefficients

$$\begin{aligned} A_0 &= 1, & B_0 &= p^2, \\ A_{-1} &= 1, & B_{-1} &= p^2, \\ A_\infty &= 0, & B_\infty &= -\ell(\ell + 1) + q^2, \end{aligned} \quad (\text{S53})$$

we obtain the indices

$$\begin{aligned} x_0^\pm &= \pm ip, & x_{-1}^\pm &= \pm ip, \\ x_\infty^+ &= 1/2 + \sqrt{(\ell + 1/2)^2 - q^2}, & x_\infty^- &= 1/2 - \sqrt{(\ell + 1/2)^2 - q^2}. \end{aligned} \quad (\text{S54})$$

Consequently, the solutions $R(z)$ in Eq. (S50) can be written as the standard form :

$$R = \left(\frac{z}{z+1} \right)^{ip} {}_2F_1(-\ell_q, \ell_q + 1, 1 - 2ip; z+1), \quad (\text{S55})$$

with the hypergeometric function ${}_2F_1(-\ell_q, \ell_q + 1, 1 - 2ip; z+1)$.

The standard form can be expressed through a set of linearly independent solutions (R_3, R_4) , where the hypergeometric function ${}_2F_1(-\ell_q, \ell_q + 1, 1 - 2ip; z+1)$ transforms into two another linearly independent functions w_3 and w_4 :

$$\begin{aligned} R_3 &\equiv \left(\frac{z}{z+1} \right)^{ip} (-z)^{\ell_q} w_3, & w_3 &\equiv (-z)^{\ell_q} {}_2F_1(-\ell_q, -\ell_q - 2ip, -2\ell_q, -z^{-1}), \\ R_4 &\equiv \left(\frac{z}{z+1} \right)^{ip} (-z)^{-\ell_q - 1} w_4, & w_4 &\equiv (-z)^{-\ell_q - 1} {}_2F_1(\ell_q + 1, \ell_q + 1 - 2ip, 2\ell_q + 2, -z^{-1}). \end{aligned} \quad (\text{S56})$$

Physically, (R_3, R_4) represent the solutions described by the centrifugal potential. These centrifugal solutions can be transformed into the ingoing and outgoing solutions (R_1, R_2) near the horizon:

$$\begin{aligned} R_1(z) &= \left(\frac{z}{z+1} \right)^{ip} w_1, & w_1 &\equiv {}_2F_1(-\ell_q, \ell_q + 1, 1 + 2ip; -z), \\ R_2(z) &= \left(\frac{z}{z+1} \right)^{ip} z^{-2ip} w_2, & w_2 &\equiv {}_2F_1(-\ell_q - 2ip, \ell_q + 1 - 2ip, 1 - 2ip; z+1). \end{aligned} \quad (\text{S57})$$

The relation between these two sets of solutions as $z \rightarrow 0$ (near horizon) is

$$\begin{aligned} R_3 &= f_{13}R_1 + f_{23}R_2, \\ R_4 &= f_{14}R_1 + f_{24}R_2, \end{aligned} \quad (\text{S58})$$

with the transformation coefficients

$$\begin{aligned} f_{13} &= (-1)^{\ell_q} \frac{\Gamma(-2\ell_q)\Gamma(-2ip)}{\Gamma(-\ell_q)\Gamma(-2ip - \ell_q)}, \\ f_{23} &= (-1)^{\ell_q} \frac{\Gamma(-2\ell_q)\Gamma(2ip)}{\Gamma(-\ell_q + 2ip)\Gamma(-\ell_q)}, \\ f_{14} &= (-1)^{1-\ell_q} \frac{\Gamma(2\ell_q + 2)\Gamma(-2ip)}{\Gamma(\ell_q + 1)\Gamma(\ell_q - 2ip + 1)}, \\ f_{24} &= (-1)^{1-\ell_q} \frac{\Gamma(2\ell_q + 2)\Gamma(2ip)}{\Gamma(\ell_q + 1)\Gamma(\ell_q + 2ip + 1)}. \end{aligned} \quad (\text{S59})$$

The general solution $R(z)$ is represented by

$$\begin{aligned} R(z) &= AR_3 + BR_4 \\ &= (Af_{13} + Bf_{14})R_1 + (Af_{23} + Bf_{24})R_2 \\ &\simeq (Af_{13} + Bf_{14})z^{ip} + (Af_{23} + Bf_{24})z^{-ip}(z \rightarrow 0) \end{aligned} \quad (\text{S60})$$

where A and B are the linear coefficients in the (R_3, R_4) basis. Imposing the purely ingoing boundary condition at the event horizon (the reflectivity $\mathcal{R} \equiv \frac{Af_{13} + Bf_{14}}{Af_{23} + Bf_{24}} = 0$). Then we obtain the relation between A and B

$$Af_{13} + Bf_{14} = 0. \quad (\text{S61})$$

Overlap matching and analytic expression for $\delta\nu$

In the overlap region, we connect the far-region solutions with the near-region solutions to obtain the complex shift $\delta\nu$. Using the properties of confluent hypergeometric functions

$$\begin{aligned} &U(-n_r - \delta\nu, 2\ell_q + 2; 2kr) \\ &= \frac{\Gamma(-2\ell_q - 1)}{\Gamma(-n_r - \delta\nu - 2\ell_q - 1)} U(-n_r - \delta\nu, 2\ell_q + 2; 2kr) \\ &+ \frac{(2kr)^{-2\ell_q - 1} \Gamma(2\ell_q + 1)}{\Gamma(-n_r - \delta\nu)} U(-n_r - \delta\nu - 2\ell_q - 1, -2\ell_q; 2kr), \end{aligned} \quad (\text{S62})$$

and Gamma functions

$$\begin{aligned} \frac{\Gamma(-2\ell_q - 1)}{\Gamma(-n_r - \delta\nu - 2\ell_q - 1)} &= (-1)^{n_r} \frac{\Gamma(2\ell_q + n_r + 2)}{\Gamma(2\ell_q + 2)}, \\ \frac{\Gamma(2\ell_q + 1)}{\Gamma(-n_r - \delta\nu)} &= (-1)^{n_r + 1} \delta\nu \Gamma(n_r + 1) \Gamma(2\ell_q + 1), \end{aligned} \quad (\text{S63})$$

the far-region solution's asymptotic behavior in the overlap region ($2kr \rightarrow 0$) is

$$\begin{aligned} R_{\text{far}}(r) &= (2kr)^{\ell_q} e^{-kr} U(-n_r - \delta\nu, 2\ell_q + 2; 2kr) \\ &\simeq (-1)^{n_r} \frac{\Gamma(2\ell_q + n_r + 2)}{\Gamma(2\ell_q + 2)} (2kr)^{\ell_q} + (-1)^{n_r + 1} \Gamma(n_r + 1) \Gamma(2\ell_q + 1) \delta\nu (2kr)^{-\ell_q - 1}. \end{aligned} \quad (\text{S64})$$

Meanwhile, the near-region solution's asymptotic behavior for $r \gg M$ in the overlap region is

$$R_{\text{near}}(r) \simeq A \left(\frac{-r}{r_+ - r_-} \right)^{\ell_q} + B \left(\frac{-r}{r_+ - r_-} \right)^{-\ell_q - 1}. \quad (\text{S65})$$

where

$$\begin{aligned} R_3 &= (-z)^{\ell_q} w_3 \simeq (-z)^{\ell_q} = \left(\frac{-r}{r_+ - r_-} \right)^{\ell_q}, \\ R_4 &= (-z)^{-\ell_q - 1} w_4 \simeq (-z)^{-\ell_q - 1} = \left(\frac{-r}{r_+ - r_-} \right)^{-\ell_q - 1}, \end{aligned} \quad (\text{S66})$$

Matching these two solutions (Eq. (S64) and Eq. (S65)) in the overlap region determines the coefficients A and B

$$A = (-1)^{n_r + \ell_q} [2k(r_+ - r_-)]^{\ell_q} \frac{\Gamma(2\ell_q + n_r + 2)}{\Gamma(2\ell_q + 2)}, \quad (\text{S67})$$

$$B = (-1)^{n_r + \ell_q} [2k(r_+ - r_-)]^{-\ell_q - 1} \Gamma(n_r + 1) \Gamma(2\ell_q + 1) \delta\nu. \quad (\text{S68})$$

Considering the relation $Af_{13} + Bf_{14} = 0$ from Eq. (S61), we derive the expression of $\delta\nu$:

$$\begin{aligned} \delta\nu &= 2ip [2k(r_+ - r_-)]^{2\ell_q + 1} \\ &\times \frac{\Gamma(2\ell_q + n_r + 2)}{\Gamma(n_r + 1)} \left[\frac{\Gamma(\ell_q + 1)}{\Gamma(2\ell_q + 1) \Gamma(2\ell_q + 2)} \right]^2 \\ &\times \left| \frac{\Gamma(1 + \ell_q + 2ip)}{\Gamma(1 + 2ip)} \right|^2. \end{aligned} \quad (\text{S69})$$

III. GRAVITATIONAL-WAVE POWER FROM ELECTRICALLY CHARGED SCALAR CLOUDS

Due to the temporal oscillations of the energy-momentum tensor $T_{\mu\nu}$ of the real scalar field

$$T_{\mu\nu}(t, \mathbf{x}) = \partial_\mu \psi \partial_\nu \psi - g_{\mu\nu} \left(g^{ab} \frac{1}{2} \partial_a \psi \partial_b \psi + \frac{1}{2} \mu^2 \psi^2 \right), \quad (\text{S70})$$

the scalar clouds emits GWs. We consider the gravitational perturbation

$$\hat{g}_{\mu\nu} = g_{\mu\nu} + h_{\mu\nu}, \quad (\text{S71})$$

where $\hat{g}_{\mu\nu}$ is the spacetime metric, $g_{\mu\nu}$ is the background metric and $h_{\mu\nu}$ is a small gravitational perturbation. To obtain the sourced wave equation for the source $T_{\mu\nu}$, we introduce the trace-reversed metric perturbation $\bar{h}_{\mu\nu} = h_{\mu\nu} - \frac{1}{2} \eta_{\mu\nu} h^\rho_\rho$ satisfying

$$\square \bar{h}_{\mu\nu} = -16\pi T_{\mu\nu}(\mathbf{x}, t), \quad (\text{S72})$$

under the Lorenz gauge $\partial^\mu \bar{h}_{\mu\nu} = 0$. The above wave equation can be rewritten as an equation of $h_{\mu\nu}$

$$\square h_{\mu\nu} = -16\pi \left(T_{\mu\nu} - \frac{1}{2} T^\rho_\rho g_{\mu\nu} \right). \quad (\text{S73})$$

The GW emission of the scalar clouds includes the contributions from both the self-annihilation of a single mode with $\omega_{n\ell m}$ and the transition between different modes $\omega_{n\ell m} \rightarrow \omega_{n'\ell' m'}$ [16]. If the cloud is occupied by the mode $\psi \propto e^{-i\omega_{n\ell m} t + im\phi}$ with $\omega_{n\ell m}$, its energy-momentum tensor $T_{\mu\nu} \propto e^{-i2\omega t + i2m\phi}$ oscillates at a frequency of $2\omega_{n\ell m}$, so that the GW frequency $\tilde{\omega}$ and azimuthal quantum number \tilde{m} satisfy the relationship

$$\tilde{\omega} = 2\omega_{n\ell m}, \quad \tilde{m} = 2m. \quad (\text{S74})$$

On the other hand, if two modes with $\omega_{n\ell m}$ and $\omega_{n'\ell' m'}$ are occupied, an interference term oscillating at the difference frequency $\omega_{n\ell m} - \omega_{n'\ell' m'}$ appears in the energy-momentum tensor $T_{\mu\nu}$, producing gravitational waves at frequency $\omega_{n\ell m} - \omega_{n'\ell' m'}$.

However, the probability of the scalar cloud being occupied by multiple modes simultaneously during its spontaneous growth is expected to be small [3], unless the initial amplitudes of these modes are sufficiently large [69, 70] or the scalar fields possess sufficiently strong non-gravitational self-interactions [71]. Therefore, the self-annihilation radiation process is generally dominated [21]. In the following discussion of the GW emission, we will focus on that produced by the self-annihilation process.

Given the solution to Eq. (S73), the GW power P_{GW} is defined as

$$P_{\text{GW}} \equiv \frac{dE_{\text{GW}}}{dt} = \frac{1}{32\pi} \int g^{\mu\rho} g^{\nu\sigma} \dot{h}_{\mu\nu}^{\text{TT}} \dot{h}_{\rho\sigma}^{\text{TT}} dS, \quad (\text{S75})$$

where $\dot{h}_{\mu\nu}^{\text{TT}}$ denotes the time derivative of the perturbation in the transverse-traceless (TT) gauge [72]. Notably, the GW radiation from the self-annihilation lies in the short-wavelength regime, which makes the standard quadrupole radiation formula inapplicable. In the self-annihilation process, the corresponding GW frequency is about $\tilde{\omega} = 2\omega_{n\ell m} \approx 2\mu$. Thus, the GW emission from the self-annihilation process has a wavelength $\tilde{\lambda} \sim \frac{2\pi}{\tilde{\omega}} \approx \frac{\pi}{\mu}$. In addition, the radius of the cloud is about $r_c \sim \frac{1}{\alpha\mu}$. Consequently, the gravitational wavelength $\tilde{\lambda}$ is much shorter than the radius of the cloud r_c for $\alpha \ll 1$

$$\tilde{\lambda} \sim \frac{\pi}{\mu} \ll r_c \sim \frac{1}{\alpha\mu}. \quad (\text{S76})$$

Analytical estimates for the GW emission from the scalar clouds can be obtained using two approximations: the flat-spacetime approximation [17, 49] and the Schwarzschild approximation [39]. The former approximation tends to underestimate the GW radiation, while the latter tends to overestimate it. For simplicity, we calculate the GW power from the electrically charged clouds around the magnetic BH in the flat-spacetime approximation.

III.a. General setup: GW equation and homogeneous-mode expansion

The solution $h_{\mu\nu}$ satisfying Eq. (S73) and entering Eq. (S75) can be expanded in a basis of the homogeneous outgoing-mode $u_{\mu\nu}^{(\tilde{j})}$ at the future null infinity

$$h_{\mu\nu} = \sum_{\tilde{j}} C_{\tilde{j}} u_{\mu\nu}^{(\tilde{j})}, \quad (\text{S77})$$

where \tilde{j} indicates the collection of indices to specify each mode and the homogeneous out-mode $u_{\mu\nu}^{(\tilde{j})}$ satisfies the source-free (homogeneous) wave equation

$$\square u_{\mu\nu}^{(\tilde{j})} = 0. \quad (\text{S78})$$

Substituting Eq. (S77) into Eq. (S75) and using the orthogonality of the outgoing modes (equivalently, time-averaging over several GW periods so that cross terms vanish), we obtain

$$P_{\text{GW}} = \frac{1}{64\pi} \sum_{\tilde{j}} \tilde{\omega}^2 |C_{\tilde{j}}|^2 J_{\tilde{j}} \quad (\text{S79})$$

with

$$J_{\tilde{j}} = \int g^{\mu\rho} g^{\nu\sigma} u_{\mu\nu}^{(\tilde{j})\text{TT}} u_{\rho\sigma}^{(\tilde{j})\text{TT}} dS. \quad (\text{S80})$$

Applying Green's theorem and integration by parts, $C_{\tilde{j}}$ is given in [17] as

$$C_{\tilde{j}} = 8\pi \frac{\langle u^{(\tilde{j})\text{TT}}, T \rangle}{\tilde{\omega} J_{\tilde{j}}}. \quad (\text{S81})$$

Here, under the gauge transformation $u_{\mu\nu}^{\text{TT}} \rightarrow u_{\mu\nu} = u_{\mu\nu}^{\text{TT}} + \delta u_{\mu\nu}$ with $\delta u_{\mu\nu} = \nabla_{\mu}\xi_{\nu} + \nabla_{\nu}\xi_{\mu}$, one has $\langle \delta u, T \rangle = 0$. Then, the inner product $\langle u^{(\tilde{j})}, T \rangle$ can be calculated without imposing a special gauge choice.

Consequently, the GW power can be expressed by using the homogeneous solution $u^{(\tilde{j})}$

$$P_{\text{GW}} = \pi \sum_{\tilde{j}} \frac{|\langle u^{(\tilde{j})}, T \rangle|^2}{J_{\tilde{j}}}. \quad (\text{S82})$$

III.b. Outgoing modes in the Newman-Penrose formalism

To construct the homogeneous solutions, we can employ the Newman-Penrose (NP) formalism with the Kinnersley null tetrad [73]

$$l^{\mu} = \frac{1}{\Delta} (r^2 + a^2, 1, 0, a), \quad (\text{S83})$$

$$n^{\mu} = \frac{1}{2\Sigma} (r^2 + a^2, -\Delta, 0, a), \quad (\text{S84})$$

$$m^{\mu} = \frac{1}{\sqrt{2}(r + ia\cos\theta)} \left(ia\sin\theta, 0, 1, \frac{i}{\sin\theta} \right). \quad (\text{S85})$$

In this tetrad, the metric can be expressed as

$$g_{\mu\nu} = -l_{\mu}n_{\nu} - n_{\mu}l_{\nu} + m_{\mu}m_{\nu}^* + m_{\nu}m_{\mu}^*. \quad (\text{S86})$$

For the gravitational perturbation, the Newman-Penrose quantities ψ_0 and $\rho_{\text{NP}}^{-4}\psi_4$ describe the ingoing and outgoing gravitational waves respectively and they are given by

$$\psi_0 = -C_{\alpha\beta\gamma\delta} l^{\alpha} m^{\beta} l^{\gamma} m^{\delta}, \quad \psi_4 = -C_{\alpha\beta\gamma\delta} n^{\alpha} m^{*\beta} n^{\gamma} m^{*\delta}, \quad (\text{S87})$$

with the Weyl tensor $C_{\alpha\beta\gamma\delta}$ and $\rho_{\text{NP}} \equiv \frac{-1}{r-ia\cos\theta}$. The quantities ψ_0 and $\rho_{\text{NP}}^{-4}\psi_4$ satisfy the Teukolsky equation [74]

$$\begin{aligned} & \left[\frac{(r^2 + a^2)^2}{\Delta} - a^2 \sin^2 \theta \right] \frac{\partial^2 \psi}{\partial t^2} + \frac{4Mar}{\Delta} \frac{\partial^2 \psi}{\partial t \partial \phi} + \left[\frac{a^2}{\Delta} - \frac{1}{\sin^2 \theta} \right] \frac{\partial^2 \psi}{\partial \phi^2} \\ & - \Delta^{-s} \frac{\partial}{\partial r} \left(\Delta^{s+1} \frac{\partial \psi}{\partial r} \right) - \frac{1}{\sin \theta} \frac{\partial}{\partial \theta} \left(\sin \theta \frac{\partial \psi}{\partial \theta} \right) - 2s \left[\frac{a(r-M)}{\Delta} + \frac{i \cos \theta}{\sin^2 \theta} \right] \frac{\partial \psi}{\partial \phi} \\ & - 2s \left[\frac{M(r^2 - a^2)}{\Delta} - r - ia \cos \theta \right] \frac{\partial \psi}{\partial t} + (s^2 \cot^2 \theta - s) \psi = 0, \end{aligned} \quad (\text{S88})$$

with $s = \pm 2$. The field quantity ψ can be separated as the radial part ${}_s\tilde{R}_{\tilde{\ell}\tilde{m}}^{\tilde{\omega}}(r)$ and angular part ${}_s\tilde{S}_{\tilde{\ell}\tilde{m}}^{\tilde{\omega}}(\theta)$

$$\psi = e^{-i\tilde{\omega}t} e^{i\tilde{m}\phi} {}_s\tilde{R}_{\tilde{\ell}\tilde{m}}^{\tilde{\omega}}(r) {}_s\tilde{S}_{\tilde{\ell}\tilde{m}}^{\tilde{\omega}}(\theta). \quad (\text{S89})$$

The separated radial and angular equations of Eq. (S88) are

$$\Delta^{-s} \frac{d}{dr} \left(\Delta^{s+1} \frac{d {}_s\tilde{R}_{\tilde{\ell}\tilde{m}}^{\tilde{\omega}}}{dr} \right) + \left[\frac{\tilde{K}^2 - 2is(r-M)\tilde{K}}{\Delta} + 4is\tilde{\omega}r - \lambda \right] {}_s\tilde{R}_{\tilde{\ell}\tilde{m}}^{\tilde{\omega}} = 0, \quad (\text{S90})$$

$$\begin{aligned} & \frac{1}{\sin \theta} \frac{d}{d\theta} \left(\sin \theta \frac{d {}_s\tilde{S}_{\tilde{\ell}\tilde{m}}^{\tilde{\omega}}}{d\theta} \right) + \left(a^2 \tilde{\omega}^2 \cos^2 \theta - \frac{\tilde{m}^2}{\sin^2 \theta} - 2a\tilde{\omega}s \cos \theta \right. \\ & \left. - \frac{2\tilde{m}s \cos \theta}{\sin^2 \theta} - s^2 \cot^2 \theta + s + {}_sA_{\tilde{\ell}\tilde{m}} \right) {}_s\tilde{S}_{\tilde{\ell}\tilde{m}}^{\tilde{\omega}} = 0, \end{aligned} \quad (\text{S91})$$

where $\tilde{K} = (r^2 + a^2)\tilde{\omega} - a\tilde{m}$, $\lambda = {}_sA_{\tilde{\ell}\tilde{m}} + a^2\tilde{\omega}^2 - 2a\tilde{m}\tilde{\omega}$.

Here, ${}_s\tilde{S}_{\tilde{\ell}\tilde{m}}^{\tilde{\omega}}(\theta)$ is the spin-weighted spheroidal harmonic. In the limit $a\tilde{\omega} \ll 1$, the spin-weighted spheroidal harmonics reduce to the spin-weighted spherical harmonics with the eigenvalue ${}_sA_{\tilde{\ell}\tilde{m}} = \tilde{\ell}(\tilde{\ell}+1) - s(s+1)$

$$\begin{aligned} {}_s\tilde{Y}_{\tilde{\ell}\tilde{m}}(\theta, \phi) &= e^{i\tilde{m}\phi} \sqrt{\frac{(\tilde{\ell}+\tilde{m})!(\tilde{\ell}-\tilde{m})!}{(\tilde{\ell}+s)!(\tilde{\ell}-s)!}} \sqrt{\frac{2\tilde{\ell}+1}{4\pi}} \sin^{2\tilde{\ell}}(\theta/2) \\ & \times \sum_{r=0}^{\tilde{\ell}-s} \binom{\tilde{\ell}-s}{r} \binom{\tilde{\ell}+s}{r+s-\tilde{m}} (-1)^{\tilde{\ell}-r-s+\tilde{m}} \cot^{2r+s-\tilde{m}}(\theta/2). \end{aligned} \quad (\text{S92})$$

Additionally, the asymptotic behavior of ${}_s\tilde{R}_{\tilde{\ell}\tilde{m}}^{\tilde{\omega}}(r)$ for outgoing-mode is

$${}_s\tilde{R}_{\tilde{\ell}\tilde{m}}^{\tilde{\omega}} \sim \begin{cases} e^{i(\tilde{\omega}-\tilde{m}\Omega_H)\tilde{R}_*} & (\tilde{R}_* \rightarrow -\infty), \\ Z_{\text{in}} \frac{e^{-i\tilde{\omega}\tilde{R}_*}}{r} + Z_{\text{out}} \frac{e^{i\tilde{\omega}\tilde{R}_*}}{r^{2s+1}} & (\tilde{R}_* \rightarrow +\infty), \end{cases} \quad (\text{S93})$$

where \tilde{R}_* is the tortoise coordinate.

The homogeneous metric perturbation can be reconstructed from the Teukolsky functions ${}_s\tilde{R}_{\tilde{\ell}\tilde{m}}^{\tilde{\omega}}(r)$ and angular part ${}_s\tilde{S}_{\tilde{\ell}\tilde{m}}^{\tilde{\omega}}(\theta)$. The $u_{\mu\nu}$ is given by Chrzanowski [75] in the outgoing radiation gauge $u_{\mu\nu}n^\nu = 0$

$$\begin{aligned} u_{\mu\nu}(\tilde{\ell}, \tilde{m}, \tilde{\omega}, \mathcal{P}) &= (-n_\mu n_\nu \mathcal{A} - m_\mu m_\nu \mathcal{B} + n_{(\mu} m_{\nu)} \mathcal{C}) {}_{-2}\tilde{R}_{\tilde{\ell}\tilde{m}}^{\tilde{\omega}}(r) {}_{-2}\tilde{S}_{\tilde{\ell}\tilde{m}}^{\tilde{\omega}}(\theta) e^{i\tilde{m}\phi - i\tilde{\omega}t} \\ & + \mathcal{P} \left(-n_\mu n_\nu \mathcal{A}^* - m_\mu^* m_\nu^* \mathcal{B}^* + n_{(\mu} m_{\nu)}^* \mathcal{C}^* \right) {}_{+2}\tilde{R}_{\tilde{\ell}\tilde{m}}^{\tilde{\omega}}(r) {}_{+2}\tilde{S}_{\tilde{\ell}\tilde{m}}^{\tilde{\omega}}(\theta) e^{i\tilde{m}\phi - i\tilde{\omega}t}, \end{aligned} \quad (\text{S94})$$

where the operators

$$\mathcal{A} = \rho_{\text{NP}}^{*-4} (\delta_{\text{NP}} - 3\alpha_{\text{NP}}^* - \beta_{\text{NP}} + 5\pi_{\text{NP}}^*) (\delta_{\text{NP}} - 4\alpha_{\text{NP}}^* + \pi_{\text{NP}}^*), \quad (\text{S95})$$

$$\mathcal{B} = \rho_{\text{NP}}^{*-4} (\Delta_{\text{NP}} + 5\mu_{\text{NP}}^* - 3\gamma_{\text{NP}}^* + \gamma_{\text{NP}}) (\Delta_{\text{NP}} + \mu_{\text{NP}}^* - 4\gamma_{\text{NP}}^*), \quad (\text{S96})$$

$$\begin{aligned} \mathcal{C} &= \rho_{\text{NP}}^{*-4} [(\delta_{\text{NP}} + 5\pi_{\text{NP}}^* + \beta_{\text{NP}} - 3\alpha_{\text{NP}}^* + \tau_{\text{NP}}) (\Delta_{\text{NP}} + \mu_{\text{NP}}^* - 4\gamma_{\text{NP}}^*) \\ & + (\Delta_{\text{NP}} + 5\mu_{\text{NP}}^* - \mu_{\text{NP}} - 3\gamma_{\text{NP}}^* - \gamma_{\text{NP}}) (\delta_{\text{NP}} - 4\alpha_{\text{NP}}^* + \pi_{\text{NP}}^*)], \end{aligned} \quad (\text{S97})$$

with the Newman-Penrose variables $\alpha_{\text{NP}}, \beta_{\text{NP}}, \gamma_{\text{NP}}, \pi_{\text{NP}}, \mu_{\text{NP}}$ [73, 74] and $\Delta_{\text{NP}} = n^\mu \nabla_\mu, \delta_{\text{NP}} = m^\mu \nabla_\mu$. The polarization-state parameters $\mathcal{P} = \pm 1$ correspond to the even-parity and odd-parity perturbations respectively [76, 77]. Here m_μ and n_μ denote four-vectors and are unrelated to the quantum numbers m and n .

From Eq. (S93) and Eq. (S94), the asymptotic behavior of outgoing waves in the TT gauge is at the far region $r \gg M$

$$u_{IJ} \simeq \frac{Z_{\text{out}}}{2} \tilde{\omega}^2 \frac{e^{-i\tilde{\omega}(t-r)}}{r} \times \begin{pmatrix} \hat{u}_{\theta\theta} & \hat{u}_{\theta\phi} \\ \hat{u}_{\phi\theta} & \hat{u}_{\phi\phi} \end{pmatrix} \quad (\text{S98})$$

where the subscript IJ denotes the angular θ, ϕ components and the matrix of \hat{u} can be rewritten as

$$r^2 \begin{pmatrix} \hat{u}_+ & \hat{u}_\times \sin \theta \\ \hat{u}_\times \sin \theta & -\hat{u}_+ \sin^2 \theta \end{pmatrix} = \begin{cases} r^2 \mathbb{S}_{IJ} & (P = +1), \\ r^2 \mathbb{V}_{IJ} & (P = -1). \end{cases} \quad (\text{S99})$$

Here, the explicit expressions of $\mathbb{S}_{IJ}, \mathbb{V}_{IJ}$ are as follows

$$\mathbb{S}_{IJ} = e^{i\tilde{m}\phi} \begin{pmatrix} -_2\tilde{S}_{\tilde{\ell}\tilde{m}}^\omega + +_2\tilde{S}_{\tilde{\ell}\tilde{m}}^\omega & i \sin \theta \left(-_2\tilde{S}_{\tilde{\ell}\tilde{m}}^\omega - +_2\tilde{S}_{\tilde{\ell}\tilde{m}}^\omega \right) \\ i \sin \theta \left(-_2\tilde{S}_{\tilde{\ell}\tilde{m}}^\omega - +_2\tilde{S}_{\tilde{\ell}\tilde{m}}^\omega \right) & -\sin^2 \theta \left(-_2\tilde{S}_{\tilde{\ell}\tilde{m}}^\omega + +_2\tilde{S}_{\tilde{\ell}\tilde{m}}^\omega \right) \end{pmatrix}, \quad (\text{S100})$$

$$\mathbb{V}_{IJ} = e^{i\tilde{m}\phi} \begin{pmatrix} -_2\tilde{S}_{\tilde{\ell}\tilde{m}}^\omega - +_2\tilde{S}_{\tilde{\ell}\tilde{m}}^\omega & i \sin \theta \left(-_2\tilde{S}_{\tilde{\ell}\tilde{m}}^\omega + +_2\tilde{S}_{\tilde{\ell}\tilde{m}}^\omega \right) \\ i \sin \theta \left(-_2\tilde{S}_{\tilde{\ell}\tilde{m}}^\omega + +_2\tilde{S}_{\tilde{\ell}\tilde{m}}^\omega \right) & -\sin^2 \theta \left(-_2\tilde{S}_{\tilde{\ell}\tilde{m}}^\omega - +_2\tilde{S}_{\tilde{\ell}\tilde{m}}^\omega \right) \end{pmatrix}. \quad (\text{S101})$$

Substituting Eq. (S98) into Eq. (S80), we have

$$J_{\tilde{j}} = \int g^{\mu\rho} g^{\nu\sigma} u_{\mu\nu}^{(\tilde{j})\text{TT}} u_{\rho\sigma}^{(\tilde{j})\text{TT}} dS \quad (\text{S102})$$

$$\simeq 2|Z_{\text{out}}|^2 \tilde{\omega}^4 \quad (\text{S103})$$

for both $\mathcal{P} = \pm 1$.

Consequently, from Eq. (S75), the GW power can be rewritten as

$$P_{\text{GW}} = \frac{\pi}{2} \left| \frac{\langle u, T \rangle}{Z_{\text{out}}} \right|^2 \tilde{\omega}^{-4}, \quad (\text{S104})$$

with the outgoing coefficient Z_{out} for the asymptotic outgoing waves.

III.c. GW emission in the flat-spacetime approximation

We now need to derive explicit expressions of the outgoing coefficient Z_{out} and the inner product $\langle u, T \rangle$ that appear in the GW power formula Eq. (S103) in the flat-spacetime approximation.

In the flat spacetime, the Teukolsky radial equation (S90) can be written as

$$\frac{d^2 s \tilde{R}_{\tilde{\ell}\tilde{m}}}{d\tilde{r}^2} + \frac{2s+2}{\tilde{r}} \frac{d_s \tilde{R}_{\tilde{\ell}\tilde{m}}}{d\tilde{r}} + \left[1 + \frac{2is}{\tilde{r}} - \frac{(\tilde{\ell}-s)(\tilde{\ell}+s+1)}{\tilde{r}^2} \right] s \tilde{R}_{\tilde{\ell}\tilde{m}} = 0, \quad (\text{S105})$$

where the radial coordinate is rescaled

$$\tilde{r} \equiv \tilde{\omega} r. \quad (\text{S106})$$

The regular homogeneous solution with $s = +2$ can be expressed using confluent hypergeometric function U

$$+_2\tilde{R}_{\tilde{\ell}\tilde{m}} = e^{-i\tilde{r}} \tilde{r}^{\tilde{\ell}-2} U(\tilde{\ell}-1, 2\tilde{\ell}+2, 2i\tilde{r}), \quad (\text{S107})$$

where $U(\tilde{\ell}-1, 2\tilde{\ell}+2, 0) = 1$ makes the radial function $+_2\tilde{R}_{\tilde{\ell}\tilde{m}}$ regular at $\tilde{r} = 0$. Thus, the asymptotic behavior of $+_2\tilde{R}_{\tilde{\ell}\tilde{m}}$ at the far region $\tilde{r} \gg 1$ is

$$+_2\tilde{R}_{\tilde{\ell}\tilde{m}} \approx \frac{\Gamma(2\tilde{\ell}+2)}{(2i)^{\tilde{\ell}+3} \Gamma(\tilde{\ell}-1)} \frac{e^{i\tilde{r}}}{\tilde{r}^5} + \frac{\Gamma(2\tilde{\ell}+2)}{(-2i)^{\tilde{\ell}-1} \Gamma(\tilde{\ell}+3)} \frac{e^{-i\tilde{r}}}{\tilde{r}}. \quad (\text{S108})$$

Therefore, from the above asymptotic behavior, the outgoing coefficient Z_{out} for the asymptotic outgoing waves is

$$Z_{\text{out}} = \frac{\Gamma(2\tilde{\ell} + 2)}{(2i)^{\tilde{\ell}+3}\Gamma(\tilde{\ell} - 1)}\tilde{\omega}^{-5}. \quad (\text{S109})$$

Next, we calculate the full inner product $\langle u, T \rangle$. For notational simplicity, we set the GW-related functions $\tilde{R} := {}_{+2}\tilde{R}_{\tilde{\ell}\tilde{m}}(r)$ and ${}_{+s}\tilde{Y} := {}_{+s}\tilde{Y}_{\tilde{\ell}\tilde{m}}(\theta, \phi)$. On the other hand, the scalar-field functions $R := R_{\ell m}(r)$ and $Y := Y_{\ell m}(\theta, \phi)$ are defined.

In the flat-spacetime approximation, the Kinnersley tetrad and the Newman-Penrose variables in Eq. (S94) become

$$l^\mu = (1, 1, 0, 0), \quad n^\mu = \left(\frac{1}{2}, -\frac{1}{2}, 0, 0 \right), \quad m^\mu = \frac{1}{\sqrt{2}r} \left(0, 0, 1, \frac{i}{\sin \theta} \right). \quad (\text{S110})$$

and

$$\rho_{\text{NP}} = -\frac{1}{r}, \quad \beta_{\text{NP}} = -\alpha_{\text{NP}} = \frac{\cot \theta}{2\sqrt{2}r}, \quad \mu_{\text{NP}} = -\frac{1}{2r}, \quad \pi_{\text{NP}} = \tau_{\text{NP}} = \gamma_{\text{NP}} = 0. \quad (\text{S111})$$

Applying the operators $\mathcal{A}, \mathcal{B}, \mathcal{C}$ in Eq. (S94) to the combination of the GW-related functions \tilde{R}, \tilde{Y} and phase factor $e^{-i\tilde{\omega}t}$ yields Eqs. (S164)–(S168) in the Sec. III III.d. Therefore, the local inner product $u_{\mu\nu}^* T^{\mu\nu}$ is

$$u_{\mu\nu}^* T^{\mu\nu} = (-T_{nn}\mathcal{A}_{-2}^* - T_{m^*m^*}\mathcal{B}_{-2}^* + T_{nm^*}\mathcal{C}_{-2}^*) + \mathcal{P}(-T_{nn}\mathcal{A}_{+2} - T_{mm}\mathcal{B}_{+2} + T_{nm}\mathcal{C}_{+2}), \quad (\text{S112})$$

where $\mathcal{A}_{-2}^*, \mathcal{A}_{+2}, \mathcal{B}_{-2}^*, \mathcal{B}_{+2}, \mathcal{C}_{-2}^*, \mathcal{C}_{+2}$ denote the complex conjugates of the above operators actions for GW-related functions (Eqs. (S164)–(S168)) and they also are given by Eqs. (S170)–(S175). Additionally, $T_{nn}, T_{mm}, T_{m^*m^*}, T_{nm}, T_{nm^*}$ are the projections of the energy-momentum $T_{\mu\nu}$ onto the Kinnersley null vectors n_μ, m_μ, m_μ^* , as detailed in Eqs. (S176)–(S178).

North/south selection rules and helicity-polarized emission

By performing the angular integration of the local inner product $u_{\mu\nu}^* T^{\mu\nu}$, we obtain the angular inner product in the rescaled radial coordinate \tilde{r}

$$\int \hat{u}_{ab}^* \hat{T}^{ab} d\Omega = \frac{e^{-i(2\omega - \tilde{\omega})t}}{16} \mathcal{F}_{\tilde{\ell}\tilde{m}}(\tilde{r}) = \frac{\mathcal{F}_{\tilde{\ell}\tilde{m}}(\tilde{r})}{16}, \quad (\text{S113})$$

with the quantum numbers $\tilde{\ell}$ and \tilde{m} for GW modes and the function

$$\begin{aligned} \mathcal{F}_{\tilde{\ell}\tilde{m}}(\tilde{r}) = & -\tilde{r}^2 \tilde{R}^*(\tilde{r}) \left(\frac{i}{2}R(\tilde{r}) + R_{,\tilde{r}}(\tilde{r}) \right)^2 I_1 \\ & - \tilde{r}^2 \left[-2i\tilde{R}_{,\tilde{r}}^*(\tilde{r}) + \left(-2 - \frac{2i}{\tilde{r}} + \frac{\tilde{\ell}^2 + \tilde{\ell} - 2}{\tilde{r}^2} \right) \tilde{R}^*(\tilde{r}) \right] R^2(\tilde{r}) I_2 \\ & + 2\tilde{r}^2 \left(-i\tilde{R}^*(\tilde{r}) + \tilde{R}_{,\tilde{r}}^*(\tilde{r}) + \frac{2}{\tilde{r}}\tilde{R}^*(\tilde{r}) \right) \left(\frac{i}{2}R(\tilde{r}) + R_{,\tilde{r}}(\tilde{r}) \right) R(\tilde{r}) I_3. \end{aligned} \quad (\text{S114})$$

Here, I_1, I_2, I_3 are the angular integrals over the angular coordinates (θ, ϕ) . In the following, we focus on the north-south modes of the scalar clouds with $\ell = q, m = \pm q$

$$Y_{qq\pm q}^\pm \begin{cases} Y_{qqq}^+ = A_q e^{iq\phi} (\cos \frac{\theta}{2})^{2q}, & m = q, \\ Y_{qq-q}^- = A_{-q} e^{-iq\phi} (\sin \frac{\theta}{2})^{2q}, & m = -q, \end{cases} \quad (\text{S115})$$

with the normalization coefficients A_q, A_{-q}

$$A_q = A_{-q} = \sqrt{\frac{2q+1}{4\pi}}. \quad (\text{S116})$$

The north-south modes possess the strongest superradiant instability around the magnetic BH. Furthermore, we focus on the dominant GW emission mode $\tilde{\ell} = 2\ell, \tilde{m} = 2m$ in the following analysis. For convenience in notation, we adopt the notation $Y^+ \equiv Y_{qqq}^+$, $Y^- \equiv Y_{qq-q}^-$ for the charged scalar field modes, and ${}_{-2}\tilde{Y} \equiv {}_{-2}\tilde{Y}_{\tilde{\ell}\tilde{m}}$, ${}_{+2}\tilde{Y} \equiv {}_{+2}\tilde{Y}_{\tilde{\ell}\tilde{m}}$ for the GW emission modes.

For the odd-parity perturbation $\mathcal{P} = -1$, one can find $I_1 = -I_1$, $I_2 = -I_2$ and $I_3 = -I_3$ under the parity inversion $(\theta, \phi) \rightarrow (\pi - \theta, \phi + \pi)$. Thus, we have

$$I_1 = \int \left[(\eth \eth {}_{-2}\tilde{Y})^* \sum_{\pm} (Y^{\pm})^2 - (\eth^* \eth^* {}_{+2}\tilde{Y})^* \sum_{\pm} (Y^{\pm})^2 \right] d\Omega = 0, \quad (\text{S117})$$

$$I_2 = \int \left[({}_{-2}\tilde{Y})^* \sum_{\pm} (\eth^* Y^{\pm})^2 - ({}_{+2}\tilde{Y})^* \sum_{\pm} (\eth Y^{\pm})^2 \right] d\Omega = 0, \quad (\text{S118})$$

$$I_3 = \int \left[(\eth^* {}_{-2}\tilde{Y})^* \sum_{\pm} (\eth^* Y^{\pm}) Y^{\pm} - (\eth^* {}_{+2}\tilde{Y})^* \sum_{\pm} (\eth Y^{\pm}) Y^{\pm} \right] d\Omega = 0. \quad (\text{S119})$$

Intuitively, the configuration of the scalar clouds with the north-south modes around the magnetic BH is invariant under the parity inversion. This leads to the non-radiation of odd-parity GWs, which are the characteristic twisting or toroidal modes.

Furthermore, for the even-parity perturbation $\mathcal{P} = 1$, the angular integrals are

$$I_1 = \int \left[(\eth \eth {}_{-2}\tilde{Y})^* \sum_{\pm} (Y^{\pm})^2 + (\eth^* \eth^* {}_{+2}\tilde{Y})^* \sum_{\pm} (Y^{\pm})^2 \right] d\Omega, \quad (\text{S120})$$

$$I_2 = \int \left[({}_{-2}\tilde{Y})^* \sum_{\pm} (\eth^* Y^{\pm})^2 + ({}_{+2}\tilde{Y})^* \sum_{\pm} (\eth Y^{\pm})^2 \right] d\Omega, \quad (\text{S121})$$

$$I_3 = \int \left[(\eth^* {}_{-2}\tilde{Y})^* \sum_{\pm} (\eth^* Y^{\pm}) Y^{\pm} + (\eth^* {}_{+2}\tilde{Y})^* \sum_{\pm} (\eth Y^{\pm}) Y^{\pm} \right] d\Omega. \quad (\text{S122})$$

In Sec. III III.d, our calculation of the angular integrals I_1, I_2, I_3 reveals that the azimuthal angle ϕ integration

$$\int_0^{2\pi} e^{\pm i4q\phi} d\phi = 0, \quad 4q = 2N \in \mathbb{Z}, \quad (\text{S123})$$

vanishes for the angular inner product with $m = q, \tilde{m} = -2q$ and $m = -q, \tilde{m} = 2q$. For instance, the square of the north cloud mode gives $(Y^+)^2 \propto e^{+i2q\phi}$. If the GW mode is chosen with $\tilde{m} = +2q$, the spin-weighted spherical harmonic ${}_{-2}\tilde{Y}_{\tilde{\ell}\tilde{m}}^* \propto e^{-i2q\phi}$ leads to their phases ϕ cancellation and non-zero angular integrals. Conversely, a mismatch with $\tilde{m} = -2q$ produces the above phase factor $e^{+i4q\phi}$, which integrates to zero due to azimuthal phase ϕ single-valuedness. Consequently, the angular integrals I_1, I_2, I_3 vanish, resulting in the absence of the corresponding GW emission. The underlying physics mirrors the angular-momentum selection rules in quantum transitions [78].

In other words, the north scalar cloud governed by Y^+ with $\ell = q, m = q$ radiates GWs exclusively in the mode $\tilde{\ell} = 2q, \tilde{m} = +2q$, with explicit angular integrals

$$I_1^+ = 8\pi \tilde{A}_0^* A_q^2 \sqrt{(\tilde{\ell} - 1)\tilde{\ell}(\tilde{\ell} + 1)(\tilde{\ell} + 2)} B(q + 1, 3q + 1), \quad (\text{S124})$$

$$I_2^+ = 2\pi q^2 A_q^2 [\tilde{A}_{-2}^* I_{-2}^+(q) + \tilde{A}_{+2}^* I_{+2}^+(q)], \quad (\text{S125})$$

$$I_3^+ = 4\pi q A_q^2 [\tilde{A}_{-2}^* J_{-2}^+(q) + \tilde{A}_{+2}^* J_{+2}^+(q)]. \quad (\text{S126})$$

where

$$I_{-2}^+(q) = 2[B(q + 3, 3q - 1) - B(q + 2, 3q - 1) + \frac{1}{4}B(q + 1, 3q - 1)], \quad (\text{S127})$$

$$I_{+2}^+(q) = 2[B(q + 1, 3q + 1) + B(q, 3q + 1) + \frac{1}{4}B(q - 1, 3q + 1)], \quad (\text{S128})$$

$$J_{-2}^+(q) = 2(q - 1)B(q + 3, 3q - 1) - (3q - 1)B(q + 2, 3q - 1) + qB(q + 1, 3q - 1), \quad (\text{S129})$$

$$J_{+2}^+(q) = 2(q + 1)B(q + 1, 3q + 1) + (1 - q)B(q, 3q + 1) - qB(q - 1, 3q + 1), \quad (\text{S130})$$

with the Beta functions B [65] and the normalization coefficients $\tilde{A}_0, \tilde{A}_{\pm 2}$ for $s = 0, \pm 2$ spin-weighted spherical harmonics

$$\tilde{A}_0 = \frac{1}{\sqrt{4\pi B(2q+1, 2q+1)}}, \quad \tilde{A}_{-2} = \tilde{A}_{+2} = \frac{1}{\sqrt{4\pi B(2q+3, 2q-1)}}. \quad (\text{S131})$$

Conversely, the south cloud governed by Y^- with $\ell = q, m = -q$ radiates only GWs in the mode $\tilde{\ell} = 2q, \tilde{m} = -2q$, with the explicit angular integrals

$$I_1^- = 8\pi \tilde{A}_0^* A_{-q}^2 \sqrt{(\tilde{\ell}-1)\tilde{\ell}(\tilde{\ell}+1)(\tilde{\ell}+2)} B(3q+1, q+1), \quad (\text{S132})$$

$$I_2^- = 2\pi q^2 A_{-q}^2 [\tilde{A}_{-2}^* I_{-2}^-(q) + \tilde{A}_{+2}^* I_{+2}^-(q)], \quad (\text{S133})$$

$$I_3^- = 4\pi q A_{-q}^2 [\tilde{A}_{-2}^* J_{-2}^-(q) + \tilde{A}_{+2}^* J_{+2}^-(q)], \quad (\text{S134})$$

where

$$I_{-2}^-(q) = 2[B(3q+3, q-1) - B(3q+2, q-1) + \frac{1}{4}B(3q+1, q-1)], \quad (\text{S135})$$

$$I_{+2}^-(q) = 2[B(3q+1, q+1) - 3B(3q, q+1) + \frac{9}{4}B(3q-1, q+1)], \quad (\text{S136})$$

$$J_{-2}^-(q) = (q-1) \left[2B(3q+3, q-1) - B(3q+2, q-1) \right], \quad (\text{S137})$$

$$J_{+2}^-(q) = -(q+1) \left[3B(3q, q+1) - 2B(3q+1, q+1) \right]. \quad (\text{S138})$$

It is noteworthy that the angular integrals I_2 and I_3 contain Beta functions $B(q-1, \dots)$. For $q = 1$, the angular integrals develop a logarithmic divergence originating from the polar behavior of Y^\pm . We restrict the analysis to $q > 1$ in the analytic evaluation, and leave the $q \leq 1$ case to a separate gauge-covariant treatment. This is distinct from the Kerr BH case, where the scalar cloud radiates GWs only with $\tilde{\ell} = \tilde{m} = 2\ell$.

A crucial comparison concerns the relative magnitudes between the angular integrals for the north scalar cloud (Eqs. (S124)–(S126)) and those for the south scalar cloud (Eqs. (S132)–(S134)). Clearly, for the first angular integral I_1 , the integral I_1^+ is equal to I_1^-

$$I_1^+ = I_1^-. \quad (\text{S139})$$

For the second angular integral I_2 , I_2^+ and I_2^- are not equal, differing by an $\mathcal{O}(1)$ factor, yet share the same order of magnitude:

$$\frac{I_2^+}{I_2^-} = \frac{I_{-2}^+(q) + I_{+2}^+(q)}{I_{-2}^-(q) + I_{+2}^-(q)} \approx \begin{cases} 1.97, & q = 2, \\ 2.53, & q = 3, \\ 3.15, & q = 5, \\ 3.76, & q = 10. \end{cases} \quad (\text{S140})$$

For the third angular integral I_3 , I_3^+ and I_3^- are also unequal, typically opposite in sign, yet of the same order of magnitude:

$$\frac{I_3^+}{I_3^-} = \frac{J_{-2}^+(q) + J_{+2}^+(q)}{J_{-2}^-(q) + J_{+2}^-(q)} \approx \begin{cases} -4.08, & q = 2, \\ -3.72, & q = 3, \\ -3.75, & q = 5, \\ -3.95, & q = 10. \end{cases} \quad (\text{S141})$$

Enhancement scaling with the reduced orbital index ℓ_q of the GW power

Next, we perform the radial integration of the angular inner product $\int \hat{u}_{ab}^* T^{ab} d\Omega$ to obtain the full inner product $\langle u, T \rangle$

$$\langle u, T \rangle = \int \left(\int \hat{u}_{ab}^* T^{ab} d\Omega \right) \tilde{r}^2 d\tilde{r} = \frac{\int \mathcal{F}(\tilde{r}) \tilde{r}^2 d\tilde{r}}{16\tilde{\omega}^3} \quad (\text{S142})$$

For the bound-state solution of the scalar field given by Eq. (S18), we transform the radial coordinate r into a dimensionless radial coordinate $\tilde{r} \equiv \tilde{\omega}r$ and get

$$R_{,\tilde{r}\tilde{r}} + \frac{2}{\tilde{r}}R_{,\tilde{r}} + \left[-\frac{\beta^2}{4} + \frac{\ell(\ell+1)-q^2}{\tilde{r}^2} - \frac{n\beta}{\tilde{r}} \right] R = 0, \quad (\text{S143})$$

where $\beta \equiv \frac{k}{\omega} \approx \frac{\mu M}{n}$. Moreover, the radial integral of $\mathcal{F}(\tilde{r})$ containing I_1, I_2, I_3 is given by Eq. (S229) in Sec. III III.d

$$\begin{aligned} \int \mathcal{F}_{\tilde{\ell}\tilde{m}}(\tilde{r}) \tilde{r}^2 d\tilde{r} &= \int (2iI_2 + iI_3) \tilde{r}^4 \tilde{R}_{,\tilde{r}}^* R^2 d\tilde{r} + \int \left(2I_2 + I_3 + \frac{I_1}{4} + \frac{\beta^2}{4} I_1 \right) \tilde{r}^4 \tilde{R}^* R^2 d\tilde{r} \\ &+ \int (I_1 + 2I_3) \tilde{r}^4 \tilde{R}_{,\tilde{r}}^* (RR') d\tilde{r} + \int (-iI_1 - 2iI_3) \tilde{r}^4 \tilde{R}^* (RR') d\tilde{r} \\ &+ \int (2iI_2 + 2iI_3 + n\beta I_1) \tilde{r}^3 \tilde{R}^* R^2 d\tilde{r} + \int (4I_3) \tilde{r}^3 \tilde{R}^* (RR') d\tilde{r} \\ &+ \int \left[-(\tilde{\ell}^2 + \tilde{\ell} - 2)I_2 - \ell_q(\ell_q + 1)I_1 \right] \tilde{r}^2 \tilde{R}^* R^2 d\tilde{r}. \end{aligned} \quad (\text{S144})$$

In [17], the angular integrals for the Kerr case satisfy the relationship $I_1 = -2I_3$, $I_2 = \frac{\ell(\ell+1)}{(\ell-1)(\ell+2)} I_1$. This relationship, however, does not hold for the magnetic BH case due to the different angular function $Y_{q\ell m}$ in the charged case compared to the neutral Kerr BH.

The bound-state function (Eq. (S21)) for the charged scalar field in the far region can be rewritten as

$$\begin{aligned} R(r) &\simeq A'_R (2kr)^{\ell_q} e^{-kr} U(-n_r, 2\ell_q + 2; 2kr) \\ &\simeq A'_R e^{-kr} (-1)^{n_r} \Gamma(n_r + 1) L_{n_r}^{(2\ell_q + 1)}(0) \left[(2kr)^{\ell_q} + \frac{-n_r}{2\ell_q + 2} (2kr)^{\ell_q + 1} + \dots \right] \\ &= A_R e^{-\frac{\beta}{2}\tilde{r}} \left(\frac{\beta}{2} \right)^{\ell_q} \left[\tilde{r}^{\ell_q} + (\beta\gamma) \tilde{r}^{\ell_q + 1} + \dots \right], \end{aligned} \quad (\text{S145})$$

where generalized Laguerre polynomials $L_{n_r}^{(2\ell_q + 1)}(0)$ [65], the normalization coefficient A_R and parameter γ are given by

$$L_{n_r}^{(2\ell_q + 1)}(0) = \frac{\Gamma(n_r + 2\ell_q + 2)}{\Gamma(2\ell_q + 2)\Gamma(n_r + 1)}, \quad \gamma = \frac{-n_r}{2\ell_q + 2}, \quad (\text{S146})$$

$$A_R = (-1)^{n_r+1} \frac{\sqrt{2E_c}}{\omega} (2k)^{3/2} \frac{2^{\ell_q} \Gamma(n_r + 2\ell_q + 2)}{\Gamma(2\ell_q + 2)} \sqrt{\frac{\Gamma(n_r + 1)}{2n\Gamma(n_r + 2\ell_q + 2)}}, \quad (\text{S147})$$

with $n = n_r + \ell_q + 1$ and the total cloud energy $E_c \equiv \int T_{tt} r^2 dr d\Omega$. Substituting Eq. (S145) into Eq. (S144) and Eq. (S142), the full inner product $\langle u, T \rangle$ takes the form neglecting terms of order $\mathcal{O}(\beta^2)$

$$\begin{aligned} \langle u, T \rangle &\simeq \frac{A_R^2}{16\tilde{\omega}^3} \left(\frac{\beta}{2} \right)^{2\ell_q} \left[\left(2I_2 + \frac{I_1}{4} + I_3 \right) \left(f^{(2)}(\beta) + 2\beta\gamma f^{(3)}(\beta) \right) \right. \\ &+ (-6iI_2 - 2iI_3) \left(f^{(1)}(\beta) + 2\beta\gamma f^{(2)}(\beta) \right) + n\beta I_1 f^{(1)}(\beta) \\ &+ \left(-(\tilde{\ell}^2 + \tilde{\ell} - 2)I_2 - \ell_q(\ell_q + 1)I_1 \right) \left(f^{(0)}(\beta) + 2\beta\gamma f^{(1)}(\beta) \right) \\ &+ \left(-iI_1 - 4iI_2 - 4iI_3 \right) \left(\ell_q f^{(1)}(\beta) + \beta \left((2\ell_q + 1)\gamma - \frac{1}{2} \right) f^{(2)}(\beta) \right) \\ &+ \left(-4I_1 - 4I_3 \right) \left(\ell_q f^{(0)}(\beta) + \beta \left((2\ell_q + 1)\gamma - \frac{1}{2} \right) f^{(1)}(\beta) \right) \\ &\left. - (I_1 + 2I_3) \left(\ell_q(2\ell_q - 1) f^{(0)}(\beta) + 2\beta \ell_q \left((2\ell_q + 1)\gamma - 1 \right) f^{(1)}(\beta) \right) \right]. \end{aligned} \quad (\text{S148})$$

where we defined

$$f^{(N)} \equiv \int_0^\infty \tilde{R}^* \tilde{r}^{2\ell_q + 2 + N} e^{-\beta\tilde{r}} d\tilde{r}, \quad (\text{S149})$$

with $\tilde{R}^*(\tilde{r}) = e^{i\tilde{r}}\tilde{r}^{\tilde{\ell}-2}{}_2F_1(\tilde{\ell}-1, 2\tilde{\ell}+2; -2i\tilde{r})$. The integration of $f^{(0)}$ can be performed as

$$\begin{aligned}
f^{(0)} &= \int_0^\infty \tilde{r}^{2\ell_q+\tilde{\ell}} e^{-(\beta-i)\tilde{r}} F(\tilde{\ell}-1, 2\tilde{\ell}+2; -2i\tilde{r}) d\tilde{r} \\
&= \frac{\Gamma(2\ell_q+\tilde{\ell}+1)}{(\beta-i)^{2\ell_q+\tilde{\ell}+1}} {}_2F_1\left(\tilde{\ell}-1, 2\ell_q+\tilde{\ell}+1; 2\tilde{\ell}+2; \frac{-2i}{\beta-i}\right) \\
&\simeq \Gamma(2\ell_q+\tilde{\ell}+1) (-i)^{-(2\ell_q+\tilde{\ell}+1)} \left(H_0 - i\beta \left[(2\ell_q+\tilde{\ell}+1)H_0 + \frac{(\tilde{\ell}-1)(2\ell_q+\tilde{\ell}+1)}{\tilde{\ell}+1} H_1 \right] \right. \\
&\quad + \beta^2 \left[-\frac{(2\ell_q+\tilde{\ell}+1)(2\ell_q+\tilde{\ell}+2)}{2} H_0 - \frac{(\tilde{\ell}-1)(2\ell_q+\tilde{\ell}+1)(2\ell_q+\tilde{\ell}+2)}{\tilde{\ell}+1} H_1 \right. \\
&\quad \left. \left. - \frac{(\tilde{\ell}-1)\tilde{\ell}(2\ell_q+\tilde{\ell}+1)(2\ell_q+\tilde{\ell}+2)}{(\tilde{\ell}+1)(2\tilde{\ell}+3)} H_2 \right] + O(\beta^3) \right), \tag{S150}
\end{aligned}$$

where

$$H_0 \equiv {}_2F_1\left(\tilde{\ell}-1, 2\ell_q+\tilde{\ell}+1, 2\tilde{\ell}+2; 2\right) \tag{S151}$$

$$H_1 \equiv {}_2F_1\left(\tilde{\ell}, 2\ell_q+\tilde{\ell}+2, 2\tilde{\ell}+3; 2\right) \tag{S152}$$

$$H_2 \equiv {}_2F_1\left(\tilde{\ell}+1, 2\ell_q+\tilde{\ell}+3, 2\tilde{\ell}+4; 2\right). \tag{S153}$$

and $f^{(N)}$ with $N > 0$ are given by differentiating $f^{(0)}$ as

$$f^{(N)} = (-1)^N \frac{d^N f^{(0)}}{d\beta^N}. \tag{S154}$$

Therefore, for the scalar clouds of the north-south modes Y^\pm , the full inner products are

$$\langle u, T \rangle^\pm \simeq \frac{A_R^2}{16} \left(\frac{\beta}{2}\right)^{2\ell_q} \Gamma(2\ell_q+\tilde{\ell}+1) (-i)^{-(2\ell_q+\tilde{\ell}+1)} \Sigma^\pm, \tag{S155}$$

where

$$\Sigma^\pm \equiv I_1^\pm C_1 + I_2^\pm C_2 + I_3^\pm C_3 \tag{S156}$$

and

$$\begin{aligned}
C_1 &= - \left(2\ell_q^2 + \frac{9}{2}\ell_q + \frac{(\tilde{\ell}+1)(\tilde{\ell}+2)}{4} \right) H_0 - \frac{(\tilde{\ell}-1)(\tilde{\ell}+2)(2\ell_q+\tilde{\ell}+1)}{2(\tilde{\ell}+1)} H_1 \\
&\quad - \frac{\tilde{\ell}(\tilde{\ell}-1)(2\ell_q+\tilde{\ell}+1)(2\ell_q+\tilde{\ell}+2)}{2(\tilde{\ell}+1)(2\tilde{\ell}+3)} H_2, \tag{S157}
\end{aligned}$$

$$\begin{aligned}
C_2 &= -(\tilde{\ell}-1)(4\ell_q+3\tilde{\ell}+4)H_0 - \frac{2(\tilde{\ell}-1)(2\ell_q+\tilde{\ell}+1)(2\ell_q+2\tilde{\ell}+1)}{\tilde{\ell}+1} H_1 \\
&\quad - \frac{4\tilde{\ell}(\tilde{\ell}-1)(2\ell_q+\tilde{\ell}+1)(2\ell_q+\tilde{\ell}+2)}{(\tilde{\ell}+1)(2\tilde{\ell}+3)} H_2, \tag{S158}
\end{aligned}$$

$$C_3 = -\tilde{\ell}(\tilde{\ell}+1)H_0 - 2(\tilde{\ell}-1)(2\ell_q+\tilde{\ell}+1)H_1 - \frac{2\tilde{\ell}(\tilde{\ell}-1)(2\ell_q+\tilde{\ell}+1)(2\ell_q+\tilde{\ell}+2)}{(\tilde{\ell}+1)(2\tilde{\ell}+3)} H_2. \tag{S159}$$

Consequently, substituting the outgoing coefficient Z_{out} in Eq. (S109) and the full inner product $\langle u, T \rangle$ in Eq. (S155) into Eq. (S104), the GW power of the modes $\tilde{\ell} = 2q, \tilde{m} = \pm 2q$ from the north-south scalar clouds Y^\pm are respectively

$$P_{\text{GW}}^\pm = C_{n\ell\ell_q}^\pm \left(\frac{E_c}{M}\right)^2 \alpha^{4\ell_q+8}, \tag{S160}$$

where

$$C_{n\ell\ell_q}^{\pm} = \frac{2^{2\tilde{\ell}+3}\pi}{n^{4\ell_q+8}} \frac{\Gamma(\tilde{\ell}-1)^2}{\Gamma(2\tilde{\ell}+2)^2} \frac{\Gamma(2\ell_q+\tilde{\ell}+1)^2}{\Gamma(2\ell_q+2)^4} \frac{\Gamma(n+\ell_q+1)^2}{\Gamma(n-\ell_q)^2} |\Sigma^{\pm}|^2. \quad (\text{S161})$$

The parametric scaling of Eq. (S160) can be understood by contrasting the present charged scalar cloud with the neutral Kerr case. At leading order in the small-coupling limit $\alpha \ll 1$, the scalar clouds around Kerr BHs constructed from spherical harmonics (approximated by spheroidal harmonics), the angular integrals entering the full inner product $\langle u, T \rangle$ satisfy simple identities, $I_1 = -2I_3$ and $I_2 = \frac{\ell(\ell+1)}{(\ell-1)(\ell+2)} I_1$ [17]. When substituted into the general radial integrand in Eq. (S144), these relations enforce cancellations among the leading terms in the small- β expansion, so that the first nonvanishing contribution arises only at higher order in $\beta \sim \alpha/n$. This is the origin of the extra α^2 suppression in the Kerr result $P_{\text{GW}} \propto \alpha^{4\ell+10}$ [17]. In the magnetic case, however, the cloud's angular dependence is governed by monopole harmonics $Y_{q\ell m}$, for which the Kerr identities among I_1, I_2, I_3 no longer hold. As a result, the lowest-order piece of the overlap survives, removing the Kerr cancellation and reducing the parametric suppression by two powers of α . At the same time, the centrifugal behavior in the bound-state wavefunction is controlled by the reduced orbital index ℓ_q (so that $R(r) \sim r^{\ell_q}$ at small r), which further strengthens the overlap relative to the neutral case. Combining these two effects yields the scaling $P_{\text{GW}} \propto \alpha^{4\ell_q+8}$. The comparison between the neutral and charged cases is illustrated in Fig. 2.

A useful intuitive picture is to view the radial overlap as an oscillatory volume integral. The outgoing GW mode carries a rapidly varying phase $\sim e^{i\tilde{\omega}r}$ with $\tilde{\omega} \simeq 2\mu$, so for $r \gtrsim 1/\mu$ the integrand oscillates within a wavelength and the contributions from different radius largely cancel. Meanwhile, the cloud extends to $r_c \sim 1/(\alpha\mu) \gg 1/\mu$ for $\alpha \ll 1$, so most of the cloud's volume lies in this strongly canceling regime. The net overlap therefore receives its dominant contribution from the near-origin region $r \lesssim 1/\mu$, where the phase varies slowly and the integrand can add coherently. Since smaller ℓ_q weakens the small- r suppression ($R \sim r^{\ell_q}$ is less suppressed than r^ℓ), the coherent near-origin contribution is enhanced, leading to a larger GW power.

III.d. Technical ingredients

In this subsection we evaluate the inner product between the homogeneous metric perturbation and the matter source, which decomposes into an angular part and a radial part.

Local inner product $u_{\mu\nu}^* T^{\mu\nu}$ in the Chrzanowski formalism

The Chrzanowski formula Eq. (S94) of the homogeneous perturbation is

$$u_{\mu\nu}(\tilde{\ell}, \tilde{m}, \tilde{\omega}, P) = (-n_\mu n_\nu \mathcal{A} - m_\mu m_\nu \mathcal{B} + n_{(\mu} m_{\nu)} \mathcal{C}) +_2 R_{\tilde{\ell}\tilde{m}}^{\tilde{\omega}}(r) -_2 S_{\tilde{\ell}\tilde{m}}^{\tilde{\omega}}(\theta) e^{i\tilde{m}\phi - i\tilde{\omega}t} + P \left(-n_\mu n_\nu \mathcal{A}^* - m_\mu^* m_\nu^* \mathcal{B}^* + n_{(\mu} m_{\nu)}^* \mathcal{C}^* \right) +_2 R_{\tilde{\ell}\tilde{m}}^{\tilde{\omega}}(r) +_2 S_{\tilde{\ell}\tilde{m}}^{\tilde{\omega}}(\theta) e^{i\tilde{m}\phi - i\tilde{\omega}t}, \quad (\text{S162})$$

and then the results of applying the operators in Eqs. (S95)–(S97) to the functions $\pm_2 R_{\tilde{\ell}\tilde{m}} \pm_2 Y_{\tilde{\ell}\tilde{m}} e^{-i\tilde{\omega}t}$

$$\mathcal{A} \left(\tilde{R}_{-2} \tilde{Y} e^{-i\tilde{\omega}t} \right) = \frac{\tilde{r}^2}{2\tilde{\omega}^2} \tilde{R} \tilde{\partial} \tilde{\partial}_{-2} \tilde{Y} e^{-i\tilde{\omega}t}, \quad (\text{S163})$$

$$\mathcal{A}^* \left(\tilde{R}_{+2} \tilde{Y} e^{-i\tilde{\omega}t} \right) = \frac{\tilde{r}^2}{2\tilde{\omega}^2} \tilde{R} \tilde{\partial}^* \tilde{\partial}^*_{+2} \tilde{Y} e^{-i\tilde{\omega}t}, \quad (\text{S164})$$

$$\mathcal{B} \left(\tilde{R}_{-2} \tilde{Y} e^{-i\tilde{\omega}t} \right) = \frac{\tilde{r}^4}{4\tilde{\omega}^2} \left[2i\tilde{R}_{,\tilde{r}} + \left(-2 + \frac{2i}{\tilde{r}} + \frac{\tilde{\ell}^2 + \tilde{\ell} - 2}{\tilde{r}^2} \right) \tilde{R} \right] -_2 \tilde{Y} e^{-i\tilde{\omega}t}, \quad (\text{S165})$$

$$\mathcal{B}^* \left(\tilde{R}_{+2} \tilde{Y} e^{-i\tilde{\omega}t} \right) = \frac{\tilde{r}^4}{4\tilde{\omega}^2} \left[2i\tilde{R}_{,\tilde{r}} + \left(-2 + \frac{2i}{\tilde{r}} + \frac{\tilde{\ell}^2 + \tilde{\ell} - 2}{\tilde{r}^2} \right) \tilde{R} \right] +_2 \tilde{Y} e^{-i\tilde{\omega}t}, \quad (\text{S166})$$

$$\mathcal{C} \left(\tilde{R}_{-2} \tilde{Y} e^{-i\tilde{\omega}t} \right) = \frac{\tilde{r}^3}{\sqrt{2\tilde{\omega}^2}} \left(i\tilde{R} + \tilde{R}_{,\tilde{r}} + \frac{2}{\tilde{r}} \tilde{R} \right) \tilde{\partial}_{-2} \tilde{Y} e^{-i\tilde{\omega}t}, \quad (\text{S167})$$

$$\mathcal{C}^* \left(\tilde{R}_{+2} \tilde{Y} e^{-i\tilde{\omega}t} \right) = \frac{\tilde{r}^3}{\sqrt{2\tilde{\omega}^2}} \left(i\tilde{R} + \tilde{R}_{,\tilde{r}} + \frac{2}{\tilde{r}} \tilde{R} \right) \tilde{\partial}^* +_2 \tilde{Y} e^{-i\tilde{\omega}t}. \quad (\text{S168})$$

Therefore, the local inner product can be given by

$$u_{\mu\nu}^* T^{\mu\nu} = (-\hat{T}_{nn}\mathcal{A}_{-2}^* - \hat{T}_{m^*m^*}\mathcal{B}_{-2}^* + \hat{T}_{nm^*}\mathcal{C}_{-2}^*) + P(-\hat{T}_{nn}\mathcal{A}_{+2} - \hat{T}_{mm}\mathcal{B}_{+2} + \hat{T}_{nm}\mathcal{C}_{+2}), \quad (\text{S169})$$

where $\mathcal{A}_{-2}^*, \mathcal{A}_{+2}, \mathcal{B}_{-2}^*, \mathcal{B}_{+2}, \mathcal{C}_{-2}^*, \mathcal{C}_{+2}$ are the complex conjugates of the above results Eqs. (S164)–(S168)

$$\mathcal{A}_{-2}^* = \frac{\tilde{r}^2}{2\tilde{\omega}^2} \tilde{R}^* (\eth \eth_{-2} \tilde{Y})^* e^{i\tilde{\omega}t}, \quad (\text{S170})$$

$$\mathcal{A}_{+2} = \frac{\tilde{r}^2}{2\tilde{\omega}^2} \tilde{R}^* (\eth^* \eth^*_{+2} \tilde{Y})^* e^{i\tilde{\omega}t}, \quad (\text{S171})$$

$$\mathcal{B}_{-2}^* = \frac{\tilde{r}^4}{4\tilde{\omega}^2} \left[-2i\tilde{R}_{,\tilde{r}}^* + \left(-2 - \frac{2i}{\tilde{r}} + \frac{\tilde{\ell}^2 + \tilde{\ell} - 2}{\tilde{r}^2} \right) \tilde{R}^* \right] (-_2 \tilde{Y})^* e^{i\tilde{\omega}t}, \quad (\text{S172})$$

$$\mathcal{B}_{+2} = \frac{\tilde{r}^4}{4\tilde{\omega}^2} \left[-2i\tilde{R}_{,\tilde{r}}^* + \left(-2 - \frac{2i}{\tilde{r}} + \frac{\tilde{\ell}^2 + \tilde{\ell} - 2}{\tilde{r}^2} \right) \tilde{R}^* \right] (+_2 \tilde{Y})^* e^{i\tilde{\omega}t}, \quad (\text{S173})$$

$$\mathcal{C}_{-2}^* = \frac{\tilde{r}^3}{\sqrt{2}\tilde{\omega}^2} \left(-i\tilde{R}^* + \tilde{R}_{,\tilde{r}}^* + \frac{2}{\tilde{r}} \tilde{R}^* \right) (\eth_{-2} \tilde{Y})^* e^{i\tilde{\omega}t}, \quad (\text{S174})$$

$$\mathcal{C}_{+2} = \frac{\tilde{r}^3}{\sqrt{2}\tilde{\omega}^2} \left(-i\tilde{R}^* + \tilde{R}_{,\tilde{r}}^* + \frac{2}{\tilde{r}} \tilde{R}^* \right) (\eth_{+2} \tilde{Y})^* e^{i\tilde{\omega}t}, \quad (\text{S175})$$

and $T_{nn}, T_{mm}, T_{m^*m^*}, T_{nm}, T_{nm^*}$ are the projections of the energy-momentum $T_{\mu\nu}$ on the Kinnersley null vectors n_μ, m_μ, m_μ^*

$$T_{nn} \equiv T_{\mu\nu} n^\mu n^\nu = \frac{\tilde{\omega}^2}{8} \left(\frac{i}{2} R + R_{,\tilde{r}} \right)^2 Y^2 e^{-2i\tilde{\omega}t}, \quad (\text{S176})$$

$$T_{mm} \equiv T_{\mu\nu} m^\mu m^\nu = \frac{\tilde{\omega}^2}{4\tilde{r}^2} R^2 (\eth Y)^2 e^{-2i\tilde{\omega}t}, \quad (\text{S177})$$

$$T_{m^*m^*} \equiv T_{\mu\nu} m^{*\mu} m^{*\nu} = \frac{\tilde{\omega}^2}{4\tilde{r}^2} R^2 (\eth^* Y)^2 e^{-2i\tilde{\omega}t}, \quad (\text{S178})$$

$$T_{nm} \equiv T_{\mu\nu} n^\mu m^\nu = \frac{\tilde{\omega}^2}{4\sqrt{2}\tilde{r}} \left(\frac{i}{2} R + R_{,\tilde{r}} \right) R (\eth Y) Y e^{-2i\tilde{\omega}t},$$

$$T_{nm^*} \equiv T_{\mu\nu} n^\mu m^{*\nu} = \frac{\tilde{\omega}^2}{4\sqrt{2}\tilde{r}} \left(\frac{i}{2} R + R_{,\tilde{r}} \right) R (\eth^* Y) Y e^{-2i\tilde{\omega}t}.$$

Angular source integrals I_1, I_2, I_3 and the $(\tilde{\ell}, \tilde{m}) = (2q, \pm 2q)$ selection rule

In this section, we calculate the three angular integrals I_1, I_2, I_3 in Eqs. (S120)–(S122) for even-parity perturbation $\mathcal{P} = +1$.

For the first angular integral I_1 , we can use the eth operator [79] to act on the spin-weighted spherical harmonics

$$\eth ({}_s Y_{\tilde{\ell}\tilde{m}}) = +\sqrt{(\tilde{\ell}-s)(\tilde{\ell}+s+1)} {}_{s+1} Y_{\tilde{\ell}\tilde{m}}, \quad \eth^* ({}_s Y_{\tilde{\ell}\tilde{m}}) = -\sqrt{(\tilde{\ell}+s)(\tilde{\ell}-s+1)} {}_{s-1} Y_{\tilde{\ell}\tilde{m}}. \quad (\text{S179})$$

Thus, the angular integral I_1 can be written as

$$I_1 = \int \left[(\eth \eth_{-2} \tilde{Y})^* \sum_{\pm} (Y^{\pm})^2 + (\eth^* \eth^*_{+2} \tilde{Y})^* \sum_{\pm} (Y^{\pm})^2 \right] d\Omega$$

$$= 2\sqrt{(\tilde{\ell}-1)\tilde{\ell}(\tilde{\ell}+1)(\tilde{\ell}+2)} \int {}_0 \tilde{Y}_{\tilde{\ell}\tilde{m}}^* \left((Y_{qqq}^+)^2 + (Y_{qq-q}^-)^2 \right) d\Omega$$

where the $s = 0$ spin-weighted spherical harmonics with $\tilde{\ell} = 2\ell, \tilde{m} = 2m$ are given by

$${}_0 \tilde{Y}_{\tilde{\ell}\tilde{m}} = Y_{2\ell 2m} = \tilde{A}_0 e^{2im\phi} (\sin \frac{\theta}{2} \cos \frac{\theta}{2})^{2\ell}, \quad \tilde{A}_0 = \frac{1}{\sqrt{4\pi B(2q+1, 2q+1)}} \quad (\text{S181})$$

and the north-south monopole modes of the scalar cloud $\ell = q > 0$, $m = \pm q$

$$Y_{qq\pm q}^{\pm} \begin{cases} Y_{qqq}^+ = A_q e^{iq\phi} (\cos \frac{\theta}{2})^{2q}, & m = q, \\ Y_{qq-q}^- = A_{-q} e^{-iq\phi} (\sin \frac{\theta}{2})^{2q}, & m = -q, \end{cases} \quad (\text{S182})$$

with the normalization coefficients $\tilde{A}_0, A_{\pm q}$

$$A_q = A_{-q} = \sqrt{\frac{2q+1}{4\pi}}. \quad (\text{S183})$$

Thus, we can obtain the following equations

$${}_0\tilde{Y}_{\tilde{\ell}\tilde{m}}^*(Y^+)^2 = \tilde{A}_0^* A_q^2 (\sin \frac{\theta}{2})^{2q} (\cos \frac{\theta}{2})^{6q}, \quad m = q, \tilde{m} = 2q, \quad (\text{S184})$$

$${}_0\tilde{Y}_{\tilde{\ell}\tilde{m}}^*(Y^+)^2 = \tilde{A}_0^* A_q^2 e^{i4q\phi} (\sin \frac{\theta}{2})^{2q} (\cos \frac{\theta}{2})^{6q}, \quad m = q, \tilde{m} = -2q, \quad (\text{S185})$$

$${}_0\tilde{Y}_{\tilde{\ell}\tilde{m}}^*(Y^-)^2 = \tilde{A}_0^* A_{-q}^2 (\sin \frac{\theta}{2})^{6q} (\cos \frac{\theta}{2})^{2q}, \quad m = -q, \tilde{m} = -2q, \quad (\text{S186})$$

$${}_0\tilde{Y}_{\tilde{\ell}\tilde{m}}^*(Y^-)^2 = \tilde{A}_0^* A_{-q}^2 e^{-i4q\phi} (\sin \frac{\theta}{2})^{6q} (\cos \frac{\theta}{2})^{2q}, \quad m = -q, \tilde{m} = 2q. \quad (\text{S187})$$

Then we integrate the above equations over the angles and find

$$\int_0^{2\pi} e^{\pm i4q\phi} d\phi = 0 \quad (\text{S188})$$

for Eq. (S185) and Eq. (S187). The underlying physics is the same as that determining the angular-momentum selection rules in quantum transitions [78]. In other words, for the angular integral I_1 , only the north scalar field mode Y^+ with $\ell = q, m = q$ contributes to the GW mode with $\tilde{\ell} = 2q, \tilde{m} = 2q$. Conversely, only the south scalar field mode Y^- with $\ell = q, m = -q$ contributes to the GW mode with $\tilde{\ell} = 2q, \tilde{m} = -2q$. Consequently, we have the angular integrals for the GW mode with $\tilde{\ell} = 2q, \tilde{m} = 2q$

$$\begin{aligned} & \int {}_0\tilde{Y}_{\tilde{\ell}\tilde{m}}^*(Y_{qqq}^+)^2 d\Omega \\ &= 4\pi \tilde{A}_0^* A_q^2 \int_0^\pi (\sin \frac{\theta}{2})^{2q+1} (\cos \frac{\theta}{2})^{6q+1} d\theta = 4\pi \tilde{A}_0^* A_q^2 \int_0^1 u^q (1-u)^{3q} du \\ &= 4\pi \tilde{A}_0^* A_q^2 B(q+1, 3q+1) = 4\pi \tilde{A}_0^* A_q^2 \frac{\Gamma(q+1)\Gamma(3q+1)}{\Gamma(4q+2)}, \end{aligned} \quad (\text{S189})$$

and for the GW mode with $\tilde{\ell} = 2q, \tilde{m} = -2q$

$$\begin{aligned} & \int {}_0\tilde{Y}_{\tilde{\ell}\tilde{m}}^*(Y_{qq-q}^-)^2 d\Omega \\ &= 4\pi \tilde{A}_0^* A_{-q}^2 \int_0^\pi (\sin \frac{\theta}{2})^{6q+1} (\cos \frac{\theta}{2})^{2q+1} d\theta = 4\pi \tilde{A}_0^* A_{-q}^2 \int_0^1 u^{3q} (1-u)^q du \\ &= 4\pi \tilde{A}_0^* A_{-q}^2 B(3q+1, q+1) = 4\pi \tilde{A}_0^* A_{-q}^2 \frac{\Gamma(3q+1)\Gamma(q+1)}{\Gamma(4q+2)}, \end{aligned} \quad (\text{S190})$$

Here, we set $u = \sin^2 \frac{\theta}{2}$. Substituting the above integrals into Eq. (S180), the angular integrals I_1^+ for the north mode Y^+ and I_1^- for south mode are given by

$$I_1^+ = 8\pi \tilde{A}_0^* A_q^2 \sqrt{(\tilde{\ell}-1)\tilde{\ell}(\tilde{\ell}+1)(\tilde{\ell}+2)} B(q+1, 3q+1), \quad (\text{S191})$$

$$I_1^- = 8\pi \tilde{A}_0^* A_{-q}^2 \sqrt{(\tilde{\ell}-1)\tilde{\ell}(\tilde{\ell}+1)(\tilde{\ell}+2)} B(3q+1, q+1). \quad (\text{S192})$$

Next, we calculate the second angular integral I_2 :

$$I_2 = \int \left({}_{-2}\tilde{Y} \right)^* \left((\tilde{\partial}^* Y_{qqq}^+)^2 + (\tilde{\partial}^* Y_{qq-q}^-)^2 \right) + \left({}_{+2}\tilde{Y} \right)^* \left((\tilde{\partial} Y_{qqq}^+)^2 + (\tilde{\partial} Y_{qq-q}^-)^2 \right) d\Omega, \quad (\text{S193})$$

where the $s = \pm 2$ spin-weighted spherical harmonics with $\tilde{\ell} = 2\ell, \tilde{m} = 2m$ are

$${}_{-2}Y_{\tilde{\ell}\tilde{m}} = \tilde{A}_{-2}e^{i\tilde{m}\phi}(\sin \frac{\theta}{2})^{\tilde{\ell}-s}(\cos \frac{\theta}{2})^{\tilde{\ell}+s} = \tilde{A}_{-2}e^{i\tilde{m}\phi}(\sin \frac{\theta}{2})^{2q+2}(\cos \frac{\theta}{2})^{2q-2}, \quad (\text{S194})$$

$${}_{+2}Y_{\tilde{\ell}\tilde{m}} = \tilde{A}_{+2}e^{i\tilde{m}\phi}(\sin \frac{\theta}{2})^{\tilde{\ell}-s}(\cos \frac{\theta}{2})^{\tilde{\ell}+s} = \tilde{A}_{+2}e^{i\tilde{m}\phi}(\sin \frac{\theta}{2})^{2q-2}(\cos \frac{\theta}{2})^{2q+2}, \quad (\text{S195})$$

with the normalization coefficients

$$\tilde{A}_{-2} = \tilde{A}_{+2} = \frac{1}{\sqrt{4\pi B(2q+3, 2q-1)}}. \quad (\text{S196})$$

Since the monopole harmonics Y^\pm are not spin-weighted spherical harmonics and do not satisfy Eq. (S179), we directly compute the action of the \eth operator [79]

$$\eth := -\left(\partial_\theta + \frac{i}{\sin \theta} \partial_\phi - s \cot \theta\right), \quad (\text{S197})$$

$$\eth^* := -\left(\partial_\theta - \frac{i}{\sin \theta} \partial_\phi + s \cot \theta\right) \quad (\text{S198})$$

for the scalar field ($s = 0$) on the monopole harmonics Y^\pm :

$$\eth Y_{qq\pm q}^\pm = \begin{cases} \eth Y_{qqq}^+ = q A_q e^{iq\phi} \cos \frac{\theta}{2}^{2q-1} \left(\frac{1+2 \sin^2 \frac{\theta}{2}}{2 \sin \frac{\theta}{2}} \right) \\ \eth Y_{qq-q}^- = -q A_{-q} e^{-iq\phi} \sin \frac{\theta}{2}^{2q-1} \left(\frac{1+2 \cos^2 \frac{\theta}{2}}{2 \cos \frac{\theta}{2}} \right) \end{cases} \quad (\text{S199})$$

$$\eth^* Y_{qq\pm q}^\pm = \begin{cases} \eth^* Y_{qqq}^+ = q A_q e^{iq\phi} \cos \frac{\theta}{2}^{2q-1} \left(\frac{2 \sin^2 \frac{\theta}{2}-1}{2 \sin \frac{\theta}{2}} \right) \\ \eth^* Y_{qq-q}^- = -q A_{-q} e^{-iq\phi} \sin \frac{\theta}{2}^{2q-1} \left(\frac{2 \cos^2 \frac{\theta}{2}-1}{2 \cos \frac{\theta}{2}} \right) \end{cases} \quad (\text{S200})$$

Similarly, for the angular integral I_2 , only the north scalar field mode Y^+ with $\ell = q, m = q$ contributes to the GW mode with $\tilde{\ell} = 2q, \tilde{m} = 2q$. Conversely, only the south scalar field mode Y^- with $\ell = q, m = -q$ contributes to the GW mode with $\tilde{\ell} = 2q, \tilde{m} = -2q$. Therefore, the angular integrals I_2^+ for the north mode Y^+ and I_2^- for south mode Y^- are

$$\begin{aligned} I_2^+ &= \int \left({}_{-2}\tilde{Y} \right)^* \left(\eth^* Y_{qqq}^+ \right)^2 + \left({}_{+2}\tilde{Y} \right)^* \left(\eth Y_{qqq}^+ \right)^2 d\Omega \\ &= 2\pi q^2 A_q^2 [\tilde{A}_{-2}^* I_{-2}^+(q) + \tilde{A}_{+2}^* I_{+2}^+(q)], \end{aligned} \quad (\text{S201})$$

$$\begin{aligned} I_2^- &= \int \left({}_{-2}\tilde{Y} \right)^* \left(\eth^* Y_{qq-q}^- \right)^2 + \left({}_{+2}\tilde{Y} \right)^* \left(\eth Y_{qq-q}^- \right)^2 d\Omega \\ &= 2\pi q^2 A_{-q}^2 [\tilde{A}_{-2}^* I_{-2}^-(q) + \tilde{A}_{+2}^* I_{+2}^-(q)], \end{aligned} \quad (\text{S202})$$

where

$$I_{-2}^+(q) = 2[B(q+3, 3q-1) - B(q+2, 3q-1) + \frac{1}{4}B(q+1, 3q-1)], \quad (\text{S203})$$

$$I_{+2}^+(q) = 2[B(q+1, 3q+1) + B(q, 3q+1) + \frac{1}{4}B(q-1, 3q+1)], \quad (\text{S204})$$

$$I_{-2}^-(q) = 2[B(3q+3, q-1) - B(3q+2, q-1) + \frac{1}{4}B(3q+1, q-1)], \quad (\text{S205})$$

$$I_{+2}^-(q) = 2[B(3q+1, q+1) - 3B(3q, q+1) + \frac{9}{4}B(3q-1, q+1)]. \quad (\text{S206})$$

We now proceed to the calculation of the final angular integral I_3

$$I_3 = \int \left[(\eth^* {}_{-2}\tilde{Y})^* \sum_{\pm} (\eth^* Y^\pm) Y^\pm + (\eth^* {}_{+2}\tilde{Y})^* \sum_{\pm} (\eth Y^\pm) Y^\pm \right] d\Omega \quad (\text{S207})$$

where Eq. (S198) and Eqs. (S194)–(S195) yield

$$(\tilde{\mathcal{D}}^*_{-2}\tilde{Y}_{2q,2q})^* = 2\tilde{A}_{-2}^*e^{-i2q\phi}(\sin\frac{\theta}{2})^{2q+1}(\cos\frac{\theta}{2})^{2q-3}[(q-1)(\sin\frac{\theta}{2})^2 - q] \quad (\text{S208})$$

$$(\tilde{\mathcal{D}}^*_{+2}\tilde{Y}_{2q,2q})^* = 2\tilde{A}_{+2}^*e^{-i2q\phi}(\sin\frac{\theta}{2})^{2q-3}(\cos\frac{\theta}{2})^{2q+1}[(q+1)(\sin\frac{\theta}{2})^2 - q] \quad (\text{S209})$$

$$(\tilde{\mathcal{D}}^*_{-2}\tilde{Y}_{2q,-2q})^* = 2(q-1)\tilde{A}_{-2}^*e^{+i2q\phi}(\sin\frac{\theta}{2})^{2q+3}(\cos\frac{\theta}{2})^{2q-3} \quad (\text{S210})$$

$$(\tilde{\mathcal{D}}^*_{+2}\tilde{Y}_{2q,-2q})^* = 2(q+1)\tilde{A}_{+2}^*e^{+i2q\phi}(\sin\frac{\theta}{2})^{2q-1}(\cos\frac{\theta}{2})^{2q+1} \quad (\text{S211})$$

Similarly, the selection rule in Eq. (S188) also holds, substituting Eqs. (S200) and Eqs. (S182) into the integral I_3 . For the angular integral I_3 , only the north scalar field mode Y^+ ($\ell = q, m = q$) contributes to the GW mode with $\tilde{\ell} = 2q, \tilde{m} = 2q$. While only the south scalar field mode Y^- ($\ell = q, m = -q$) contributes to the GW mode with $\tilde{\ell} = 2q, \tilde{m} = -2q$. The resulting integrals are

$$I_3^+ = 4\pi q A_{+q}^2 [\tilde{A}_{-2}^* J_{-2}^+(q) + \tilde{A}_{+2}^* J_{+2}^+(q)], \quad (\text{S212})$$

$$I_3^- = 4\pi q A_{-q}^2 [\tilde{A}_{-2}^* J_{-2}^-(q) + \tilde{A}_{+2}^* J_{+2}^-(q)], \quad (\text{S213})$$

where

$$J_{-2}^+(q) = 2(q-1) B(q+3, 3q-1) - (3q-1) B(q+2, 3q-1) + q B(q+1, 3q-1), \quad (\text{S214})$$

$$J_{+2}^+(q) = 2(q+1) B(q+1, 3q+1) + (1-q) B(q, 3q+1) - q B(q-1, 3q+1), \quad (\text{S215})$$

$$J_{-2}^-(q) = (q-1) \left[2B(3q+3, q-1) - B(3q+2, q-1) \right], \quad (\text{S216})$$

$$J_{+2}^-(q) = -(q+1) \left[3B(3q, q+1) - 2B(3q+1, q+1) \right]. \quad (\text{S217})$$

Radial source integral of the function $\mathcal{F}_{\tilde{\ell}\tilde{m}}(\tilde{r})$

The function $\mathcal{F}_{\tilde{\ell}\tilde{m}}(\tilde{r})$ of the angular inner product $\int \hat{u}_{ab}^* \hat{T}^{ab} d\Omega$ in Eq. (S113) is given by

$$\begin{aligned} \mathcal{F}_{\tilde{\ell}\tilde{m}}(\tilde{r}) = & -\tilde{r}^2 \tilde{R}^* \left(\frac{i}{2} R + R_{,\tilde{r}} \right)^2 I_1 - \tilde{r}^2 \left[-2i\tilde{R}_{,\tilde{r}}^* + \left(-2 - \frac{2i}{\tilde{r}} + \frac{\tilde{\ell}^2 + \tilde{\ell} - 2}{\tilde{r}^2} \right) \tilde{R}^* \right] R^2 I_2 \\ & - \tilde{r}^2 \left(2i\tilde{R}^* - 2\tilde{R}_{,\tilde{r}}^* - \frac{4}{\tilde{r}}\tilde{R}^* \right) \left(\frac{i}{2} R + R_{,\tilde{r}} \right) R I_3. \end{aligned} \quad (\text{S218})$$

For the first term containing the angular integral I_1 in the $\mathcal{F}_{\tilde{\ell}\tilde{m}}(\tilde{r})$ function

$$-\tilde{r}^2 \tilde{R}^* \left(\frac{i}{2} R + R_{,\tilde{r}} \right)^2 I_1 = -\tilde{r}^2 \tilde{R}^* (R'^2 + iRR' - R^2/4) I_1, \quad (\text{S219})$$

we perform the radial integration separately for each component of the term. Then using integration by parts and the radial equation (S143) in a dimensionless radial coordinate \tilde{r} for the charged scalar field,

$$R_{,\tilde{r}\tilde{r}} + \frac{2}{\tilde{r}} R_{,\tilde{r}} + \left[-\frac{\beta^2}{4} + \frac{\ell(\ell+1) - q^2}{\tilde{r}^2} - \frac{n\beta}{\tilde{r}} \right] R = 0, \quad (\text{S220})$$

we obtain

$$\begin{aligned} I_1 & \int \left(-\tilde{r}^2 \tilde{R}^* R'^2 \right) \tilde{r}^2 d\tilde{r} \\ & = I_1 \left[\int \tilde{r}^2 \tilde{R}_{,\tilde{r}}^* (\tilde{r}^2 RR') d\tilde{r} + \int 2\tilde{r} \tilde{R}^* (\tilde{r}^2 RR') d\tilde{r} + \int \tilde{r}^4 \tilde{R}^* (RR'') d\tilde{r} \right] \\ & = I_1 \left[\int \tilde{r}^2 \tilde{R}_{,\tilde{r}}^* (\tilde{r}^2 RR') d\tilde{r} + \int \left(\frac{\beta^2}{4} \tilde{r}^4 - \ell_q(\ell_q+1) \tilde{r}^2 + n\beta \tilde{r}^3 \right) \tilde{R}^* R^2 d\tilde{r} \right] \end{aligned} \quad (\text{S221})$$

and

$$I_1 \left[- \int i\tilde{r}^4 \tilde{R}^* (RR') d\tilde{r} + \int \tilde{r}^4 \tilde{R}^* (R^2/4) d\tilde{r} \right]. \quad (\text{S222})$$

For the second term containing the angular integral I_2 in the $\mathcal{F}_{\tilde{\ell}\tilde{m}}(\tilde{r})$ function

$$- \tilde{r}^2 \left[-2i\tilde{R}_{,\tilde{r}}^* + \left(-2 - \frac{2i}{\tilde{r}} + \frac{\tilde{\ell}^2 + \tilde{\ell} - 2}{\tilde{r}^2} \right) \tilde{R}^* \right] R^2 I_2, \quad (\text{S223})$$

we also integrate the term over the radial coordinate

$$2iI_2 \int \tilde{r}^4 \tilde{R}_{,\tilde{r}}^* R^2 dr + I_2 \int \tilde{r}^4 \left(2 + \frac{2i}{\tilde{r}} - \frac{\tilde{\ell}^2 + \tilde{\ell} - 2}{\tilde{r}^2} \right) \tilde{R}^* R^2 d\tilde{r}. \quad (\text{S224})$$

For the third term containing the angular integral I_3 in the $\mathcal{F}_{\tilde{\ell}\tilde{m}}(\tilde{r})$ function

$$- \tilde{r}^2 \left(2i\tilde{R}^* - 2\tilde{R}_{,\tilde{r}}^* - \frac{4}{\tilde{r}}\tilde{R}^* \right) \left(\frac{i}{2}R + R_{,\tilde{r}} \right) RI_3, \quad (\text{S225})$$

the radial integration is carried out for each component of this term

$$-I_3 \int 2i\tilde{r}^4 \tilde{R}^* (iR^2/2 + RR') d\tilde{r} = I_3 \int \tilde{r}^4 \tilde{R}^* (R^2) d\tilde{r} - I_3 \int 2i\tilde{r}^4 \tilde{R}^* (RR') d\tilde{r}, \quad (\text{S226})$$

$$I_3 \int 2\tilde{r}^4 \tilde{R}_{,\tilde{r}}^* (R'R + iR^2/2) d\tilde{r} = I_3 \int 2\tilde{r}^2 \tilde{R}_{,\tilde{r}}^* (\tilde{r}^2 R'R) d\tilde{r} + I_3 \int 2\tilde{r}^4 \tilde{R}_{,\tilde{r}}^* (iR^2/2) d\tilde{r}, \quad (\text{S227})$$

$$I_3 \int 4\tilde{r}^3 \tilde{R}^* (iR^2/2 + RR') d\tilde{r} = I_3 \int 2i\tilde{r}^3 \tilde{R}^* R^2 d\tilde{r} + I_3 \int 4\tilde{r}^3 \tilde{R}^* (RR') d\tilde{r}. \quad (\text{S228})$$

Summing the radial integrals of all three terms containing angular integrals I_1, I_2, I_3 and rearranging yields the radial integral of the function $\mathcal{F}_{\tilde{\ell}\tilde{m}}(\tilde{r})$

$$\begin{aligned} \int \mathcal{F}_{\tilde{\ell}\tilde{m}}(\tilde{r}) \tilde{r}^2 d\tilde{r} &= \int (2iI_2 + iI_3) \tilde{r}^4 \tilde{R}_{,\tilde{r}}^* R^2 d\tilde{r} + \int \left(2I_2 + I_3 + \frac{I_1}{4} + \frac{\beta^2}{4} I_1 \right) \tilde{r}^4 \tilde{R}^* R^2 d\tilde{r} \\ &\quad + \int (I_1 + 2I_3) \tilde{r}^4 \tilde{R}_{,\tilde{r}}^* (RR') d\tilde{r} + \int (-iI_1 - 2iI_3) \tilde{r}^4 \tilde{R}^* (RR') d\tilde{r} \\ &\quad + \int (2iI_2 + 2iI_3 + n\beta I_1) \tilde{r}^3 \tilde{R}^* R^2 d\tilde{r} + \int (4I_3) \tilde{r}^3 \tilde{R}^* (RR') d\tilde{r} \\ &\quad + \int \left[-(\tilde{\ell}^2 + \tilde{\ell} - 2)I_2 - \ell_q(\ell_q + 1)I_1 \right] \tilde{r}^2 \tilde{R}^* R^2 d\tilde{r}. \end{aligned} \quad (\text{S229})$$

IV. MASS EVOLUTION AND GRAVITATIONAL-WAVE WAVEFORM OF ELECTRICALLY CHARGED SCALAR CLOUDS

IV.a. Coupled BH-cloud mass and spin evolution for charged scalar clouds

The coupled evolution equations for the BH-cloud system are given by

$$\frac{dM}{dt} = -2\omega_I M_c, \quad (\text{S230})$$

$$\frac{dJ}{dt} = -\frac{2m\omega_I}{\omega_R} M_c, \quad (\text{S231})$$

$$\frac{dM_c}{dt} = 2\omega_I M_c - P_{\text{GW}}. \quad (\text{S232})$$

where P_{GW} denotes the GW energy loss from the cloud. The BH angular-momentum evolution Eq. (S231) follows from Eq. (S230) by using $\delta J/\delta M = m/\omega_R$ [3]. In many superradiant scenarios one has a clear hierarchy $\tau_{\text{SR}} \ll \tau_{\text{GW}}$ at

early times, so that the GW term can be neglected to leading order and the cloud grows approximately exponentially, $M_c \propto \exp(2\omega_I t)$. As the cloud extracts spin, Ω_H decreases and the system approaches the superradiant threshold $m\Omega_H \simeq \omega_R$, causing $\omega_I \propto (m\Omega_H - \omega_R) \rightarrow 0$ and leading to saturation when $m\Omega_H = \omega_R$. Afterwards the evolution is governed by GW emission and the cloud decays.

Motivated by this hierarchy, we adopt a simplified model in which the mass of the cloud M_c grows exponentially with a fixed growth rate ω_I , given by the initial BH spin a and mass M

$$M_c(t) \approx M_{c,i} \exp(2\omega_I t), \quad (\text{S233})$$

where $M_{c,i}$ is the initial mass of the cloud. The approximation can estimate the e-folding growth timescale τ_e analytically. Under the assumption that the cloud grows from a single scalar particle $M_{c,i} = \mu$, the growth timescale can be estimated as

$$\frac{\tau_e}{M} \simeq \frac{1}{2M\omega_I} \sim \frac{1}{\alpha^{4\ell_q+6}}, \quad (\text{S234})$$

where $\omega_I \sim \mu\alpha^{4\ell_q+5}$ in Eq. (S39) is used. We utilize the two orders of magnitude difference in the maximum growth rates between the neutral scalar cloud (211 mode) at $\alpha \approx 0.30$ around a Kerr BH and the charged scalar cloud around a magnetic BH with $N = 2q = 3$ magnetic charges at $\alpha \approx 0.45$ illustrated in Fig. S3 to estimate the e-folding growth timescales:

$$\tau_e^{(N=3)} \sim \frac{4.93 \times 10^{-6}}{2 \times 10^{-6}} \left(\frac{M}{M_\odot} \right) \text{s} \approx 2.47 \left(\frac{M}{M_\odot} \right) \text{s}, \quad (\text{S235})$$

$$\tau_e^{(211)} \sim \frac{4.93 \times 10^{-6}}{2 \times 2 \times 10^{-8}} \left(\frac{M}{M_\odot} \right) \text{s} \approx 1.23 \times 10^2 \left(\frac{M}{M_\odot} \right) \text{s}. \quad (\text{S236})$$

Growth timescales for neutral and charged scalar clouds around stellar-mass ($10M_\odot$), intermediate-mass ($10^4 M_\odot$), and supermassive ($10^6 M_\odot$) BHs are shown in Table S1. The corresponding scalar masses are estimated by restoring physical units. Using $\alpha \equiv \frac{GM/c^2}{\hbar/\mu c}$, one finds

$$\mu \simeq \alpha \left(\frac{\hbar c}{GM_\odot/c^2} \right) \left(\frac{M_\odot}{M} \right) \text{ eV}, \quad (\text{S237})$$

where we use $\hbar c \simeq 0.2 \text{ GeV} \cdot \text{fm}$ and $GM_\odot/c^2 \simeq 1.5 \text{ km}$.

BH mass M	Charged $N = 3$ ($q = 1.5$, $M\omega_I \sim 10^{-6}$)	Neutral 211 mode ($M\omega_I \sim 2 \times 10^{-8}$)
$10 M_\odot$	$\sim 2.47 \times 10^1 \text{ s} (\approx 0.41 \text{ min})$	$\sim 1.23 \times 10^3 \text{ s} (\approx 20.5 \text{ min})$
$10^4 M_\odot$	$\sim 2.47 \times 10^4 \text{ s} (\approx 6.86 \text{ hr})$	$\sim 1.23 \times 10^6 \text{ s} (\approx 14.3 \text{ d})$
$10^6 M_\odot$	$\sim 2.47 \times 10^6 \text{ s} (\approx 28.6 \text{ d})$	$\sim 1.23 \times 10^8 \text{ s} (\approx 3.9 \text{ yr})$

TABLE S1. E-folding timescale $\tau_e \equiv (2\omega_I)^{-1}$ estimated using $\tau_e^{(N=3)} \simeq 2.47(M/M_\odot) \text{ s}$ and $\tau_e^{(211)} \simeq 1.23 \times 10^2(M/M_\odot) \text{ s}$.

Importantly, while the approximation above provides a useful reference scale, it assumes that GW losses remain subdominant during the growth phase. This is well justified for the neutral Kerr case, but it can fail for charged clouds around magnetic BHs because the GW luminosity grows rapidly with the coupling $\alpha \equiv \mu M$. In that regime, GW losses may become important already during the growth stage and can quench the instability before the spin-extraction saturation condition $m\Omega_H = \omega_R$ is reached. The cloud then approaches a GW-limited maximum mass set by the competition between the linear growth term $2\omega_I M_c$ and the nonlinear GW-loss term $\propto -M_c^2$. Therefore, a full numerical evolution of Eqs. (S230)–(S232) is required to capture both the spin-down suppression of ω_I and GW quenching. Based on the framework provided in [37], we have developed a code to simulate the evolution of charged scalar clouds around our magnetic BHs.

The result is shown by the solid orange curve (“full”) in Fig. S4, alongside the matched approximation (dashed). We numerically integrate Eqs. (S230)–(S232) self-consistently, updating Ω_H (and thus $\omega_I = \omega_I[M(t), a(t)]$) and the GW luminosity $P_{\text{GW}} = P_{\text{GW}}[M_c(t); \alpha(t), \dots]$ at each time step using the cloud model of Sec. II. This captures both spin-down suppression of ω_I near $m\Omega_H \simeq \omega_R$ and GW quenching during the growth phase. Consequently, while the neutral case is well described by the matched treatment, in the charged case it overestimates the peak cloud

mass and produces an artificially sharp turnover, whereas the full evolution yields a smaller, broader maximum and a longer effective timescale. The BH spin evolution is shown in the bottom panels of Fig. S4 for the same runs. During the superradiant growth stage the cloud extracts angular momentum from the BH, leading to a monotonic decrease of $a(t)/M(t) = J(t)/M(t)^2$ and a progressive reduction of the horizon frequency Ω_H . This spin-down acts as a self-regulating mechanism: as the system approaches the threshold $m\Omega_H \simeq \omega_R$, the growth rate $\omega_I \propto (m\Omega_H - \omega_R)$ is suppressed and the evolution slows. For the neutral Kerr case, GW losses remain negligible during growth, so the matched treatment captures the main spin-down phase accurately and the full evolution yields an essentially identical $a(t)$. By contrast, for charged clouds around magnetic BHs, GW emission can become important already during the growth stage and quenches the instability before the idealized saturation point is reached; consequently the BH spin decreases only modestly and then freezes once the cloud enters the GW-limited regime, consistent with the smaller peak cloud mass and the broader turnover seen in the full evolution.

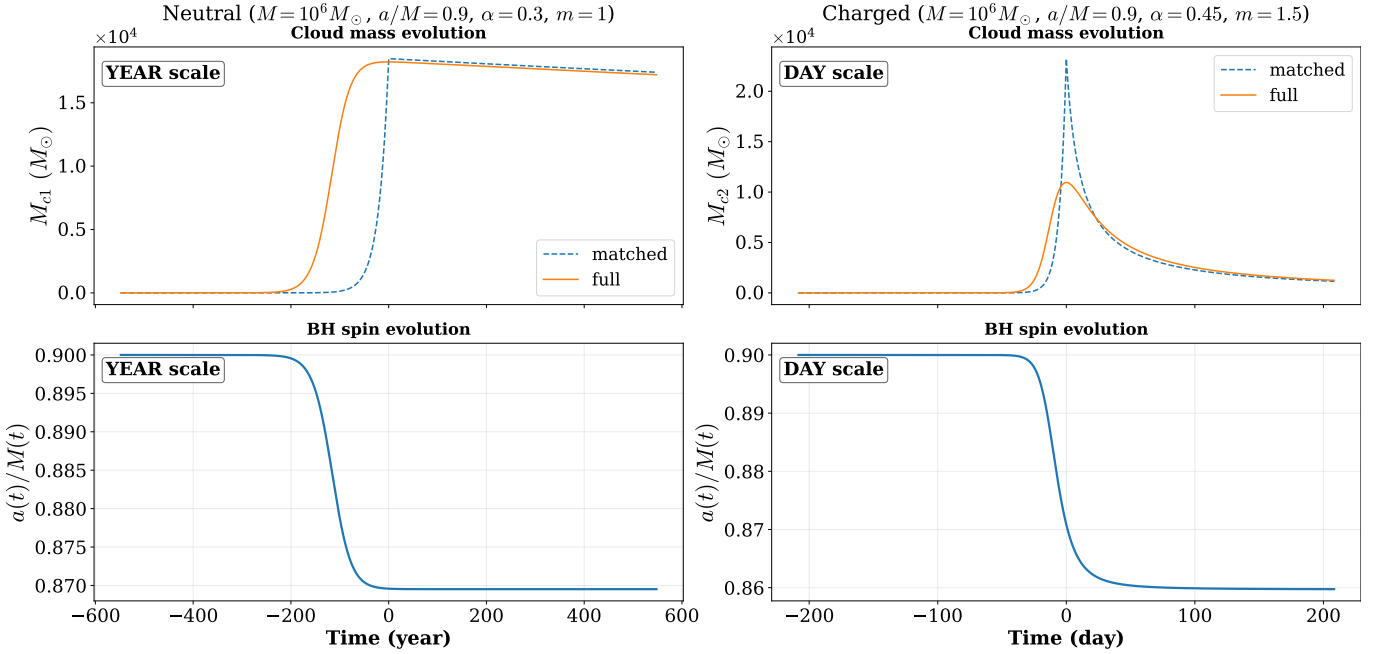


FIG. S4. Time evolution of the scalar cloud mass (top) and BH dimensionless spin (bottom) for a neutral (left) and a charged (right) scalar around a spinning BH with $M = 10^6 M_\odot$ and $a/M = 0.9$. The corresponding boson masses are $\mu \simeq 4.0 \times 10^{-17}$ eV ($\alpha = 0.3$) and $\mu \simeq 6.0 \times 10^{-17}$ eV ($\alpha = 0.45$). For the cloud mass, the dashed curve (“matched”) treats the superradiant growth and the GW-driven decay as two separate stages, neglecting P_{GW} during the growth and switching to a pure GW-decay evolution after saturation, whereas the solid curve (“full”) shows the self-consistent numerical solution of Eqs. (S230)–(S232) including GW losses throughout the evolution. In contrast, the spin evolution shown in the bottom panels corresponds to the full self-consistent solution. While the neutral case is well approximated by the matched treatment, for the charged case GW emission is already relevant during the growth stage, resulting in a longer effective evolution timescale and a reduced peak cloud mass relative to the matched estimate.

IV.b. Waveform construction: circularly polarized instantaneous strain

The TT-gauge gravitational wave can be packaged into the complex strain

$$h(t, \theta, \phi) \equiv h_+(t, \theta, \phi) - i h_\times(t, \theta, \phi), \quad (\text{S238})$$

which admits the standard expansion in spin-weighted (-2) spherical harmonics,

$$h(t, \theta, \phi) = \frac{1}{r} \sum_{\ell, m} h_{\ell m}(t) {}_{-2}Y_{\ell m}(\theta, \phi). \quad (\text{S239})$$

In the present magnetic-BH setup, the GW emission is helicity-polarized and the north/south clouds excite different azimuthal sectors. We focus on the dominant GW modes $h_{2q,\pm 2q}$, and the expansion of the complex strain becomes

$$h(t, \theta, \phi) \simeq \frac{1}{r} \left[(h_{2q,2q})_{-2} Y_{2q,2q}(\theta, \phi) + (h_{2q,-2q})_{-2} Y_{2q,-2q}(\theta, \phi) \right] e^{-i\tilde{\omega}t}, \quad (\text{S240})$$

and the plus/cross polarizations follow from $h_+ = \text{Re}[h]$, $h_\times = -\text{Im}[h]$. Here, $h_{2q,\pm 2q}$ are time-independent complex amplitudes. For a monochromatic real signal, the time average gives $\langle |\dot{h}_{2q,\pm 2q}(t)|^2 \rangle = \frac{1}{2}\tilde{\omega}^2 |h_{2q,\pm 2q}|^2$, and therefore

$$P_{\text{GW}}^\pm = \frac{1}{16\pi} \left\langle |\dot{h}_{2q,\pm 2q}(t)|^2 \right\rangle \simeq \frac{\tilde{\omega}^2}{32\pi} |h_{2q,\pm 2q}|^2. \quad (\text{S241})$$

Equivalently, the power fixes the magnitude of $h_{2q,\pm 2q}$,

$$|h_{2q,\pm 2q}| = \frac{2\sqrt{2\pi P_{\text{GW}}^\pm}}{\tilde{\omega}}. \quad (\text{S242})$$

Crucially, the phase of each mode is not determined by the power, but is carried by the complex inner product $\langle u, T \rangle$. Using the outgoing coefficient Z_{out} in Eq. (S109) and the full inner products $\langle u, T \rangle^\pm$ derived in Eq. (S155), the complex mode amplitudes are

$$h_{2q,2q} = \frac{\tilde{\omega}^2}{2} Z_{\text{out}}(\tilde{\ell} = 2q) \langle u, T \rangle^+, \quad h_{2q,-2q} = \frac{\tilde{\omega}^2}{2} Z_{\text{out}}(\tilde{\ell} = 2q) \langle u, T \rangle^-. \quad (\text{S243})$$

By construction, Eqs. (S241) and (S243) are consistent: the former fixes the normalization via $|h_{\ell m}|$, while the latter provides the full complex amplitudes (including the intrinsic phases). Consequently, the two complex amplitudes $h_{2q,2q}$ and $h_{2q,-2q}$ are treated as independent and computed from their respective overlaps $\langle u, T \rangle^\pm$. This form automatically retains the phases δ_\pm originating from $\langle u, T \rangle^\pm$ for the modes $h_{2q,\pm 2q}$

$$h_{2q,2q} = |h_{2q,2q}| e^{i\delta_+}, \quad h_{2q,-2q} = |h_{2q,-2q}| e^{i\delta_-}. \quad (\text{S244})$$

As a result, the plus and cross polarization h_+, h_\times are reconstructed as

$$h_+ = \frac{1}{r} \left[|h_{2q,2q}|_{-2} S_{2q,2q}(\theta) \cos(\tilde{\omega}t - 2q\phi - \delta_+) + |h_{2q,-2q}|_{-2} S_{2q,-2q}(\theta) \cos(\tilde{\omega}t + 2q\phi - \delta_-) \right], \quad (\text{S245})$$

$$h_\times = \frac{1}{r} \left[|h_{2q,2q}|_{-2} S_{2q,2q}(\theta) \sin(\tilde{\omega}t - 2q\phi - \delta_+) + |h_{2q,-2q}|_{-2} S_{2q,-2q}(\theta) \sin(\tilde{\omega}t + 2q\phi - \delta_-) \right], \quad (\text{S246})$$

which are as shown in Fig. 3.

Furthermore, we define the instantaneous strain envelope

$$|h(t, \theta, \phi)| \equiv \sqrt{h_+^2(t, \theta, \phi) + h_\times^2(t, \theta, \phi)}, \quad (\text{S247})$$

It is straightforward to see that the instantaneous envelope of the magnetic-BH case does not contain the fast phase $\tilde{\omega}t$

$$\begin{aligned} |h(\theta, \phi)|^2 &\equiv h_+^2 + h_\times^2 \\ &= \frac{1}{r^2} \left[|h_{2q,2q}|^2_{-2} S_{2q,2q}^2(\theta) + |h_{2q,-2q}|^2_{-2} S_{2q,-2q}^2(\theta) \right. \\ &\quad \left. + 2 |h_{2q,2q}| |h_{2q,-2q}|_{-2} S_{2q,2q}(\theta)_{-2} S_{2q,-2q}(\theta) \cos(\delta_- - \delta_+ - 4q\phi) \right]. \end{aligned} \quad (\text{S248})$$

In particular, all dependence on the phase $\tilde{\omega}t$ cancels identically: the envelope is insensitive to the GW oscillation at frequency $\tilde{\omega}$ and depends only on (θ, ϕ) and on the intrinsic relative phase $\delta_- - \delta_+$ of the two helicity sectors. The instantaneous length $|h|$ remains nearly constant on the cycle-scale timescale. This behaviour corresponds to (approximately) circular polarization at fixed sky location.

By contrast, for a neutral scalar cloud around a Kerr BH typically, which (keeping only a single GW mode $(2\ell, 2\ell)$) yields the form of polarizations given by Eq. (22) of [37]

$$h_+^{(\text{Kerr})}(t) = h_p \cos(\tilde{\omega}t), \quad h_\times^{(\text{Kerr})}(t) = h_x \sin(\tilde{\omega}t + \delta_{\text{Kerr}}), \quad (\text{S249})$$

where h_p and h_x are (slowly varying) amplitudes and δ_{Kerr} is the relative phase between the two polarizations. In this case the instantaneous strain envelope,

$$|h^{(\text{Kerr})}(t)|^2 \equiv (h_+^{(\text{Kerr})}(t))^2 + (h_\times^{(\text{Kerr})}(t))^2 = h_p^2 \cos^2(\tilde{\omega}t) + h_x^2 \sin^2(\tilde{\omega}t + \delta_{\text{Kerr}}), \quad (\text{S250})$$

does not generally eliminate the GW phase $\tilde{\omega}t$. Indeed, the above envelope can be rewritten as

$$|h^{(\text{Kerr})}(t)|^2 = \frac{1}{2} \left(h_p^2 + h_x^2 \right) + \frac{1}{2} \left[h_p^2 \cos(2\tilde{\omega}t) - h_x^2 \cos(2\tilde{\omega}t + 2\delta_{\text{Kerr}}) \right], \quad (\text{S251})$$

so that a residual modulation at frequency $2\tilde{\omega}$ persists unless special conditions are met. The cancellation occurs only in the circular limit, e.g. when $h_p = h_x$ and $\delta_{\text{Kerr}} = \pm\pi/2$. Generically, however, $h_p \neq h_x$ and/or $\delta_{\text{Kerr}} \neq \pm\pi/2$, corresponding to elliptical polarization: its instantaneous length $|h^{(\text{Kerr})}(t)|$ oscillates, producing the $2\tilde{\omega}$ breathing. This should be contrasted with the magnetic-BH case in (S248), where the north/south contributions enter as a coherent sum and $|h|$ becomes independent of $\tilde{\omega}t$, reflecting an (approximately) circularly polarized signal at fixed sky location. Those quantities tracks the slowly varying amplitude during the cloud evolution and the circularly (elliptically) polarized signal is shown in the middle panels of Fig. 3.

This cancellation admits a simple geometric interpretation in terms of the instantaneous TT deformation of a ring of freely-falling test particles. Consider an initially circular ring in the transverse plane, with position vectors $x_0^a = (x_0, y_0)$. In the linearized regime $|h| \ll 1$, the TT strain acts as an instantaneous linear map on separations,

$$x^a(t) \simeq \left(\delta^a{}_b + \frac{1}{2} h^a{}_b(t) \right) x_0^b. \quad (\text{S252})$$

For a fixed sky location, the non-trivial 2×2 TT strain matrix in the transverse plane may be written in the standard *linear* polarization basis $(+, \times)$ as

$$h_{ab}(t) = \begin{pmatrix} h_+(t) & h_\times(t) \\ h_\times(t) & -h_+(t) \end{pmatrix} \equiv h_+(t) e_{ab}^+ + h_\times(t) e_{ab}^\times, \quad (\text{S253})$$

where $e_{ab}^+ = \text{diag}(1, -1)$ and e_{ab}^\times has off-diagonal entries. Equivalently, one may use the *circular* polarization (helicity) basis (R, L) ,

$$h_{ab}(t) = h_R(t) e_{ab}^R + h_L(t) e_{ab}^L, \quad e_{ab}^{R/L} = \frac{1}{\sqrt{2}} (e_{ab}^+ \pm i e_{ab}^\times), \quad h_{R/L} = \frac{1}{\sqrt{2}} (h_+ \mp i h_\times). \quad (\text{S254})$$

Applying the full matrix $h_{ab}(t)$ to an initially circular ring gives the deformed curve shown in figure S5. The instantaneous eigenvalues follow from $\det(h - \lambda I) = 0$, yielding

$$\lambda_\pm = \pm |h|, \quad |h| \equiv \sqrt{h_+^2 + h_\times^2}, \quad (\text{S255})$$

so $|h|$ controls the instantaneous strain magnitude (the envelope governing how “elliptical” the deformation is). In the eigenvector (principal-axis) basis, the map in eq. (S252) becomes $\text{diag}(1 + \frac{1}{2}|h|, 1 - \frac{1}{2}|h|)$, hence the principal stretches (semi-axes, in units of the original radius) are

$$a_{\text{ellipse}} = 1 + \frac{1}{2}|h|, \quad b_{\text{ellipse}} = 1 - \frac{1}{2}|h|. \quad (\text{S256})$$

The time dependence enters in two distinct ways. First, $|h|(t)$ may vary, producing a genuine “breathing” of the semi-axes. In figure S5, the Kerr row exhibits such an axis breathing, consistent with the residual $2\tilde{\omega}$ modulation in eq. (S251). Second, even if $|h|$ is (approximately) independent of the fast phase $\tilde{\omega}t$ (as in eq. (S248)), the eigenvectors of h_{ab} can still rotate in time, corresponding to a time-dependent polarization angle $\theta(t)$. Writing the principal-axis directions in the transverse plane, one finds

$$\tan(2\theta(t)) = \frac{h_\times(t)}{h_+(t)}. \quad (\text{S257})$$

For an (approximately) circularly polarized waveform, h_+ and h_\times have comparable amplitudes with a $\pm\pi/2$ relative phase (equivalently, a single-helicity component in the (R, L) basis), so $|h|$ remains nearly constant while $\theta(t)$ advances linearly; in particular one finds $2\theta(t) \simeq \tilde{\omega}t \pmod{\pi}$, i.e. $\theta(t) \simeq \tilde{\omega}t/2$. Thus the same ellipse rotates in the plane while keeping (approximately) fixed axis lengths, precisely the rotating pattern seen in the magnetic-BH panels of figure S5.

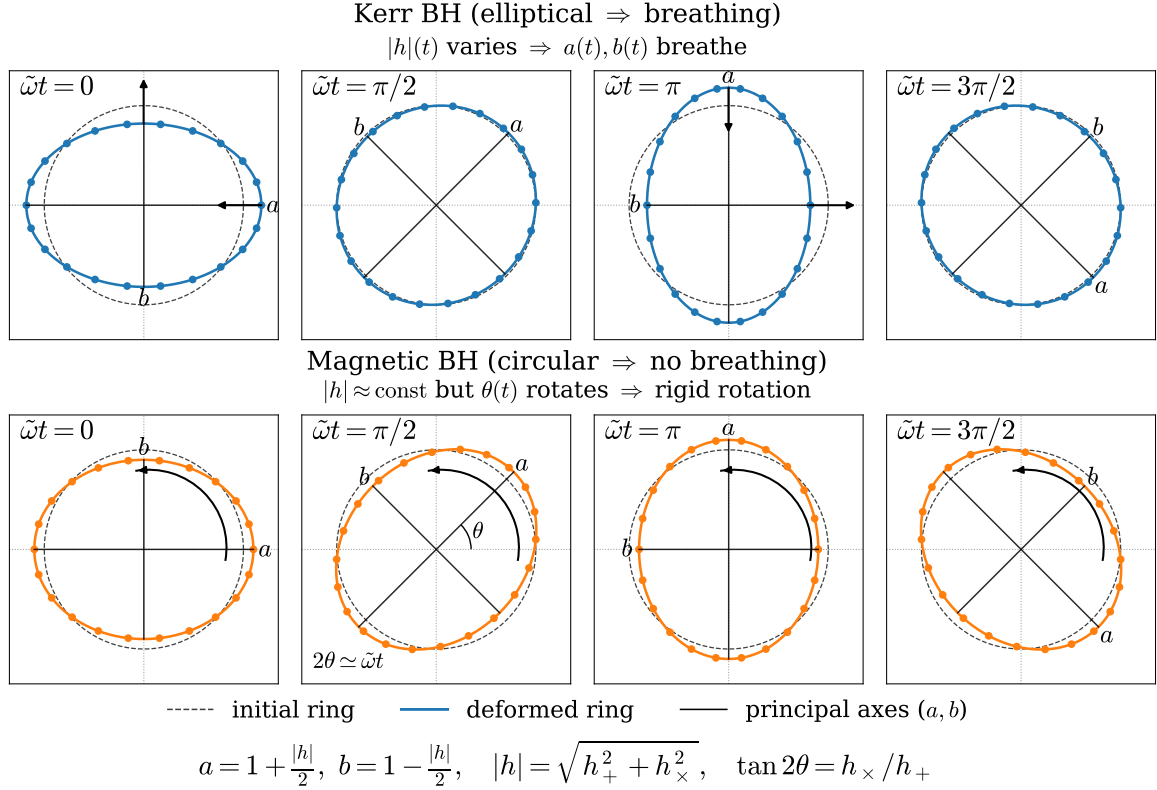


FIG. S5. Schematic comparison of the instantaneous TT deformation induced by the GW polarizations for a Kerr BH (top row) and for the magnetic-BH setup (bottom row). Each panel shows the deformation of an initially circular ring of test particles (grey dashed circle) at four phases $\tilde{\omega}t = \{0, \pi/2, \pi, 3\pi/2\}$. For the Kerr case we illustrate the generic elliptical-polarization form $h_+^{(\text{Kerr})} = h_p \cos(\tilde{\omega}t)$ and $h_\times^{(\text{Kerr})} = h_x \sin(\tilde{\omega}t + \delta_{\text{Kerr}})$, for which the instantaneous envelope $|h^{(\text{Kerr})}|$ typically oscillates at $2\tilde{\omega}$ (“breathing”). For the magnetic-BH case the signal is (approximately) circularly polarized at fixed sky location, since the coherent superposition of the $\tilde{m} = \pm 2q$ helicity sectors in Eq. (S240) yields an envelope $|h|$ independent of the fast phase $\tilde{\omega}t$ in Eq. (S248). The arrows indicate the qualitative evolution: alternating stretching/squeezing for Kerr versus a rigid rotation at nearly constant $|h|$ for the magnetic-BH case.

IV.c. Breathing amplitude and the Stokes parameter

At a fixed sky location, write the *real* GW polarizations in terms of the complex positive-frequency amplitudes $h_{+,\times}$ as

$$h_+(t) = \frac{1}{2} (h_+ e^{-i\tilde{\omega}t} + h_+^* e^{+i\tilde{\omega}t}), \quad h_\times(t) = \frac{1}{2} (h_\times e^{-i\tilde{\omega}t} + h_\times^* e^{+i\tilde{\omega}t}). \quad (\text{S258})$$

The instantaneous magnitude controlling the TT stretching is $|h(t)|^2 \equiv h_+^2(t) + h_\times^2(t)$. Using Eq. (S258) one finds

$$\begin{aligned} |h(t)|^2 &= \frac{1}{2} (|h_+|^2 + |h_\times|^2) + \frac{1}{4} [(h_+^2 + h_\times^2) e^{-2i\tilde{\omega}t} + (h_+^{*2} + h_\times^{*2}) e^{+2i\tilde{\omega}t}] \\ &= \frac{I}{2} + \frac{|A|}{2} \cos(2\tilde{\omega}t - \varphi), \end{aligned} \quad (\text{S259})$$

where $I \equiv |h_+|^2 + |h_\times|^2$ and $A \equiv h_+^2 + h_\times^2 \equiv |A| e^{i\varphi}$. Thus a $2\tilde{\omega}$ modulation (“breathing”) is present whenever $|A| \neq 0$.

With the Stokes parameter $V \equiv 2 \text{Im}(h_+ h_\times^*)$ and $\Pi_{\text{circ}} \equiv V/I$ [Eq. (18)], one may show the identity

$$|A|^2 = |h_+^2 + h_\times^2|^2 = I^2 - V^2 = I^2 (1 - \Pi_{\text{circ}}^2). \quad (\text{S260})$$

Substituting Eq. (S260) into Eq. (S259) yields

$$|h(t)|^2 = \frac{I}{2} \left[1 + \sqrt{1 - \Pi_{\text{circ}}^2} \cos(2\tilde{\omega}t - \varphi) \right], \quad (\text{S261})$$

so the breathing amplitude is set by $\sqrt{1 - \Pi_{\text{circ}}^2}$. In particular, $|\Pi_{\text{circ}}| = 1$ gives no $2\tilde{\omega}$ modulation (rigidly rotating ellipse), whereas $|\Pi_{\text{circ}}| < 1$ yields an elliptically polarized signal with breathing, approaching the linear limit as $|\Pi_{\text{circ}}| \rightarrow 0$.